

Spectral Tailoring for Boron Neutron Capture Therapy

The research described in this thesis was performed within a cooperation of the Institute for Energy of the Joint Research Centre (JRC) of the European Commission, P.O. Box 2, 1755 ZG, Petten, The Netherlands and the Section Physics of Nuclear Reactors (PNR), of the Department of Radiation, Radionuclides & Reactors (R³) of the Faculty of Applied Sciences of the Delft University of Technology, Mekelweg 15, 2629 JB, Delft, The Netherlands.

Spectral Tailoring for Boron Neutron Capture Therapy

Proefschrift

ter verkrijging van de graad van doctor
aan de Technische Universiteit Delft,
op gezag van de Rector Magnificus prof. dr. ir. J.T. Fokkema,
voorzitter van het College voor Promoties,
in het openbaar te verdedigen
op dinsdag 26 juni 2007 om 15:00 uur

door:

Victor Alexander NIEVAART
natuurkundig ingenieur,
geboren te Apeldoorn

Dit proefschrift is goedgekeurd door de promotoren:

Prof.[em] dr. ir. H. van Dam

Prof. dr. ir. T.H.J.J. van der Hagen

Toegevoegd promotor:

Dr. ir. J.L. Kloosterman

Samenstelling promotiecommissie:

Rector Magnificus, voorzitter

Prof.[em] dr. ir. H. van Dam

Prof. dr. ir. T.H.J.J. van der Hagen

Dr. ir. J.L. Kloosterman

Prof. dr. med. W. Sauerwein

Prof. dr. ir. M. Hendriks-de Jong

Prof. dr. H.T. Wolterbeek

Dr. R.L. Moss

Technische Universiteit Delft

Technische Universiteit Delft

Technische Universiteit Delft

University Hospital Essen

Erasmus Medisch Centrum Rotterdam

Technische Universiteit Delft

Joint Research Centre Petten

© 2007 V.A. Nievaart and IOS Press

All rights reserved. No part of this book may be reproduced, stored in a retrieval system, or transmitted, in any form or by any means, without prior permission from the publisher.

ISBN 978-1-58603-762-8

Keywords: Boron Neutron Capture Therapy, Optimal Source Neutrons, Adjoint Monte Carlo

Published and distributed by IOS Press under the imprint Delft University Press

Publisher

IOS Press

Nieuwe Hemweg 6b

1013 BG Amsterdam

The Netherlands

tel: +31-20-688 3355

fax: +31-20-687 0019

email: info@iospress.nl

www.iospress.nl

www.dupress.nl

LEGAL NOTICE

The publisher is not responsible for the use which might be made of the following information.

PRINTED IN THE NETHERLANDS

This thesis consists of two parts. The first part provides a complete overview of the research performed and the second part consists of a collection of key papers:

- I. V.A. Nievaart, R.L. Moss, J.L. Kloosterman, T.H.J.J. van der Hagen and H. van Dam, "A parameter study to determine the optimal source neutron energy in Boron Neutron Capture Therapy of brain tumours," Phys.Med.Biol. 49, 4277-4292 (2004).
© 2004 IOP Publishing Ltd ; www.iop.org/journals/pmb
- II. V.A. Nievaart, D. Légrady, R.L. Moss, J.L. Kloosterman, T.H.J.J. van der Hagen and H. van Dam, "Application of adjoint Monte Carlo to accelerate simulations of mono-directional beams in treatment planning for Boron Neutron Capture Therapy," Med.Phys. 34 (4), 1321-1335 (2007).
© 2007 Am. Assoc. Phys. Med. ; www.medphys.org
- III. V.A. Nievaart, R.L. Moss, J.L. Kloosterman, T.H.J.J. van der Hagen, H. van Dam, A. Wittig, M. Malago and W. Sauerwein, "Design of a Rotating Facility for Extracorporal Treatment of an Explanted Liver with Disseminated Metastases by Boron Neutron Capture Therapy with an Epithermal Neutron Beam," Rad.Res. 166, 81-88 (2006).
© 2006 by Radiation Research Society ; www.radres.org

CONTENTS

SUMMARY	IX
SAMENVATTING	XI
PUBLICATIONS	XV
CHAPTER 1 INTRODUCTION	1
1. GENERAL INTRODUCTION	1
1.1 THE BASICS OF BNCT	1
1.1.1 <i>The four major BNCT dose components in tissue</i>	2
1.1.2 <i>Biologically weighted doses and ^{10}B compounds</i>	6
1.1.3 <i>Brief history of BNCT</i>	7
1.1.4 <i>Present status of BNCT</i>	8
1.2 SPECTRAL TAILORING FOR BNCT	9
1.2.1 <i>Search for the optimal source neutron energy for BNCT</i>	10
1.2.2 <i>The scope of this thesis</i>	10
CHAPTER 2 OPTIMAL NEUTRONS AND DOSIMETRY	13
2. OPTIMAL SOURCE NEUTRONS WITH REGARD TO DOSIMETRY IN BNCT	13
2.1 BACKGROUND ON BNCT DOSIMETRY AND RADIOBIOLOGY	13
2.2 A PARAMETER STUDY FOR BNCT OF THE BRAIN	14
2.2.1 <i>Set-up and chosen parameter ranges</i>	14
2.2.2 <i>The influence of parameter biasing on the results</i>	16
2.2.3 <i>Results: the optimal source neutron energy</i>	17
2.2.4 <i>Results: the influencing parameters</i>	19
2.2.5 <i>Results: Improvements when using the optimal source neutrons</i>	21
2.3 CONCLUSIONS	23
CHAPTER 3 ADJOINT TECHNIQUES IN BNCT	25
3. APPLICATION OF ADJOINT MONTE CARLO TECHNIQUES IN BNCT	25
3.1 BACKGROUND, THEORY AND MCNP	25
3.2 GENERAL ADJOINT SET-UP FOR BNCT	26
3.3 ADJOINT TREATMENT PLANNING WITH A MONO-DIRECTIONAL BEAM	27
3.3.1 <i>Adjoint Point Detector Technique (APDT)</i>	28
3.3.2 <i>Legendre EXpansion Technique (LEXT)</i>	29
3.4 EXAMPLE: OPTIMUM CHARACTERISTICS IN THE IRRADIATION OF A HUMAN HEAD	31
3.4.1 <i>Calculation times of forward MC, APDT and LEXT</i>	32
3.4.2 <i>Optimum irradiation locations and directions</i>	35
3.4.3 <i>Optimum source neutron energy group</i>	36
3.5 CONCLUSIONS	38
CHAPTER 4 THERMAL NEUTRON FIELD FACILITY	39
4. DESIGN OF A HOMOGENEOUS THERMAL NEUTRON FIELD FACILITY FOR BNCT	39
4.1 DESIGN OF AN IRRADIATION FACILITY FOR THE	39

EXTRA-CORPORAL TREATMENT OF LIVER CANCER WITH AN EXISTING EPITHERMAL BEAM	
4.1.1 <i>Design parameters and selected materials</i>	40
4.1.2 <i>Simulating rotation with the Monte Carlo code</i>	42
4.1.3 <i>Results of the designed liver facility at the HFR Petten</i>	42
4.2 OPTIMUM NEUTRON BEAM DESIGN AND HOLDERS FOR EXTRA-CORPORAL BNCT IRRADIATIONS	44
4.2.1 <i>Set-up of the holder models</i>	44
4.2.2 <i>Expected contributions of the source neutrons inside the models</i>	45
4.2.3 <i>Optimum source neutron energies</i>	48
4.3 CONCLUSIONS	52
CHAPTER 5 CONCLUSIONS	53
APPENDIX	57
NOMENCLATURE	61
ABBREVIATIONS	63
REFERENCES	65
ACKNOWLEDGEMENT	73
CURRICULUM VITAE	75
PAPERS I-III	77

Spectral Tailoring for Boron Neutron Capture Therapy

Since the first clinical trials on Boron Neutron Capture Therapy in the 1950s, BNCT research has been mainly focussed on the treatment of (deep-seated) brain tumours, in particular, glioblastoma multiforme. Promising work to treat other cancers at other locations and even other diseases are in progress. Therefore, the chemists, medical doctors, physicists and biologists involved in BNCT are not only continuing to investigate and improve the (brain) clinical results, but are also investigating the new applications in BNCT. The work presented in this thesis is in the field of physics and deals, from three different viewpoints, with obtaining the optimal source neutron energy to optimise BNCT. The optimal source neutron energy is defined such as to obtain as many as possible (n,α) -absorptions due to ^{10}B in the tumours and as low as possible total neutron dose in the healthy tissues and organs at risk.

Firstly, the relation between the optimal source neutron energy and the radiation biology of brain BNCT was investigated. The biological weighting factors of the four major BNCT dose components, the skin and cranium thickness, the tolerance dose in skin and brain, the ^{10}B concentration and the number of beam gammas per source neutron were varied in a theoretical study. The parameter value ranges are bounded by unexpected and/or unrealistic values. It was investigated as to what is the optimal source neutron energy for four tumours at different depths, in each of the 136 million configurations for all combinations of parameter values. By far, the modality of the optimal source neutron energies is between 1 keV and 10 keV. However, depending on where the tolerance dose is reached first, in the skin or brain, low values for ^{10}B and fast neutron related parameters in this limiting tissue result in lower or higher than modal source neutron energies.

Secondly, adjoint Monte Carlo (MC) techniques are developed to find more quickly the optimal source neutrons' location, direction and energy. The adjoint MC is very suitable for this task because the adjoint particles fly mainly towards regions that from the statistics point of view are the best directions to irradiate from. Until now it was impossible to gather acceptable statistics of adjoint MC particles which traverse the adjoint detector perpendicularly, rendering the adjoint method inapplicable for mono-directional beams. The BNCT beam available in Petten can be regarded as mono-directional. This problem is solved with the use of next event estimators or with the application of a Legendre expansion technique. In the first case, adjoint particles are transported deterministically through a beam shaped channel to a point detector far away from the geometric model. The particles will traverse the disk shaped entrance of this tube (the beam exit in the actual geometry) perpendicularly. This method is slow when many events are involved that are not contributing to the point detector, e.g. neutrons in a scattering medium. In a second approach, adjoint particles that traverse an adjoint shaped detector plane are used to estimate the Legendre coefficients for expansion of the angular adjoint function. This provides an estimate of the adjoint function for the direction normal to the detector plane. In a realistic head phantom with 10 organs at risk and 10 tumours, the two adjoint techniques are 1.8 to 3.3 times faster than the forward MC calculations when 1020

different orientations of a gamma beam with a diameter larger than 5 cm are simulated. In case of a neutron beam, only the adjoint technique based on Legendre expansion is faster, 6.6 up to 20 times, than forward MC. In general, in case of small diameter beams adjoint MC calculations are only preferable for a large number of beams and a small number of regions of interest. For larger beam sizes, fewer beams and/or many regions of interest makes the adjoint favourable over the forward calculations. As well as being able to obtain the optimal locations to irradiate from, the optimal source neutron energy at every location around the head can also be obtained with adjoint MC. Compared with the Petten beam spectrum, it is found that only thermal and low-energy epithermal source neutrons can give significant improvements to the ratio of the thermal neutron flux in tumours to organs at risk.

Thirdly, the optimal source neutron energies are determined in order to obtain a homogeneous thermal neutron fluence in a prescribed volume. Ideally, when the homogeneity, defined as the ratio of minimum to maximum thermal neutron flux, is unity, the same thermal neutron related dose can be given in every part of this volume. When using the Petten beam with its current neutron spectrum for the extracorporeal BNCT treatment of liver cancer, the best homogeneity obtained is 0.68 in a volume of 2.4 litres. This volume is spheroidal shaped and rotating. The rotation is simulated in MCNP by averaging the particle tracks in tori shaped tally volumes. With a combination of source neutrons of 30% around 0.1 eV and 70% around 10 keV, a homogeneity of 0.95 can be reached in a cuboid model. This result was obtained after calculating the detector response functions for thermal neutrons in different volume shapes (i.e. cuboid, cylinder and sphere) as a function of source neutron energy. By applying linear programming, the detector response functions of the source neutron energies were combined such that the homogeneity in each volume shape is optimised.

The outcome of the three parts of this thesis shows that 3 neutron energy regimes should be prescribed in BNCT. As well as the 10 keV epithermal source neutrons, low epithermal source neutrons of around 1 eV and thermal source neutrons with energies of 0.1 eV must be used.

Petten, May 2007,
V.A. Nievaart

Spectrum Optimalisatie voor Boron Neutron Capture Therapy

Al vanaf de eerste klinische studies naar Boron Neutron Capture Therapy¹ (BNCT) in de jaren 50 ligt de nadruk van het BNCT onderzoek voornamelijk op de behandeling van diep gesitueerde hersentumoren en wel in het bijzonder de glioblastoma multiforme. Pas de laatste decennia zijn veelbelovende ontwikkelingen gaande om andere vormen en locaties van kanker en zelfs niet kankerzijnde ziektes te gaan behandelen. Dit betekent dat de bij BNCT betrokken chemici, artsen, fysici en biologen niet alleen proberen de hersenresultaten te verbeteren maar ook onderzoek te doen naar de nieuwe BNCT toepassingen. Dit proefschrift heeft een fysische grondslag en behandelt vanuit 3 invalshoeken het verkrijgen van de optimale bronneutronenenergie om zodoende BNCT te verbeteren. De optimale bronneutronen worden gekenmerkt door een energie die zoveel mogelijk (n, α)-absorpties tengevolge van ^{10}B in de tumor genereert en tegelijkertijd een zo laag mogelijke dosis geeft in de gezonde weefsels en stralingsgevoelige organen.

De eerste invalshoek van dit proefschrift is de relatie tussen de optimale bronneutronenenergie en de radiobiologie van BNCT toegepast voor hersenen. Hiervoor zijn in deze theoretische studie de biologische weegfactoren van de vier belangrijkste BNCT dosिसcomponenten, de huid- en schedeldiktes, de tolerantiedosis in huid en hersenen, de ^{10}B concentratie en het aantal brongamma's per bronneutron in de bundel gevarieerd. Voor al deze parameters zijn intervallen gekozen die zijn begrensd door onrealistische en/of niet meer te verwachten waarden. Onderzocht is wat de optimale bronneutronenenergie is voor tumoren op 4 verschillende dieptes in elk van de 136 miljoen configuraties tengevolge van alle mogelijke combinaties van parameterwaarden. Voor veruit de meeste configuraties blijken bronneutronen met een energie tussen de 1 keV en 10 keV optimaal te zijn. Alleen voor lage waarden van de ^{10}B en snelle neutronen dosis gerelateerde parameters zijn er soms afwijkende (lagere of hogere) optimale bronneutronenenergieën. Dit geldt voor deze parameters in het weefsel (huid of hersenen) waar de tolerantiedosis als eerste wordt bereikt.

Ten tweede zijn er adjoint Monte Carlo (MC) technieken ontwikkeld om sneller de optimale locatie, richting en energie van de bronneutronen te vinden. Adjoint MC is zeer geschikt omdat de adjoint deeltjes zich voornamelijk bewegen naar die plekken die statistisch gezien het gunstigste zijn om vanuit te bestralen. Tot nu toe was het onmogelijk om genoeg adjoint MC deeltjes te verzamelen die loodrecht door het detectievlak gaan. Het verkrijgen van een goede statistiek voor de adjoint in geval van een eenrichtingsbundel was dus onmogelijk. De BNCT bundel in Petten (NL) kan worden beschouwd als een eenrichtingsbundel. Het probleem is opgelost met het gebruik van 'volgende-gebeurtenis-schatters' en door toepassing van een 'Legendre-ontwikkelings' techniek. In het eerste geval worden adjointdeeltjes

¹ In het Nederlands is BNCT vertaald als Borium Neutronenvangst Therapie.

deterministisch door een kanaal getransporteerd, die is gevormd zoals de bundel, naar een punt ver weg van de ingang. Zodoende zullen de adjointdeeltjes deze ingang (de bundelopening in werkelijkheid) loodrecht passeren. Deze methode is nadelig als veel deeltjes moeten worden gevolgd die het detectiepunt niet kunnen bereiken zoals het geval is bij neutronen in een verstrooiend medium. Bij de tweede methode worden de adjointdeeltjes die een adjointdetectorvlak passeren gebruikt voor het schatten van de Legendre coëfficiënten om zodoende de hoekafhankelijke adjointfunctie te kunnen ontwikkelen. Dit resulteert in een schatting voor de adjointfunctie in de richting loodrecht op het adjoint detectievlak. In een realistisch scenario, een hoofdphantoom met 10 tumoren in de hersenen en 10 stralingsgevoelige organen, zijn de twee adjoint technieken 1,8 tot 3,3 keer sneller dan normale voorwaartse MC berekeningen als 1020 verschillende posities van een gammabundel met een diameter groter dan 5 cm moeten worden gesimuleerd. In het geval van een neutronenbundel is alleen de Legendre techniek sneller dan normale voorwaartse MC berekeningen en wel 6,6 tot 20 keer. Voor kleine bundeldiameters kan worden geconcludeerd dat adjoint MC berekeningen voordelig zijn als er relatief veel bundelposities en weinig tumoren en/of stralingsgevoelige organen in het spel zijn. Voor grotere bundeldiameters is de adjoint methode al aantrekkelijk voor minder bundelposities en/of meer gebieden waarin de dosis berekend moet worden. Buiten de optimale bundelposities kan de adjoint techniek ook worden gebruikt om de optimale bronneutronenenergie overal rondom het hoofd te bepalen. In vergelijking met het spectrum van de Pettenbundel blijkt dat toepassing van de ene keer alleen thermische en de andere keer alleen laagepithermische bronneutronen significante verbeteringen geven in de verhouding tussen het thermische neutronenfluentietempo in de tumoren en stralingsgevoelige organen.

Ten derde is de optimale bronneutronenenergie onderzocht om een homogeen thermische neutronenfluentie te verkrijgen in een bepaald volume. Deze homogeniteit is gedefinieerd als de verhouding tussen de minimale en de maximale thermische neutronenfluentietempi in een volume. Idealiter heeft deze verhouding een waarde 1 wat betekent dat de thermische neutronen gerelateerde dosis overal in het volume hetzelfde kan zijn. In geval van behandeling van leverkanker met BNCT in Petten, waarbij de lever buiten het lichaam wordt gebracht, is de homogeniteit 0,68. Deze waarde wordt bereikt in een roterende sferoïde met een volume van 2,4 liter en gebruikmakend van het bestaande spectrum van de Pettenbundel. Met de MCNP code kan rotatie worden gesimuleerd door de geregistreerde padlengtes van de deeltjes in een torus te middelen over het torusvolume. Een mix van 30% 0,1 eV bronneutronen en 70% 10 keV bronneutronen resulteert in een homogeniteit van 0.95 in een kubusvormig model. Dit resultaat is verkregen door als functie van de bronneutronenenergie de detectorresponsiefuncties te berekenen voor thermische neutronen in verschillende modellen (te weten: kubus-, cilinder- en bolvormig). Met behulp van lineair programmeren zijn de detectorresponsiefuncties zo gecombineerd dat de homogeniteit in elke volumevorm is geoptimaliseerd.

De uitkomst van deze drie delen van het promotieonderzoek is dat 3 bronneutronenenergieregimes beschikbaar zouden moeten zijn in BNCT. Buiten de

10 keV epithermische bronneutronen moeten ook laagepithermische bronneutronen van rond de 1 eV en thermische bronneutronen met energieën van 0,1 eV beschikbaar zijn.

Petten, Mei 2007,
V.A. Nievaart

PUBLICATIONS

FIRST AUTHOR:

V.A. Nievaart, R.L. Moss, J.L. Kloosterman and T.H.J.J. van der Hagen, "Calculating the tumour-specific optimal source neutron energy for Boron Neutron Capture Therapy with particle production and adjoint Monte Carlo techniques," PHYSOR 2002, Seoul Korea, October 7-10, (2002).

V.A. Nievaart, J.L. Kloosterman, T.H.J.J. van der Hagen, R.L. Moss, "Forward and adjoint Monte Carlo calculations for investigating the use of an adjustable filter in BNCT," In: W. Sauerwein, R. Moss, A. Wittig, editors Research and Development Neutron Capture Therapy. Bologna: Monduzzi Editore, 1065-72 (2002).

V.A. Nievaart, "Maximising the α -production in brain tumours under different equivalent dose configurations in BNCT," ISNCT/YMNM3 meeting, Pisa Italy, Nov 27 - Dec 2, (2003).

V.A. Nievaart, R.L. Moss, J.L. Kloosterman, T.H.J.J. van der Hagen and H. van Dam, "A parameter study to determine the optimal source neutron energy in Boron Neutron Capture Therapy of brain tumours," Phys.Med.Biol. 49, 4277-4292 (2004).

V.A. Nievaart, R.L. Moss, J.L. Kloosterman, T.H.J.J. van der Hagen, H. van Dam, "Feasibility study for the extra-corporal treatment of liver cancer by BNCT at the HFR Petten," ISNCT-11, October 11-15, Boston, Conference proceeding, USA (2004).

V. Nievaart, A. Wittig, R. Moss, J. Rassow, W. Sauerwein, "Optimisation of treatment planning for multi-beam Boron Neutron Capture Therapy (BNCT) using epithermal neutron beams in patients with multiple metastases to the brain from malignant melanoma," Strahlentherapie und Onkologie, Abstractband zum DEGRO-Kongress, Sondernr.1, May (2006).

V.A. Nievaart, R.L. Moss, J.L. Kloosterman, T.H.J.J. van der Hagen, H. van Dam, A. Wittig, M. Malago, W. Sauerwein, "Design of a rotating facility for extra-corporal treatment of an explanted liver with disseminated metastases by BNCT with an epithermal neutron beam at the HFR in Petten", Radiation Research 166, 81-88 (2006).

V.Nievaart, R Moss, A Wittig, and W Sauerwein, "Extra-corporal treatment of Liver Metastases by BNCT at the HFR Petten", Journal of Physics: Conference Series of the Institute of Physics 41, 369-374 (2006).

Sander Nievaart, Ray Moss, Wolfgang Sauerwein, Massimo Malago, Jan Leen Kloosterman, Tim van der Hagen and Hugo van Dam, "An optimum source neutron spectrum and holder shape for extra-corporal treatment of liver cancer by BNCT,"

12th International Congress on Neutron Capture Therapy Kagawa International Conference Hall, Sunport Takamatsu, Japan, Oct 9-13 (2006).

Sander Nievaart, Ray Moss, Wolfgang Sauerwein and Andrea Wittig, "Use of linear programming to obtain an optimum, multi-beam treatment plan in BNCT," 12th International Congress on Neutron Capture Therapy Kagawa International Conference Hall, Sunport Takamatsu, Japan, Oct 9-13 (2006).

V.A. Nievaart, D. Légrady, R.L. Moss, J.L. Kloosterman, T.H.J.J. van der Hagen and H. van Dam, "Application of adjoint Monte Carlo to accelerate simulations of mono-directional beams in treatment planning for Boron Neutron Capture Therapy," Med.Phys. 34 (4), 1321-1335 (2007).

V.A. Nievaart , G.G. Daquino and R.L. Moss, "Monte Carlo based treatment planning systems for Boron Neutron Capture Therapy in Petten The Netherlands," submitted to Journal of Physics: Conference Series of the Institute of Physics (2007).

CO-AUTHOR:

Mudde, RF , Deutz, L, Nievaart, VA , & Maanen, HRE van, "LDA-measurements of the turbulence in and around a venture," In W Rodi & M Mulas (Eds.), Proceeding of Ercoftac internationa symposium of engineering turbulence modelling and measurements, Ercoftac, Sardinia, Italy, pp. 80-91 (2005).

W. Sauerwein, M. Malago, R. Moss, S. Altieri, G. Hampel, A. Wittig, V. Nievaart, L. Collette, P. Mauri, R. Huiskamp, J. Michel, G. Daquino, G. Gerken, N. Bornfeld, C.E. Broelsch, "Bor-Neutroneneinfangtherapie (BNCT) zur Behandlung diffuser, nicht resektabler Lebermetastasen," Strahlentherapie und Onkologie, Abstractband zum DEGRO-Kongress, Sondernr.1, May (2006).

A. Wittig, L. Collette, J. Heimans, P. Paquis, K. Haseslsberger, V. Barsegian, C. Loquai, G. Kaiser, R. Moss, J. Rassow, F. Stecher-Rasmussen, R. Huiskamp, V. Nievaart, S. Bührmann, P. Bet, B. Hahn, K. Hideghéty, H. Arlinghaus, W. Sauerwein, "A strategy to introduce Boron Neutron Capture Therapy (BNCT), a novel radiotherapy modality, into clinical practice," The clinical trials of the EORTC BNCT Group; Strahlentherapie und Onkologie, Abstractband zum DEGRO-Kongress, Sondernr.1, May (2006).

G.Gambarini, G.G.Daquino, R.L.Moss, M.Carrara, V.A.Nievaart, E.Vanossi, "Gel dosimetry in the BNCT facility for extra-corporal treatment of corporal of liver cancer at the HFR Petten," 10th Symposium on Neutron Dosimetry. Progress in dosimetry of neutrons and light nuclei Uppsala (SV), 12-16 June (2006).

A. Roca, G.G. Daquino, R.L. Moss, S. Nievaart, R. Schmidt F. Stecher-Rasmussen, "Determination of the neutron capture sensitivity of ionisation chambers based on

neutron capture reaction rates,” 12th International Congress on Neutron Capture Therapy Kagawa International Conference Hall, Sunport Takamatsu, Japan, Oct 9-13 (2006).

Ray Moss, Sander Nievaart, Lucien Pott, Andrea Wittig, Wolfgang Sauerwein, “Design and testing of a rotating, cooled device for extra-corporal treatment of liver cancer by BNCT in the epithermal neutron beam at the HFR Petten,” 12th International Congress on Neutron Capture Therapy Kagawa International Conference Hall, Sunport Takamatsu, Japan, Oct 9-13 (2006).

G.G.Daquino, G.Gambarini, S.Nievaart, M.Carrara, E.Vanossi, “Use of Gel dosimetry to characterize the dose distribution in the spheroidal holder for liver treatment at the HFR Petten,” 12th International Congress on Neutron Capture Therapy Kagawa International Conference Hall, Sunport Takamatsu, Japan, Oct 9-13 (2006).

P. van Lent, A. Sloetjes, A. Blom, G. Krijger, G. Koning, S. Nievaart, W. van den Berg and R. Moss, “Selective elimination of synovial macrophages by boron neutron capture therapy prevents onset of murine experimental arthritis,” *Journal of Controlled Release*, Volume 116, Issue 2, 28, pp e106-e107 (2006).

Peter van Lent, Gerard Krijger, Wouter Hofkens, Sander Nievaart, Annet Sloetjes, Gerben Koning, Ray Moss, Wim van den Berg, “Selective Elimination of Synovial Macrophages by Boron Neutron Capture Therapy prevents onset of Joint Inflammation and Cartilage Destruction during Experimental Arthritis,” submitted to *Annals of Rheumatic diseases* (2007).

Andrea Wittig, Massimo Malago, Laurence Collette, René Huiskamp, Sandra Bührmann, Victor Nievaart, Gernot M. Kaiser, Karl-Heinz Jöckel, Kurt Werner Schmid, Uta Ortmann, Wolfgang A. Sauerwein, “Uptake of two ¹⁰B-compounds in liver metastases of colorectal adenocarcinoma for extracorporeal irradiation with BNCT (EORTC trial 11001),” in preparation.

M.M. Fretz, G.C. Krijger, U.D. Woroniecka, V.A. Nievaart, W. Jiskoot, R. Moss, G.A. Koning and G. Storm, “Targeted liposomes for boron neutron capture therapy (BNCT): importance of target receptor density,” in preparation.

A. Roca, S. Nievaart, R.L. Moss, F. Stecher-Rasmussen, “Validating a MCNPX model of Mg(Ar) and TE(TE) ionisation chambers exposed to ⁶⁰Co gamma-rays,” in preparation.

Chapter 1

Introduction

1. General introduction

Boron Neutron Capture Therapy (BNCT) is a form of radiotherapy using neutrons for treating various types of cancer and some other non-malignant diseases. The basics of BNCT will be discussed in the next section followed by two sections describing theory that is important for the three successive chapters. To put the research presented in this thesis in context, a brief description of the history and present status of BNCT is given. This thesis is based on three articles in the field of BNCT published in journals covering the combined field of physics and medicine. Chapters 2, 3 and 4 are written as extended summaries of the articles with some novelties added. The full articles are printed in part II of this thesis. The motives for performing this research are explained in Section 1.2 which ends with the description of the scope of this thesis.

1.1 The basics of BNCT

The basic concept of BNCT is that cancer or other ‘bad’ cells are loaded with the isotope boron-10 (^{10}B) after which the site containing these cells is irradiated with neutrons. ^{10}B and the neutrons are non-toxic. After ^{10}B has captured a neutron, a nuclear reaction takes place and releases two heavy particles, being an alpha particle (^4He) and lithium ion (^7Li). This so-called (n, α) absorption reaction is illustrated in Figure 1.1. According to the energies, the alphas and ^7Li nuclei can be regarded as short ranged particles since they travel less than 10 μm in tissue. This range is similar to the size of a human cell and implies that the heavy particles have a high probability to kill or damage the cancer cell.

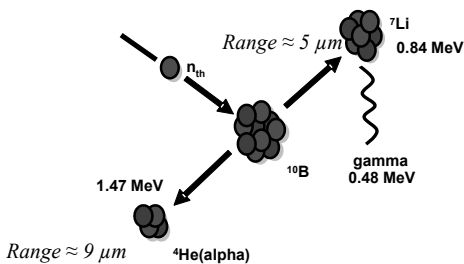


Figure 1.1. Reaction of ^{10}B with low energy neutrons which produce two highly energetic particles. In 96% of these reactions, a gamma ray is also produced.

The cell is killed when the alpha or Li particle causes a double-strand break of the DNA. This occurs when a heavy particle travels through the cell nucleus. The probability of this event together with the probability of having a neutron reacting with a ^{10}B in the first place requires that for successful BNCT the cell is loaded with around 10^9 of ^{10}B atoms [1,2].

In the field of BNCT, often the energy spectrum of the neutrons is classified in 3 parts: Thermal neutrons below 0.5 eV, epithermal neutrons between 0.5 eV and 10 keV and fast neutrons above 10 keV and below 20 MeV. It is for thermal neutrons,

indicated with n_{th} in Figure 1.1, that the probability to react with ^{10}B is high. For thermal neutrons, this probability, known as the microscopic nuclear absorption cross section¹ (σ_a) of ^{10}B is proportional with $1/v$, where v is the velocity of the incoming neutron. For example, the absorption cross section of ^{10}B for 0.025 eV neutrons is 3837 barn and only 6 barn for 10 keV neutrons. However, the neutrons slow down due to interactions with tissue. This means that the starting neutron energy, coming from the source, has to be epithermal or fast in order to become thermal in a deep seated tumour after slowing down.

BNCT is a disease targeted therapy as the neutrons will only kill the cells which are labelled with ^{10}B . Unfortunately, with the presently available ^{10}B administrating compounds, also healthy cells will contain some ^{10}B . Besides this, human tissue contains certain isotopes that react with neutrons as well. These reactions result in a dose given to the healthy tissue which should not exceed a certain limit, called the tolerance dose. These extra dose components will be further explained in the two following sections.

Although the concept of BNCT might look quite simple and despite the fact that it is seven decades after its first proposal, BNCT is still under investigation. So far, as a maximum achievement, only phase I/II² clinical trials are performed with only a relatively low number (a few hundred) of patients involved. After all these years, researchers of various disciplines are still challenged by the two key issues of BNCT: Finding a non-toxic ^{10}B administrating compound, which brings the isotope into the ‘bad’ cells only or at least significantly more than in the healthy tissue and designing a treatment beam which is developed to deliver the optimal neutrons at the right location while minimizing the dose to healthy tissue. This latter issue about finding the BNCT source neutrons with the optimal energy and direction is studied in this thesis. The research took place at the BNCT facility of the Institute for Energy, Joint Research Centre (JRC) of the European Commission in Petten, The Netherlands. The centre’s main target is to lead and participate in so-called scientific networks. For the optimisation of the *neutronics* as performed in this work, the JRC worked together with the section Physics of Nuclear Reactors (PNR) of the Delft University of Technology in The Netherlands.

1.1.1 The four major BNCT dose components in tissue


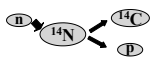
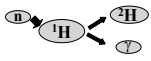
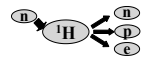
Human tissue consists mainly of hydrogen, oxygen, carbon and nitrogen. By far, most reactions of neutrons are with H and N. Together with the presence of boron in

¹ The microscopic cross section is a measure for the probability of a nuclear reaction for the nucleus and is expressed in *barn* which is 10^{-24}cm^2 [3].

² Most often clinical studies consist of four separate stages. They start from studying the effects of the treatment on healthy tissues (phase I), after which the focus is shifting towards treating the disease (phase II) and come to a scheme to treat the disease optimally (phase III) and ends with registering the treatment (phase IV).

the tissue, the majority of the total physical dose³ considered in BNCT is delivered by H, N and ¹⁰B. Because H has two types of reactions giving a physical dose, the total physical dose in BNCT consists of four components. These two H-related physical doses are described in the last two rows of Table 1.1. Rows 1 and 2 of this table describe the physical doses due to the isotopes ¹⁰B and ¹⁴N, respectively. In the remaining text the ‘physical dose’ is often shortened by writing ‘dose’. As indicated in Table 1.1 in light and dark grey, the first three dose components are related to ‘thermal’ neutron reactions while the fourth dose component is due to reactions with ‘fast’ neutrons.

Table 1.1. Overview of the four major dose components in BNCT.

Physical dose name		Dose* symbol	Reaction type	Scheme	Remarks
Thermal	Boron dose	D_B	n,α		Biological effects in tumour and normal tissue are related to ¹⁰ B micro-distribution
	Thermal neutron dose	D_p	n,p		Induced proton 620 keV
	Induced gamma-ray dose	D_γ	n,γ		Induced γ-rays 2.2 MeV
Fast	Fast neutron dose	D_n	n,n		Energy of recoiling proton is on average half the neutron energy

* According to IAEA Techdoc 1223 [4].

In a block-shaped model of H₂O, see Figure 1.2, in which realistic amounts of N and ¹⁰B are added, is the behaviour of the four dose components as a function of source neutron energy and depth in the model illustrated (see Figures 1.3 to 1.7). Light water with a few mass percent of nitrogen makes a good material to simulate average human tissue. As drawn in Figure 1.2, a spherical tumour (ø 4 cm) is positioned at 4 cm depth and contains 30 ppm of ¹⁰B which is uniformly distributed. The assumption of having a three times higher ¹⁰B-concentration in the tumour than in the healthy surroundings is a realistic ‘average’ [5,6]. The D_B (see definition Table 1.1) as a function of source neutron energy and depth in the phantom is shown in Figure 1.3. The location of the tumour is at all energies clearly visible because of

³ Physical dose is defined as the specific energy deposited around a certain point in a medium due to ionising radiation. It is written in unit Gray with symbol Gy. 1 Gy = 1 J/kg.

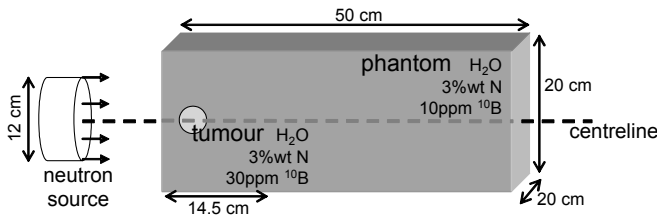


Figure 1.2. Set-up of the block shaped phantom with a tumour irradiated with neutrons.

the three times higher concentration of ¹⁰B and consequently more (n,α)-reactions. This results in the horizontal darker grey band at the full width of the figure. For source neutron energies above 1 eV and below 3 keV, the D_B is significantly higher in the first 2 cm of the tumour. Between 10 keV and 100 keV the boron dose is more uniformly distributed in the whole tumour and is still in high contrast to the healthy surroundings. This is desired. Figures 1.4 and 1.5 show the D_p and D_γ respectively, which look quite similar due to the fact that they are related to thermal neutron reactions as well. At low source neutron energies there are many thermal reactions at shallow depths. For increasing source neutron energy the majority of the thermal reactions occurs somewhat deeper until, above 1 keV, the thermal reactions are

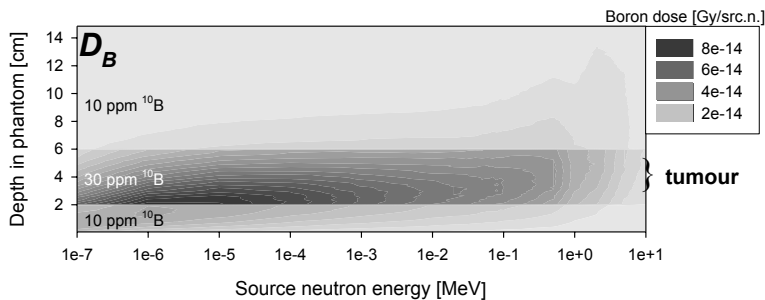


Figure 1.3. Physical boron dose per source neutron as a function of source neutron energy and depth in the light water model with tumour at the centreline.

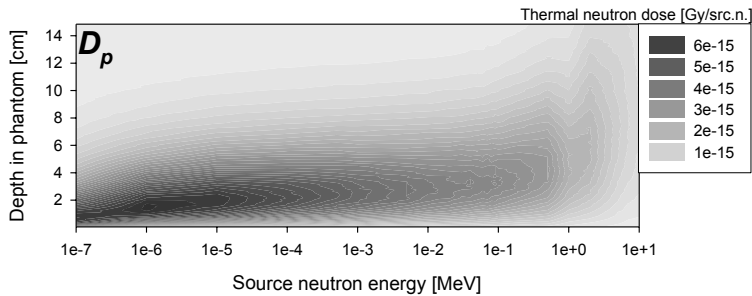


Figure 1.4. As in Figure 1.3 but for the physical thermal neutron dose per source neutron.

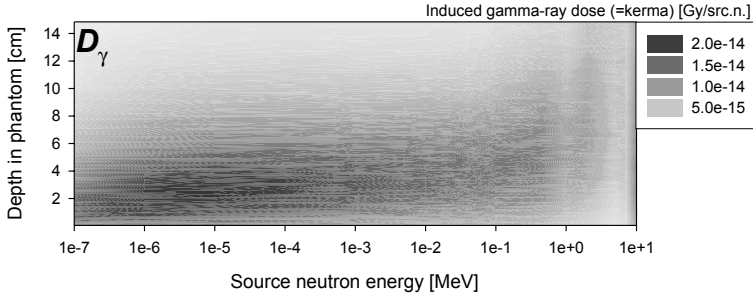


Figure 1.5. As in Figure 1.3 but for the physical gamma dose per source neutron (actually kerma).

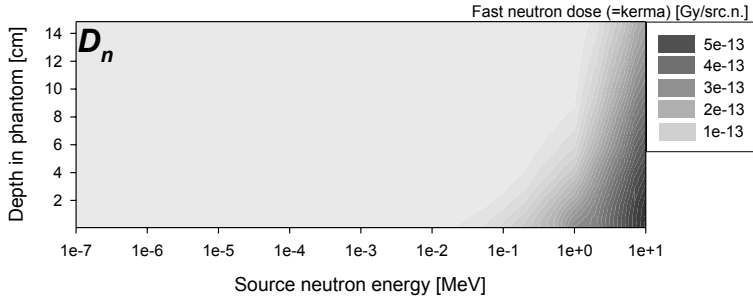


Figure 1.6. As in Figure 1.3 but for the physical fast neutron dose per source neutron (actually kerma).

‘smeared out’ stretching deeper into the phantom. The stripes and ‘folding’ behaviour around 1 MeV is due to resonances in the oxygen neutron cross section data. The typical ‘thermal-reaction’ look is also visible in Figure 1.3 but affected by the presence of the tumour. Figure 1.6 shows the D_n which is completely different from the described thermal dose figures. According to this figure, only for source neutrons above 30 keV, there is a physical fast neutron dose which increases rapidly with neutron energy. It is not visible in Figure 1.6 that D_n is already significant for source neutrons between 1 keV and 30 keV. This dose contribution can not be neglected, compared with the thermal dose components but is only significant superficially at the first 5 to 10 mm of the phantom.

The D_B and D_p presented here are determined by calculating with the Monte Carlo (MC)⁴ code MCNP4C2 from Los Alamos Laboratories [7], the alpha and proton productions, due to the ^{10}B and N respectively. Since these alphas and protons deposit their energy locally, the physical doses result from multiplying the calculated particle production densities with the released energy. The D_γ and D_n are

⁴ Monte Carlo method: Weights of simulated particles are followed when travelling through the geometry. These weights can change due to interactions with the materials. These interactions occur probabilistically and are based on the nuclear cross section data of the materials.

calculated by multiplying the photon and neutron fluxes in MCNP with energy dependent tables of kerma⁵ factors for water taken from ICRU46 [8]. Therefore, the D_γ and D_n are kermas rather than physical doses. Nevertheless, kerma and physical dose are equal in case of a charged particle equilibrium⁶ which is supposed here. Furthermore, a background dose exists due to gamma rays in the BNCT neutron beam. Figure 1.7 depicts the $D_{b\gamma}$ from these ‘beam’ gammas which will be further indicated as $D_{b\gamma}$. For mono-directional source gammas having 24 discrete energies, chosen at logarithmically equal intervals between 1 keV and 20 MeV, the plot indicates a very slowly decreasing dose as a function of depth that is hardly visible. Note that the scale is logarithmic. A typical ratio of source neutrons to source gammas is 20 which is the case at the BNCT facility in Petten.

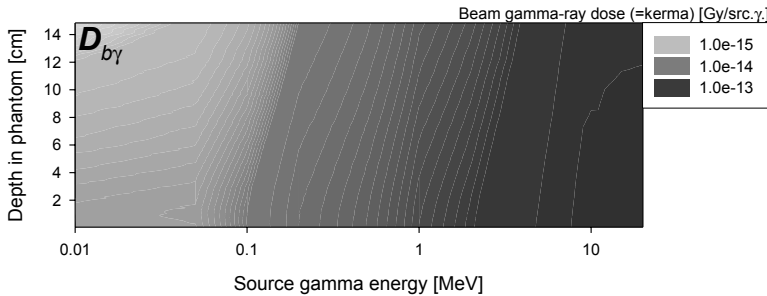


Figure 1.7. Physical gamma dose per source gamma due to (unwanted) gammas already present in the beam as a function of source gamma energy and depth in the light water model.

1.1.2 Biologically weighted doses and ^{10}B compounds

The secondary particles in BNCT, i.e. the alpha particles, protons, recoiling protons and electrons accompanying the D_B , D_p , D_n and D_γ as presented in Table 1.1, deposit their energy differently in the tissue. For example, the energy deposition along the short track of an alpha particle is very dense in comparison with that of an electron of which the track is longer. As a result, the human cells respond biologically differently when irradiated with 1 MeV alpha particles or 1 MeV gammas. This makes that the sum of the different particle energy depositions per unit of mass, the physical doses, has no biological meaning.

Many BNCT investigations aim to establish that the biological effects of D_B , D_p and D_n can be translated into gamma dose equivalents. In this way the four dose components in BNCT can be added and the (total) dose given to the patient at each point in tissue can be described. The reason to translate the doses into gamma dose

⁵ Kerma is defined as the Kinetic Energy Released per unit Mass and consists of the energy that is transferred after the first collision.

⁶ There is charged particle equilibrium when for every charged particle leaving a certain volume in an irradiated medium, another charged particle of the same type, having the same energy and direction, enters the volume.

equivalents comes from the fact that a lot of experience in conventional radiotherapy (using mainly gammas) is gathered in the last century. The translation is performed by multiplying each physical dose component by a biologically weighted factor also known as the Relative Biological Effectiveness (RBE) factor. After addition, the total dose is called the ‘total biologically weighted dose’⁷ having the symbol D_w [4]. Currently, however, after many years of research, the values of these factors are still under discussion. As will be seen in Chapter 2, the RBE factor to ‘translate’ the D_B is replaced by a Compound related Biologically Effectiveness (CBE) factor. This factor embodies the ‘normal’ boron dose related RBE but is corrected for the applied boron compound [5,9]. Up to now, only two boron compounds are approved to be given to patients in clinical BNCT trials. The first drug is Borocaptate Sodium (BSH) and the second Borono-phenylalanine (BPA) of which the chemical structures are shown in Figure 1.8 [10-13]. Due to their respective natures, the distribution of the ^{10}B over the cells and the positioning in the cells, with respect to the cell nucleus, are different. This is taken into account by the CBE factor.

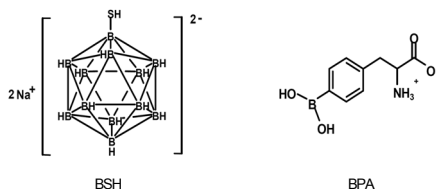


Figure 1.8. Chemical structures of BSH and BPA

1.1.3 Brief history of BNCT

(This section is partly a brief outline taken from section 1.3.2 by Philipp [14]).

The existence of neutrons was proven by Chadwick [15] twelve years after Rutherford had already postulated the existence of these particles in 1920 [16]. In 1936, after ^7Li and alpha particles were detected when ^{10}B reacts with thermal neutrons [17], Locher [18] suggested to apply this phenomenon in radiation therapy. In the early 1940s, Kruger and Zahl et al. [19-22] made some first promising radiobiological experiments in cell-cultures and mice, proving that BNCT worked as suggested. In 1941, it was Zahl et al. [22] who first proposed the use of epithermal neutrons instead of thermal neutrons, whenever humans would be treated in clinical trials. This remark of Zahl et al. about the usage of thermal and/or epithermal neutrons will be shown to play a very important role throughout this thesis.

It was not until 1950s that the first clinical trial on BNCT was started in the United States using thermal source neutrons [23]. At Brookhaven National Laboratory (BNL) and the Massachusetts Institute of Technology (MIT), 10 patients suffering from glioblastoma multiforme (a malignant type of brain tumour), were irradiated after a ^{10}B -enriched borax solution was intravenously given. The overall result, including a further 18 patients treated at MIT in a second protocol in which the skin, cranium and dura were removed, was unsatisfactory and consequently BNCT was

⁷ In Paper I the biological weighted dose, as defined for BNCT according to IAEA-TECDOC-1223, is assumed to be similar to the equivalent dose throughout the whole manuscript.

halted in the US in 1961. It was concluded that thermal neutrons do not penetrate deep enough and the boron compounds used were not very tumour selective [24]. From 1968, in Japan, clinical trials continued with the open-craniotomy procedure, where several intracerebral malignancies were treated. The Japanese professor Hatanaka who had been already involved in a clinical trial in the US, can be regarded as the catalyst of BNCT at that time. Together with other researchers, the Japanese investigated new boron compounds and treated more than 120 patients of whom some survived for a long term [25,26]. This outcome encouraged BNL and MIT to start new BNCT trials in the US in 1994 and 1996, respectively. From then onwards the focus was merely on the use of epithermal neutron beams which are able to penetrate skin and cranium and make removal of these unnecessary. In 1997, a European trial at the High Flux Reactor (HFR) in Petten (the Netherlands) started under the medical supervision of the university hospitals in Amsterdam (NL) and Essen (D), involving glioma patients [27-29]. In 1999 and 2000 respectively, similar clinical trials were started in Finland and Sweden [30,31]. All the trials mentioned so far were performed at nuclear reactors of which the 'medical' reactor at BNL in the US closed in 2000 and the Studsvik reactor in Sweden halted in 2005. In Italy (Pavia), in 2001, a very promising BNCT experiment was initiated by irradiating an explanted liver suffering from (inoperable) diffuse metastases. In 2003, a phase I/II clinical trial on skin melanoma started at a reactor in Argentina. In the same year, in Petten, a new protocol was approved and a phase I/II clinical trial started for patients suffering from melanoma metastases in the brain. This trial is performed in cooperation with the MIT. Reactor based clinical trials are also under investigation in Czech Republic, South-Korea, Taiwan and Russia. Accelerator-based BNCT is being investigated in Birmingham (UK), Italy, Argentina, Russia and in the US.

1.1.4 Present status of BNCT

The overall opinion of BNCT researchers and its critics is that *the* major improvement in BNCT is to be expected from new boron compounds that bring more ^{10}B in the tumour cells. In this respect, the application of liposomes is studied [32,33] which can be seen as bags (\varnothing 50-200nm) carrying a medicine. The liposomes can be programmed to connect only to 'bad' cells after which the medicine is transferred. The Petten BNCT group, in cooperation with the Delft University of Technology and the Universities of Utrecht and Nijmegen, are investigating the treatment of ovarian-carcinoma [34,35] and rheumatoid arthritis (after earlier studies [36,37]) using liposomes filled with BPA [38]. Other ongoing medical and biological studies concern the possibility of mixing the presently registered boron-carriers BSH and BPA [39,40] and the visualisation of the ^{10}B -uptake in cells by special microscopy (e.g. EELS [41]).

After many investigations, a major challenge in BNCT is still the translation of the several dose components into biological equivalents as discussed in section 1.1.2. It is impossible to compare the results among BNCT centres because different weighting factors have been applied or a different concept of dose-description is followed. In this respect, Riley and Binns [42,43] have started inter-comparison measurements using their own detectors and techniques at many BNCT facilities in order to standardize the used beams and enable the comparison of the results of the

treated patients. Promising and related to this issue is the development of a typical BNCT beam dependent radiobiological number which characterises the response of the cells when irradiating with this beam [44,45].

To predict the BNCT dose components as well as the neutron and gamma fluxes in patient treatment planning and experiments, MC based computer simulations are performed. The advantage of MC is the 3D-modelling capability and often the obtained precision in the results when compared with measurements whilst the disadvantage is the rather long calculation time. It is for the first reason (precision) that also physicists in conventional radiotherapy are interested and ‘variance reduction’ investigations to reduce the calculation time are in progress to overcome the MC disadvantage.

The last interesting trend in BNCT to be reported here concerns the disease targeted nature of BNCT which is most valuable when dealing with metastasised diseases. As already mentioned in Section 1.1.3, the treatment of an explanted liver full of metastases resulted in the survival of one of the patients for almost 4 years. This result encouraged many BNCT groups and also the group of Petten/Essen and Delft, to investigate the feasibility of such a project at the HFR in Petten.

1.2 Spectral tailoring for BNCT

As written in section 1.1.3, Zahl et al. was the first to propose the use of epithermal instead of thermal source neutrons. The use of epithermal source neutrons was extensively studied by Fairchild [46,47] at Brookhaven. Mainly epithermal neutrons in the range of 1 eV to 20 keV were shown to be useful for treating deep-seated brain tumours through the intact skull. The many succeeding publications discuss the characteristics of newly designed epithermal beams at the BNCT research centres [48-53]. The focus in these articles is on the application of filter and moderator materials, the shape of the beam assemblies and the quality of the resulting beam. Furthermore, these publications have in common that an existing neutron source is filtered and moderated such that it delivers neutrons in the energy range recommended by Fairchild. Actually, the spectral tailoring for BNCT consists of two parts:

1. *Defining the source neutron energies of the BNCT treatment beam in order to obtain the most ^{10}B absorption reactions in the tumour. In addition, the location, direction and dimensions of the BNCT treatment beam need to be optimised for every individual tumour size and location.*
2. *Developing and constructing the filter with the appropriate materials and obtain the from 1. resulting energies starting with an available source.*

The first part became the main issue of this PhD-research as will be further explained in Section 1.2.2.

As an example, the neutron filter in Petten has been designed and installed to let pass through only epithermal neutrons, whilst at the same time it has to reduce the unwanted photons, coming from the HFR reactor core. The design and used filter materials together with its main ‘treatment’ characteristics are given in Figure 1.9.

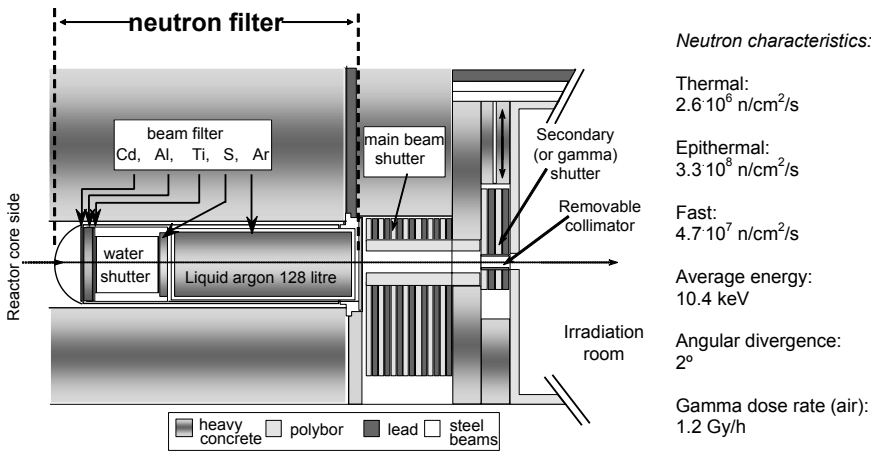


Figure 1.9. The current neutron filter for BNCT at the High Flux Reactor in Petten.

1.2.1 Search for the optimal source neutron energy for BNCT

To the knowledge of the author, there are four publications (Yanch et al. [54,55], Bisceglie et al. [56] and Bleuel et al. [57]) that deal with the tailoring of the source neutrons as described in the last section. These more fundamental investigations are mainly initiated by the development of accelerator-based neutron sources which have the ability to obtain narrow neutron energy spectra that can be varied. The publications have in common that mono-energetic and mono-directional neutrons are simulated using MC and describe the doses and fluxes realised in a phantom. Succinctly, in all these investigations the focus is on deep-seated brain tumours whilst the doses are calculated with a fixed set of CBE/RBE factors. In all these investigations, the simulated neutrons and gammas start from the source after which the resulting effects are calculated in the tumour and healthy tissues.

The publications of Yanch et al. describe the dosimetric properties as a function of discrete neutron energies, beam size, collimation and different phantom shapes. It is reported that only the geometric differences show an influence on the contribution of the individual dose components to the tumour dose. The optimal source neutron energies to treat a tumour at 7 cm depth in tissue are in the range of 4.0 eV to 40.0 keV. Bisceglie et al. conclude that an optimal source neutron energy for BNCT is in the order of a few keV's for deep-seated tumours at 5 cm. Bleuel et al. conclude that neutrons between 2 keV to 20 keV are the most desirable in BNCT.

1.2.2 The scope of this thesis

The Petten BNCT group together with the PNR department in Delft initiated a study to optimise the neutronics component of BNCT. In this respect, an investigation started to search for the optimal source neutron energies and continue the work already performed and described in Section 1.2.1. When taking into account some related challenges (see Section 1.1.4) the BNCT-physicists and medical physicists in conventional radiotherapy are currently facing, this thesis deals with the following issues:

- The influence of the dose weighting factors, and other dose related issues such as the tolerance doses in the tissues and the ^{10}B concentrations, on the optimal source neutron energy in BNCT. This issue is discussed in Chapter 2 that is based on *Paper I*.
- The development and application of adjoint MC calculation techniques. In adjoint MC the simulated particles travel ‘backwards’ which means from the tumour to the source which is the exit of the treatment beam. In realistic scenarios, this approach should be able to provide much faster the information on the optimal origin, direction and energy of the source particles compared with ‘normal’ MC. Chapter 3 and *Paper II* discuss the outcomes in all details.
- The analysis of having the optimal source neutrons not only for deep seated tumours, but also for mid-range and shallow positioned tumours. This is relevant when applying BNCT to cancer metastases which are spread throughout the brain or other organ, such as the liver. Chapter 4 describes a set-up to obtain a homogeneous (to a certain degree) thermal neutron field in a volume that contains a liver, given an epithermal neutron beam. This subject is published in *Paper III*. Chapter 4 describes also a method to obtain with adjoint-like techniques the optimal shape of the liver container and source neutron energy spectrum whenever this spectrum is free to choose.

From the knowledge obtained by studying these issues we may conclude that a ‘variable’ or set of different neutron filter(s) in BNCT would give, in every specific case, an optimal treatment from the neutrons point of view. This is essential knowledge, for designing a ‘new’ filter at the HFR in Petten or elsewhere.

It is often stated that the future of BNCT as a serious treatment relies on the availability of new boron carriers. However, this thesis shows that a better understanding of the BNCT *neutronics* gives a considerable improvement as well.

Chapter 2

Optimal neutrons and dosimetry

2. Optimal source neutrons with regard to dosimetry in BNCT

In this chapter, the optimal source neutron energy in BNCT for brain tumours is investigated as a function of several biological and physical parameters. When investigating the optimal source neutron energy for BNCT one is looking for those source neutrons which cause maximum damage to the cancer cells and ideally none, but practically only a tolerable damage to the healthy cells. For the case concerning irradiation of the human head, different types of cells (tissues) with different tolerance doses are involved. Therefore, in principle, the best source neutrons are not simply the neutrons producing the highest ^{10}B absorption rate in the tumours but the source neutrons giving the most ^{10}B absorption-reactions in the tumour before reaching the tolerance dose in one of the healthy tissues. This requires insight into the ‘dosimetry’ that is based on results coming from radiobiology.

2.1 Background on BNCT dosimetry and radiobiology

The values of the tolerance doses that are currently being used in conventional radiotherapy have been mainly determined empirically by observing the levels of early and late side effects which develop in patients who underwent radiotherapy. The vast amount of data that has been collected during the time since the introduction of radiotherapy stems from treating patients with different fractionation schemes and doses of gamma rays and megavoltage X-rays [58]. The value of the tolerance dose strongly depends on the number of fractions into which the total dose delivered to the patient was divided. Mathematical methods have been developed that allow adjusting the value of the tolerance dose depending on the number of fractions [59]. Another factor which has a profound impact on the level of the tolerance dose is the quality of radiation used for treating the patient. It is well known that the biological effect per unit dose is higher for high LET⁸ radiation as compared to low LET radiation [60]. This is due to the differences in the density of ionisation events inside a cell. While the cellular DNA repair mechanisms can cope with DNA damage that is evenly distributed inside a cell nucleus, multiple damaged sites produced by high LET radiation pose a more serious problem. Hence, at the same level of dose, high LET radiation is more effective in killing cells than low LET radiation. The need for comparing the doses of radiations of different qualities that induced the same level of biological damage triggered the introduction of the relative biological effectiveness – RBE (defined in Chapter 1). RBE values can be determined experimentally in *in vivo* and *in vitro* experiments.

⁸ In radiobiology LET stands for Linear Energy Transfer and is defined as the energy lost by charged particles due to interactions per unit of distance.

The problem with the RBE values is that their level depends on the cell system used for the experiment and the analysed endpoint [61]. Hence, when a new radiotherapy modality is developed, during which high LET radiation will be applied, it is not possible to simply recalculate the tolerance doses for irradiated organs on the basis of RBE values that were determined under laboratory conditions. Hence, no validated methods exist with the help of which the tolerance doses for high LET radiation could be calculated based on the clinical experience with low LET radiation. For ethical reasons it is not possible to determine the tolerance dose by exposing patients to various doses of high LET radiation as was done with X-rays and photons during the early days of radiotherapy [58]. This problem is especially pertinent to such complex radiotherapy modalities as BNCT, where the organs at risk are exposed to a mixed beam of both high and low LET radiations. Despite numerous radiobiological investigations it is not clear whether the effects of both radiation qualities are additive or synergistic [62,63]. In order to circumvent the radiobiological and medical issues described above, the optimal source neutron energy can be determined for a range of *RBE* values. This approach, extended by varying other parameters, such as the ^{10}B concentration, is applied in this chapter. Such an approach is at least a strong indication, as to whether there is a significant influence of the biological and clinical values on the optimal source neutron energy in BNCT and if so, what are these influencing parameters.

2.2 A parameter study for BNCT of the brain

The biological and physical parameters that are varied enclose the *RBE* factors, the ^{10}B concentration, the intensity of the gammas present in the beam and the thickness of skin and cranium. Another parameter that is chosen to vary is the tolerance dose set in skin and brain. All parameter value ranges are discussed in the next section. After setting ranges for these parameters, for every configuration, the optimal source neutron energy is calculated. The optimal source neutron energy allows most of the neutrons to react with ^{10}B present at certain tumour positions under the constraint of not exceeding a pre-set dose limit in healthy tissue.

2.2.1 Set-up and chosen parameter ranges

A cubic phantom is irradiated with neutrons from a 120 mm diameter disc shaped source with 22 discrete neutron energies, logarithmically chosen between 0.1 eV and 1 MeV. The calculations are carried out with the Monte Carlo code MCNP4C2 [7]. The MCNP geometry is shown in Figure 2.1. The neutrons are mono-directional. They first hit a layer of skin, then a layer of cranium before reaching the brain in which the tumours are located at four separate depths. All tissue compositions and densities are as defined in the ICRU46 report [8]. Small MCNP tallies (volume 78.5 mm^3) are located along the beam centre line, at every millimetre, in order to calculate the dose as a function of depth in the phantom. As will be seen in the next section, the dose is also averaged over the whole volume (1.366 litres) of the brain which is represented by the drawn hemisphere in Figure 2.1.

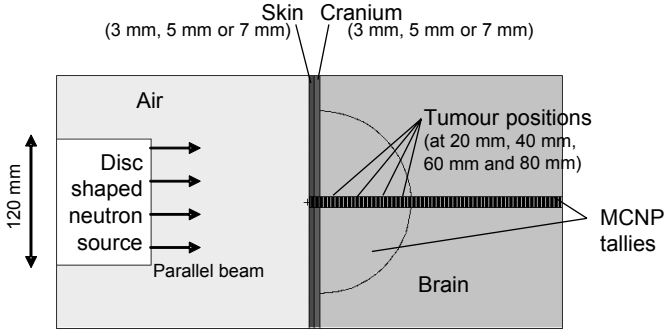


Figure 2.1. Cross section of the MCNP geometry.

The biologically weighted dose⁹ D_w in every tally i in the phantom is determined, as follows:

$$D_w = (C_B \cdot CBE_B \cdot D_B)_i + RBE_p \cdot (D_p)_i + (RBE_n \cdot D_n)_i + RBE_\gamma \cdot (D_\gamma + \lambda_{b\gamma} \cdot D_{b\gamma})_i \quad (2.1)$$

The CBE_B in this equation is the compound adjusted RBE as explained in Section 1.1.2 and the C_B is the concentration of ^{10}B . The D 's represent the absorbed doses for the thermal neutrons (p), the fast neutrons (n) and induced gammas (γ). The absorbed dose¹⁰ for the beam gammas ($b\gamma$) is given per source gamma and therefore has to be corrected with the term $\lambda_{b\gamma}$ which is defined as the ratio of source gammas to source neutrons. The ranges of these parameters are shown in Table 2.1. The ranges are mainly based on the BPA [64] and BSH [65] related treatment protocols used in Petten and on a boron uptake study [66]. Since these protocols are based on current literature, it is of no surprise that these ranges practically include all values used in BNCT literature (see Nigg [67]).

During the MCNP calculation, 10 ppm of ^{10}B is assumed in all tissues. The influence and implications of the boron concentration in the tissues is discussed in section 3.1 of Paper I. After the MCNP calculations, a post-processing program calculates all the different configurations. When combining all parameters in categories III and IV in Table 2.1, there are almost 25 million possible configurations. By ignoring double occurrences, mostly zero values, and obviously deleting physically impossible combinations, the number of possible configurations could be reduced significantly and becomes 4,527,600.

⁹ Notation here is according to IAEA-TECDOC-1223 [4]. In Paper I the used indices are different, e.g. $D_w = H$ (see Footnote 1), $D_B = D_{10B}$, $D_p = D_N$ and $D_n = D_H$.

¹⁰ The absorbed dose is also known as the physical dose.

Table 2.1. All varied parameters in this study categorized with their values, ranges and/or step sizes.

I. Thickness of skin and cranium					
Skin–Cranium [mm]: 3-3, 5-5 and 7-7					
II. Tolerance dose ratios					
$\frac{\text{skin}(\text{point}^*)}{\text{brain}(\text{point}^*)} = \frac{1}{5}, \frac{1}{3}, 1, 3 \text{ or } 5$					
$\frac{\text{skin}(\text{point}^*)}{\text{brain}(\text{volume})} = \frac{1}{5}, \frac{1}{3}, 1, 3 \text{ or } 5$					
III. Relative biological effectiveness factors and boron concentrations					
	C_B [ppm]	CBE_B [-]	RBE_p [-]	RBE_n [-]**	RBE_γ [-]
Skin	0-80 step 10	0-4 step 1	1-5 step 1	1-6 step 1	0.5-1 step 0.5
Cranium	0-20 step 10	0-2 step 1		1-6 step 1	
Brain	0-30 step 10	0-2 step 1		1-6 step 1	
IV. Beam gammas					
Source gamma energy [MeV]: 1, 5 and 10					
Number of source gammas on every source neutron (λ_{by}) [-]: 0, 1/20 and 1/10					

*) Point is defined as tally volume of 78.5 mm³

**) The RBE_n cannot exceed its previous tissue value [68].

2.2.2 The influence of parameter biasing on the results

One of the major problems when interpreting the results of this study is the presence of some parameter values a reader regards as unrealistic. The problem is that the optimal source neutron energies resulting from the ‘unwanted’ parameter value(s) cannot be recognized. It is simply impossible to produce a graph that shows the outcome of every single configuration, as every parameter needs a dimension. A solution to this problem can only be obtained interactively: first record the outcomes of all 4,527,600 configurations into a data file and after the user has selected the parameter value ranges of interest, the results are collected, processed and presented. Furthermore, due to physical and other criteria by which the parameter values are selected, not every parameter value is equally represented in the total result. This can be regarded as biasing. For example (see Table 3 in Paper I) a RBE_n ($=RBE_H$) value in skin of 6 is present in 38% of all configurations. Again the outcomes of such a parameter value cannot be ‘recognized’ in the presented results. The interactive solution proposed above is necessary to accomplish this.

To re-cap, the main interest of this study is to investigate the role of each parameter and its value for all settings.

2.2.3 Results: the optimal source neutron energy

The percentage of parameter configurations resulting in a certain optimal source neutron energy when treating tumours between 20 mm and 80 mm from the skin, under the constraint that the allowed tolerance dose in skin is three times higher than in the volume of the brain is represented in Figure 2.2. This tolerance dose ratio is comparable with the ratio as described in the EORTC protocol on ‘metastatic malignant melanoma in the brain’ [64] that prescribes not to exceed a biologically weighted dose of 22 Gy in a point in the skin and 7 Gy averaged in the brain. In Figure 2.2, the skin and cranium thicknesses are 3 mm (further referred to as the ‘3 mm phantom’).

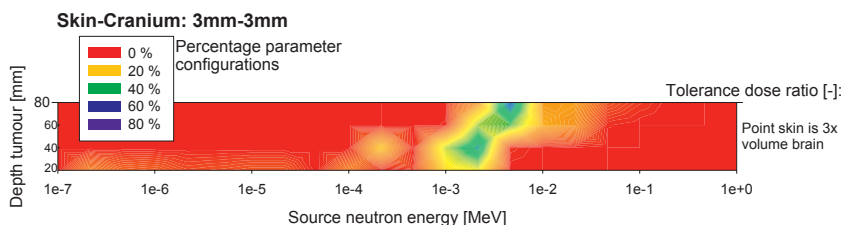


Figure 2.2. Percentage of parameter configurations resulting in a certain optimal source neutron energy as function of one tolerance dose ratio in the 3 mm phantom. The vertical axis displays the location of the tumour.

Note that Figure 2.2 is an interpolated contour plot over 22×4 grid points; 22 discrete energies on the horizontal axis times 4 depths of the tumour. It can be seen that for tumours at 20 mm depth, roughly 30% (yellow) of the configurations prescribe 1 keV source neutrons and another 40% result in 2 keV.

Although it is difficult to see in Figure 2.2, for the same depth, approximately 20% (orange) of the configurations result in 0.2 eV source neutrons. Overall, for all tumour depths the majority of the configurations prefer source neutron energies between 1 keV and 10 keV. For all ten tolerance dose ratios studied, for the 3 mm phantom, the percentage configurations with certain optimal source neutron energies are presented in Figure 2.3. The graph is an interpolation over $22 \times 10 \times 4$ grid points (energies \times tolerance ratios \times tumour depths). The results for the 5 mm and 7 mm phantoms are shown in Figures 2.4 and 2.5, respectively. Some obvious trends noticeable in Figures 2.3 to 2.5 are mentioned here and are explained further in the next section.

- The differences between the Figures 2.3 to 2.5 show that there is an influence of the skin and cranium thicknesses on the optimal source neutron results.
- The tolerance dose ratios show an influence. For every phantom, whenever the tolerance dose in skin is below or equal to the tolerance dose in brain, the same ‘image’ is obtained. The other tolerance ratios can be further classified according to ‘point’ brain or ‘volume’ brain.
- Despite the skin and cranium thicknesses, the tumours at 40 mm and 60 mm depth result mostly in 2 keV and 4 keV source neutrons, whatever phantom, whilst the tumour at 80 mm ‘needs’ source neutrons with higher energies when the skin and cranium becomes thicker.

- For the tumour at 20 mm depth, the majority of the configurations prefer lower source neutron energies whenever the skin and cranium become thicker.

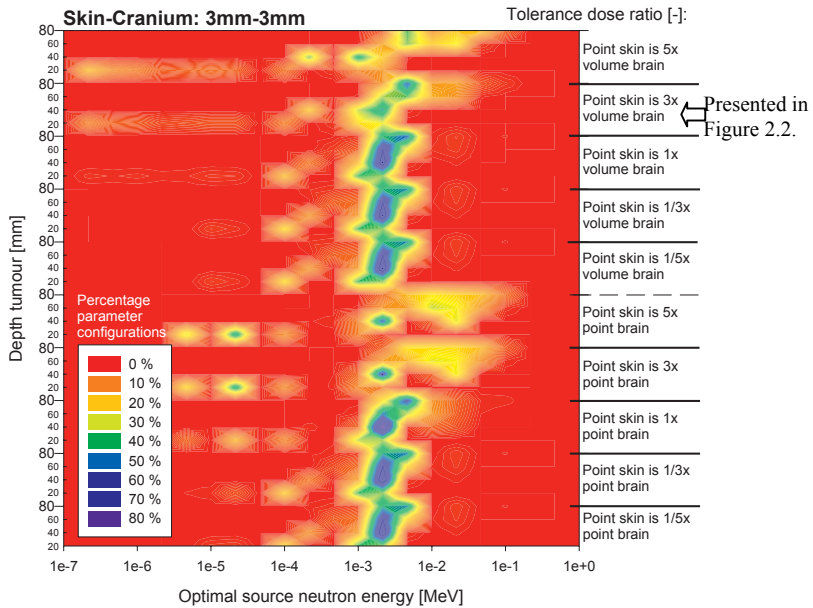


Figure 2.3. As in Figure 2.2 but for all the ten studied tolerance dose ratios (3 mm phantom).

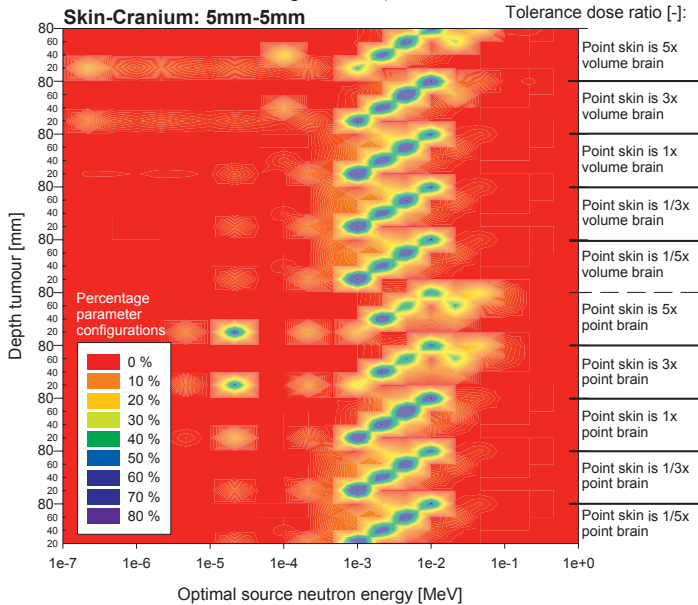


Figure 2.4. As in Figure 2.3, but for the 5 mm phantom.

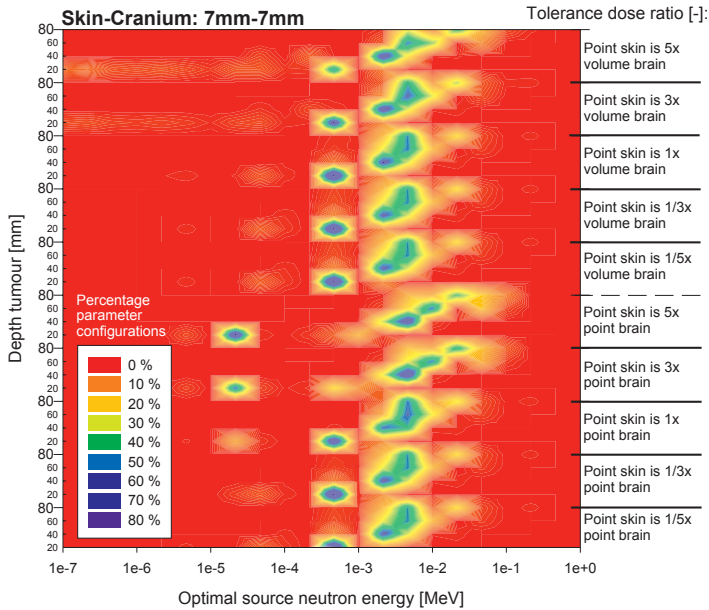


Figure 2.5. As in Figure 2.3, but for the 7 mm phantom.

2.2.4 Results: the influencing parameters

In the following, the influencing parameters are discussed in the order as presented in Table 2.1.

Category I: *Thickness of skin and cranium*

The thickness of the skin and cranium has a significant influence on the optimal source neutron energy results for the shallowest and deepest seated tumours. A transition can be seen when comparing the Figures 2.3 to 2.5.

In the case of the shallow seated tumour (at 20 mm depth), with increasing skin and cranium thickness, the majority of the optimal source neutron energies ‘moves’ from 2 keV and some 100 eV towards 1 keV and finally to 500 eV for the 7 mm phantom. The explanation for this transition is given with the help of Figure 2.6 which shows the ratios of the thermal neutron flux in the tumour located at 20 mm to the maximum flux in skin for the three studied thicknesses. The lowest curve represents the ratio of the flux in the tumour to the maximum in brain. The higher the value of the ratios, the more thermal neutrons are in the tumour than in skin or brain. This is preferable. At first sight, source neutrons greater than 100 keV are optimal but, regarding the fast neutron dose due to recoiling protons as shown in Figure 1.6 in Chapter 1, appear unusable. Furthermore, the brain-result in Figure 2.6 is slightly curved between 0.1 eV and 10 keV with a maximum around 100 eV. The skin curves become steeper with decreasing skin thickness. As a result, it seems that the skin curves prescribe ‘higher’ source neutron energies whilst the brain curve prescribes ‘lower’ energies. Consequently, there is more profit using source neutrons with higher energies with decreasing skin thickness. For the deepest seated tumour

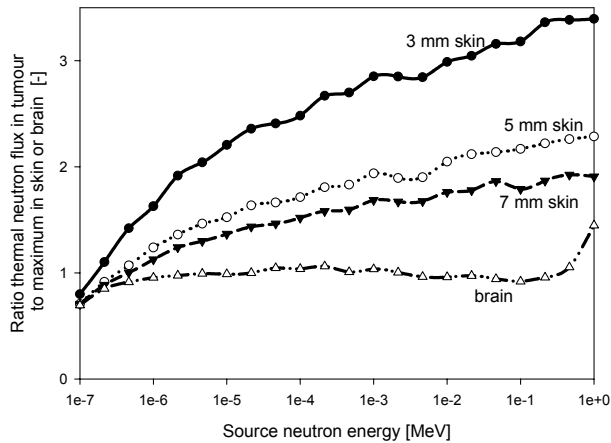


Figure 2.6. This graph belongs to the explanation given in the text for the relation between skin-cranium thicknesses and the optimal source neutron energy for shallow seated tumours.

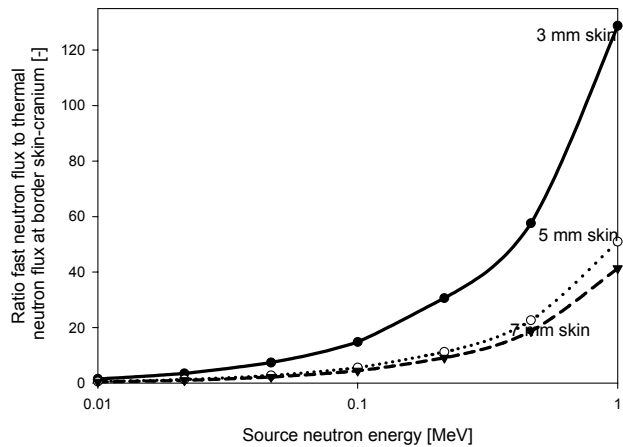


Figure 2.7. This graph belongs to the explanation given in the text for the relation between skin-cranium thicknesses and the optimal source neutron energy for deep seated tumours.

at 80 mm, a transition towards higher optimal source neutron energies is observed from 5 keV via 10 keV towards 20 keV (see Figures 2.3 to 2.5). The basic mechanisms causing this dependence on skin thickness is explained with Figure 2.7. Figure 2.7 shows the ratios of the fast neutron flux to the thermal neutron flux for the three skin thicknesses at the border between skin and cranium. The lower this

ratio the better and thus lower source neutron energies are preferable. The opposite effect is caused by that the number of thermal neutrons in the deepest seated tumour increases with increasing source neutron energy (see Figure 1.3 in Chapter 1). Although, the higher the energy of the source neutrons the better, the 3 mm skin curve is limited by a more quickly increasing fast neutron component in the skin than the other skin thicknesses. This explains the relation between the increasing energy of the optimal source neutrons and increasing skin thickness.

Category II: *Tolerance dose ratios*

An important outcome of this parameter study is that the optimal source neutron energy as a function of parameter variations shows clear dependence on the chosen tolerance dose in skin and brain (see Figures 2.3 to 2.5). Three groups, distinguished by having similar characteristics in the results, can be identified according to the tolerance ratios:

*Group 1, in which the tolerance dose in a point in the skin is lower than or equal to the tolerance dose in a point in the brain and also over the total volume of the brain. For this group the skin turns out to be the treatment limiting tissue.

*Group 2, which has a higher tolerance dose in a point in the skin than in a point in the brain. The brain turns out to be the treatment limiting tissue in the majority of the cases.

*Group 3, is the same as Group 2, except that the tolerance dose in brain is set over the whole volume of the brain, then both the skin as well as the brain can be the treatment limiting tissue.

Category III: *Relative biological effectiveness factors and boron concentrations*

According to Table 5 in Paper I, it is clear which parameters are of direct influence on the optimal source neutron energy; i.e. C_B , CBE_B and the RBE_n . For Group 1, by far, all dose limits are reached in skin at the interface with cranium. Furthermore, in the case of Group 2, the C_B and CBE_B for brain tissue and the RBE_n for all tissues are the influencing parameters. In recording the location of where the tolerance dose is exceeded, most positions are at the thermal neutron fluence peak between 20 mm and 40 mm. Finally, in the case of Group 3, a mixture of C_B and CBE_B for both skin and brain tissue and the RBE_n for all tissues, are the influencing parameters.

Category IV: *Beam gammas*

For all phantom dimensions, there is an influence notable for tumours at 20 mm and 40 mm for Groups 2 and 3. For the higher values of the gamma related parameters, the optimal source energies tend to lower energies.

2.2.5 Results: Improvements when using the optimal source neutrons

Following the above results concerning which source neutron energy ensures the maximum alpha production in the tumour, a logical follow-up question is: is it necessary to provide all these 22 source neutron energies? To investigate this, the number of alphas generated by the optimal neutrons is compared with the number of alphas as produced by each of the 22 source neutron energies as described in section 2.2.1. To clarify this, as an example, the alpha productions in the tumours obtained

with the optimal source neutron energies are compared with the alpha productions resulting from using only 10 keV source neutrons. This is done for all the 4,527,600 configurations. The improvements in alpha production when one could select in every configuration the optimal source neutron energy instead of only 10 keV source neutrons, is shown in Figure 2.8 for the 5 mm phantom. The percentage of alphas in the tumours that are produced *more* with the optimal source neutrons than with the 10 keV source neutrons, goes up to 400%. In other words: for a specific parameter setting (configuration) the optimal source neutron energy is 5 times better.

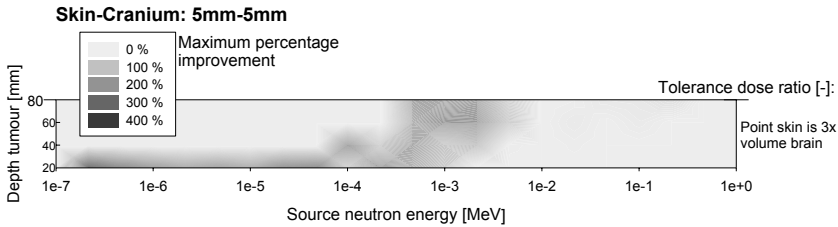


Figure 2.8. Maximum percentage improvement of the number of alphas produced with the optimal source neutron energy in comparison with the number of alphas produced with 10 keV source neutrons for one tolerance ratio (5 mm phantom).

All the percentages presented in Figure 2.8 are taken for the configurations where this improvement in alpha production is a maximum. As mentioned in Paper I, graphs like Figure 2.8 show a dependency with the tolerance ratio but then there is no significant difference concerning these graphs for the 3 mm and 7 mm phantoms. In Figure 2.8, for this particular ‘400% improvement’ case, the use of 0.2 eV source neutrons for superficially located tumours becomes a reality when dealing with very low ^{10}B related parameter values in skin (see further Table 5 in Paper I). The same article predicts that besides using 10 keV source neutrons, the availability of source neutrons with energies in the order of tens of eV will cover all configurations and assure the best alpha production possible in BNCT. In how far this prediction is true was investigated after the publication of Paper I. The results are presented here.

All possible pair-configurations out of the above mentioned 22 source neutron energy results are investigated. For example, the outcomes of the maximum improvement when using the optimal source neutron energies instead of only 0.1 eV source neutrons is combined with the results of the 2 keV source neutrons. For every pair of source neutron energies the smallest improvement values are collected. It turns out that the availability of 500 eV and 10 keV source neutrons provide the smallest difference in alpha production compared with the optimal source neutrons. However, the ‘maximum’ improvement when these 500 eV and 10 keV source neutrons are available is still 50%, for a certain parameter setting. The outcome of an attempt to minimise the maximum improvement even further is shown Figure 2.9. When 3 beams with three different source neutron energies can be chosen out of the 22 studied source neutron energies, it turns out that the best set consists of 5 eV, 500 eV and again 10 keV. With this trio the maximum improvement of having all 22 source neutron energies available is only 28%.

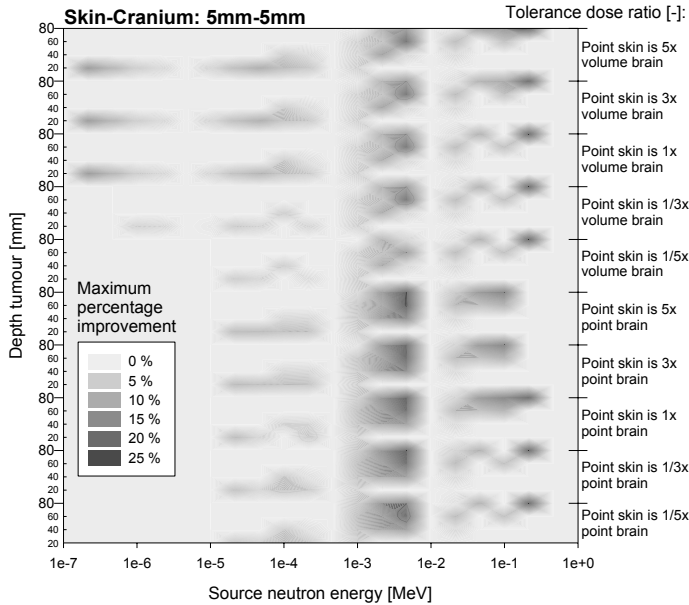


Figure 2.9. With the availability of source neutrons of 5 eV, 500 eV and 10 keV only a maximum improvement of 28% in alpha production would be achieved when using the optimal source neutron energy.

2.3 Conclusions

The optimal source neutron energy delivers a maximum of alphas in the tumour, while not exceeding tolerance dose constraints. It turns out that the definition of these tissue dependent tolerance doses greatly influence the source energy making a neutron ‘optimal’. The results presented in Figures 2.3 to 2.5 indicate that according to the ratio of the tolerance dose set in skin to brain three groups can be distinguished. The thickness of skin and cranium affects also the choice of which source neutrons are better to use. The parameters of influence are the ^{10}B concentration (C_B), the boron related CBE and the RBE for fast neutrons. It turns out that the tissue in which the tolerance dose is reached first determines the parameters causing the major deviation in the source neutron energies. Future studies will involve the field size of the beam and the influence of the shape of the phantom. Also the possibility to process user-defined ranges of the parameter values on-line, by using an interactive program, is necessary to continue and control the discussed parameter biasing.

Another important conclusion from the alpha production improvement results (see Figure 2.9), is that the availability of 5 eV, 500 eV and 10 keV source neutrons would improve the treatment plans (in this study) enormously. In this studied brain case, the nuclear physicist and/or treatment planner in BNCT could deliver, no matter what the circumstances or parameter settings, most of the alphas at the tumour location.

Chapter 3

Adjoint techniques in BNCT

3. Application of adjoint Monte Carlo techniques in BNCT

In specific cases, adjoint Monte Carlo (MC) calculations can provide the optimum setting to the treatment planner giving shorter calculation times compared with ‘normal’ forward MC. However, the adjoint method in its standard form is not applicable when dealing with mono-directional treatment beams as in BNCT. In this chapter, techniques are developed to overcome this problem and the method is demonstrated in a specific example.

3.1 Background, theory and MCNP

In reactor physics, an equation can be defined that is adjoint to the neutron transport equation. With the proper adjoint source the solutions of this adjoint equation can be physically defined as a measure of the “importance” of a neutron in contributing to the response of the detector [69]. In the field of irradiating materials, e.g. phantoms and patients, it can simply provide at defined locations (points, areas, volumes) the expected detector contribution of source particles, as a function of energy, position and starting angle. These ‘detectors’ can be tumours or organs at risk (OAR), which together, will be further mentioned as regions of interest (ROI).

In MCNP [7] the adjoint equation is solved by tracing histories ‘backward’; the normal MC method is reversed and the adjoint particle obtains after an event the energy and angle that a forward particle would normally have before this event. As stated in the manual, MCNP in forward (=normal or standard) mode is preferable when the detector volume or area is large. The adjoint mode is interesting when the detector volume or area is small but the source volume or area is large. Because the histories start in this small detector area and are traced ‘backward’, they will have a higher probability to contribute to the larger phase space region of the source¹¹. In principle, regarding the statistics, the more particles contribute to the estimate under investigation, the smaller the variance becomes. A good description of adjoint MC is given in Wagner et al. [70] and Hoogenboom [71].

An important result, as derived in Bell and Glasstone [69], is the relation between the ‘forward’ flux and the adjoint function, ϕ and ϕ^+ respectively. The total detector response, depending on the detector response function Σ_d is the integral at the right hand side of

$$\int Q(r, \Omega, E) \phi^+(r, \Omega, E) dV d\Omega dE = \int \Sigma_d(r, \Omega, E) \phi(r, \Omega, E) dV d\Omega dE \quad (3.1)$$

¹¹ In adjoint MC the forward source becomes the adjoint detector and forward detector becomes the adjoint source

in which r is the position, Ω the solid angle, E the energy and V the volume. This integral is taken over all phase-space variables and provides the same result as the integral of ϕ^+ multiplied with the source function Q . In other words: knowing the adjoint function and source function of a treatment beam enables to determine e.g. the total detector response of the flux, dose or reaction rate inside a certain area, as similarly obtained with a forward calculation.

As written in the manual, MCNP has an option called ‘SCX’ which enables to register at the detector the initial energy of the particle emitted by the source. Regardless of the mode in which MCNP is running (forward or adjoint), four possible outcomes can be gathered. These, sometimes confusing possibilities, are listed in Table 3.1.

Table 3.1. Overview MCNP modes.

MCNP mode / Particles start at source:	Obtained at detector:
Forward	Total detector response
Forward+SCX	Expected contribution of forward source particles to the forward detector response (=numerically proportional to the adjoint function)
Adjoint	Adjoint function
Adjoint+SCX	Expected contribution of adjoint source particles to the adjoint detector response (=numerically proportional to the total detector response)

Because MCNP normalizes every source description automatically, this means in BNCT that the results of the adjoint calculation are normalized to the tumour (adjoint source) instead of the neutron beam (forward source). A proper normalization is necessary as one is interested in ‘per-particle-results’ related to the real source. Although the re-normalization of the adjoint results can be derived analytically, the ‘SCX’ option provides an additional check. The normalization of adjoint results is discussed in the report by Wagner et al. [70] and also Difilippo [72].

3.2 General adjoint set-up for BNCT

In BNCT, to know the contribution of source neutrons to a reaction rate in the tumour, the adjoint source spectrum should be similar to the (n, α) capture cross section of ^{10}B . Most of the organs at risk, as defined in, for example, the melanoma metastasis of the brain protocol, are in deeper lying structures which will only suffer from the dose given by the thermal reactions. In theory, a well defined adjoint source energy spectrum should be similar to the (n, α), (n,p) and (n, γ) cross sections of ^{10}B , ^{14}N and ^1H , respectively, depending on the reaction rate of interest. These cross sections have in common that the probability to have a reaction at thermal neutron energies is orders of magnitude higher than for high energies. In practice, in

BNCT, calculating the thermal neutron flux will provide a good first estimate of how the thermal neutron related doses in the phantom will behave (see Chapter 1). In the following, the adjoint source spectrum as well as the forward detector response function are taken to be thermal and defined uniform up to 0.5 eV.

Most of the fast neutron dose is delivered at the outside in the first few centimetres of the tissue. Because the interaction of the beam-particles always starts in the skin, the fast neutron dose component can be regarded as uniform and needs only to be estimated at one location. Note that when dealing with the fast neutrons in the adjoint approach, it is difficult or maybe even impossible, as the skin will form a large adjoint source.

For all calculations presented in this chapter, a new 172 group neutron cross section library is made, according to the XMAS energy structure. All cross section tables, for nuclides present in human tissue used in BNCT, are based on JEF2.2 evaluations for 37°C and with $S(\alpha,\beta)$ thermal treatment.

3.3 Adjoint treatment planning with a mono-directional beam

Nowadays, most investigations in treatment planning focus on decreasing the computational time to obtain the doses without making concessions on the accuracy [73-75]. When less time is needed for the dose calculations, simply more time is available for optimization of a treatment plan. There are mainly three algorithms used in treatment planning to calculate the dose which are the convolution/superposition method, the pencil beam method and the MC method. The first two mentioned methods are widely applied in treatment planning and can be characterized as being fast but less accurate compared with the MC method which is accurate but needs more calculation time. Acceleration of Monte Carlo calculations by variance reduction techniques is also of great interest and is investigated in a wide area of research. Especially in treatment planning, Monte Carlo provides more accurately calculated dose rates in the heterogeneous human tissues [76,77] than with the other methods. However, the current long calculation times prevent that the MC methods can be applied for every single beam configuration for every patient.

In comparison with the above mentioned investigations, far less articles have been published in the field of adjoint MC as used in treatment planning. The existing articles [72, 78-81] all deal with gammas and it is only in the work of Lilly [82] in which the adjoint method is related to BNCT. However, Lilly uses a discrete ordinate radiation transport code to optimize a neutron filter for BNCT.

Since BNCT is worldwide still in a clinical trial phase, relatively, not many patients are treated. As a consequence, little experience exists in positioning neutron beams and making treatment plans for various locations and positions of the cancer. In this chapter, we will show that the adjoint MC technique can be an improvement for BNCT and can help the treatment planner in selecting optimum beam settings.

In the published adjoint articles mentioned above, two approaches concerning the adjoint detectors can be distinguished:

1. The adjoint detectors are formed by segmentation of a sphere or cylinder surrounding the irradiated geometry. All adjoint particles are tallied in the angular and energy bins for each segment.

2. The adjoint detectors are shaped according to the beam exit of the treatment beam. Only adjoint particles resembling the characteristics of the treatment beam, e.g. energy and angle, are tallied in the appropriate bins.

If the interest is to know the delivered dose or reaction rate of a treatment beam to a certain ROI, the first approach would be ideal if the segments are very small and the bin structure very fine. Knowing this (almost) continuous adjoint function for the phase space coordinates around the geometry, the treatment beam could be positioned everywhere and directed freely. However, to obtain reasonable statistics the segments and binning have to be coarse, as such the response of a treatment beam cannot be obtained. Nevertheless, this is useful as a way to obtain a first impression of the directions that are interesting to irradiate from [78].

The second approach delivers, together with the appropriate source function Q (see equation 3.1), the same total detector response as a forward MC calculation. However, a major drawback of this approach is that only adjoint particles at the adjoint detector can contribute with flight directions and energies in the ranges of the treatment beam; e.g. a 2 degree angular divergence requires adjoint particles arriving at the detector within an angle of 2 degrees with the normal of the adjoint detector plane. The probability that adjoint MC particles arrive at the adjoint detector within certain (narrow) boundary conditions is small and it will take a long calculation time before good statistics are obtained. As a result, the adjoint MC approach seems inapplicable for performing BNCT with a mono-directional neutron beam. To overcome this, two techniques are developed which will be discussed in the next sections.

3.3.1 Adjoint Point Detector Technique (APDT)

Since the probability that particles will traverse a plane detector perpendicularly within a narrow solid angle is very small, one has to ‘force’ them. In MCNP this ‘forcing’ technique is called DXTRAN; at every event the contribution a particle will have to a certain specified region is calculated deterministically. DXTRAN can be used in forward and adjoint mode. This specified region can be defined as a point and by positioning this point far away from the geometry and surrounding it by a beam-shaped body, a situation as depicted in Figure 3.1 arises.

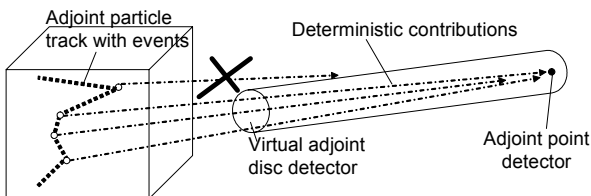


Figure 3.1. Adjoint Point Detector Technique (APDT).

For a disc shaped beam opening, the adjoint point detector is surrounded by a cylinder. As can be seen in Figure 3.1, all contributions to the adjoint point detector pass the entrance of the cylinder (almost) perpendicularly, while all others are “killed”. This entrance behaves as a virtual disc shaped adjoint detector. The further

away the adjoint point detector is positioned the more perpendicular the contributions traverse the entrance. In order to prevent angular spreading in the example discussed in section 3.4, the distance from the centre of the irradiated phantom to the beam exit (=adjoint detector disc) is chosen to be 10^4 cm. This value depends on the size of the phantom and the size of the beam exit. The normalisation factor for this adjoint technique is provided in Appendix A. As there is a possibility for a score at the adjoint point detector for every event, the relative error decreases more quickly, as compared with the analogue MCNP. A disadvantage of the technique is when a lot of particle events are involved of which many will not contribute to the point detector because these contributions ‘travel’ through the region outside the beam-shaped body (see Figure 3.1) and a lot of CPU time is wasted. Many particle events are caused by e.g. highly scattering materials and large geometric dimensions.

3.3.2 Legendre EXpansion Technique (LEXT)

The second technique to determine the adjoint function for the direction perpendicular to the adjoint detector is by use of the Functional Expansion Technique (FET). Suppose that the angular adjoint function at a certain adjoint detector for a certain energy group looks like the 2D function $f(\alpha, \beta)$ plotted in Figure 3.2. When this function behaves well, it can be expressed by

$$f(\alpha, \beta) = \sum_{l=0}^{\infty} \sum_{m=0}^{\infty} d_{l,m} \psi_l(\alpha) \psi_m(\beta) \quad (3.2)$$

in which $d_{l,m}$ are coefficients and $\psi_{l,m}$ are orthonormal basis functions. It is in the work of Beers and Pine [83] that this so-called FET is applied in MC. They accomplished that all samples contribute to the estimates of the coefficients $d_{l,m}$. This can be proven, for example, for one dimension (d_l) by combining the definition

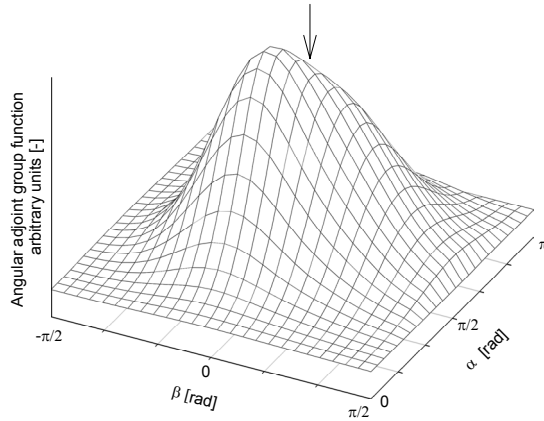


Figure 3.2. Example of an angular adjoint function in 2D at an adjoint detector for one energy group.

for the total detector response and the scalar product describing the coefficients (equation 8 and 9 in Paper II),

$$d_l = \int f(\alpha)\psi_l(\alpha)d\alpha \approx \frac{1}{N} \sum_{i=1}^N w_i \psi_l(\alpha) \quad (3.3)$$

in which N is the number of samples and w is the statistical weight. For the two dimensions (α, β) , both accompanying coefficients $d_{l,m}$ can be evaluated from N . The indices l and m have to be truncated by values of L and M such that the function f is still well approximated by the sums of the products of d and ψ . In any case, L and M should be high enough for a converged result but not too high because of the increasing relative error for every extra coefficient used. Note that there is a direct relation among the number of samples, number of used coefficients, the convergence of the result and its relative error. This relation should be investigated once for every geometric model and problem set-up (e.g. detector size, number of energy bins, material characteristics). This may be regarded as a disadvantage of the technique.

In this work it is chosen that the orthonormal basis functions are the Legendre polynomials: Legendre EXpansion Technique (LEXT). At this stage it is not well known how angular adjoint functions in different circumstances (e.g. other geometries and particle types) will look like. Therefore, investigating other base functions which describe the adjoint functions better in particular cases is expected to be subject of future studies. The Legendre polynomials are orthogonal at $(-1,1)$ and have the best pointwise convergence properties near the centre of this interval [84,85]. As a consequence, since the interest is in the normal direction, α and β have to be chosen such that the normal falls in the centre of their ranges (see the arrow in Figure 3.2). The parameterisation in Figure 3.2 is as chosen and described in Paper II. Actually, α and β are the angles which describe the directions of the adjoint particles traversing the adjoint detector and can be defined in many ways as long as the normal directions fall at the centres of the intervals. Note that the adjoint particle can cross the adjoint detector from one side only. In this parameterisation the ranges of $[-\pi/2, \pi/2]$ and $[0, \pi]$ will be linearly scaled into the Legendre range of $[-1,1]$. Functions f with steep gradients and/or zero values demand extra coefficients to describe these characteristics properly. The use of too many coefficients should be prevented and can be accomplished by truncating the angles (see Section II.F of Paper II).

Before the Legendre technique is applied, all adjoint particles will be recorded in a so-called PTRAC file written by MCNP, on a sphere surrounding the geometry. With the recorded position and flight direction information it can be determined whether an adjoint particle traversed a certain area. In a post processing program these areas can be mathematically described with a shape resembling the neutron beam exit (=adjoint detector). The number, positions and orientations of these adjoint detectors are free to choose in the post-processing program and no new MCNP calculation has to be done. As described in Paper II the weight of every adjoint particle traversing an adjoint detector is recalculated directly with the LE XT to provide its weight if it was flying in the normal direction. After this ‘weight-

adaptation' the average and relative error are calculated like in a normal tally result of MCNP.

3.4 Example: Optimum characteristics in the irradiation of a human head

The APDT and LEXT are demonstrated by calculating the total detector responses of the fluxes due to thermal neutrons and gammas¹² in 10 randomly distributed tumours and 10 OAR (in total 20 adjoint sources) in a patient suffering from brain cancer. The MCNP geometry of the patient's head is shown in Figure 3.3, as created by the program Sabrina [86]. The OAR are defined as written in the protocol in Petten used to treat metastatic malignant melanoma in the brain [64]. CT-images of the head of a patient are translated, using Scan2MCNP [87], into a MCNP geometry consisting of 47520 voxels. Each voxel can be filled with either brain tissue, soft tissue, cranium or mixtures of these.

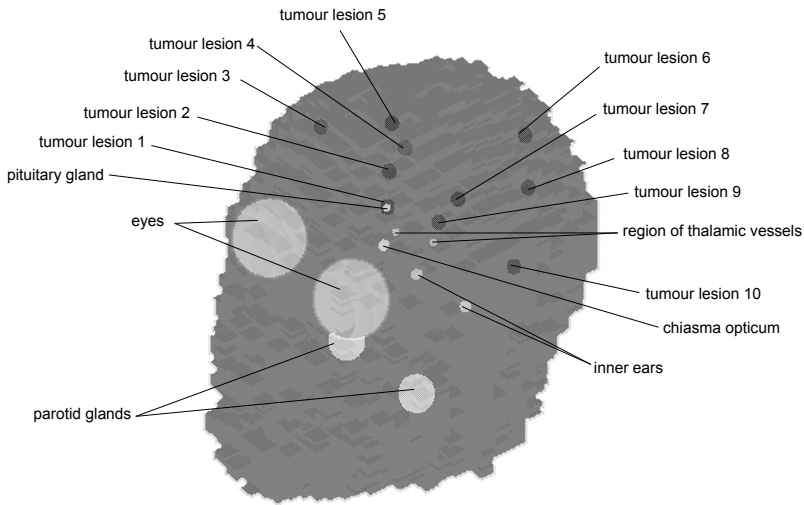


Figure 3.3. Phantom head with 10 OAR and 10 tumours which is used as an example throughout this section.

The model is surrounded by air. Figure 3.4a shows the head phantom surrounded by 60 centre points where all adjoint detector discs are positioned. These centre points are described in azimuthal and polar angles as shown for one adjoint detector disc in Figure 3.4b. At each of the 60 positions, 17 discs with different, systematically chosen orientations of their outer normals (pointing away from the phantom) are positioned. See Figure 3.4c.

¹² In the remaining text shortened as 'thermal neutron flux' and 'gamma flux'

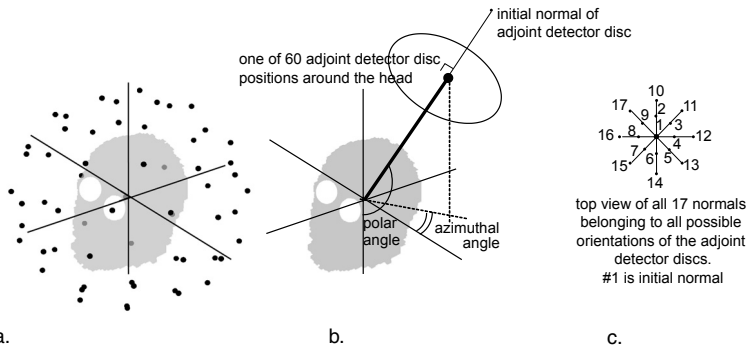


Figure 3.4. (a) MCNP head model surrounded by 60 adjoint detector disc centre points. (b) The adjoint detector centre points are described in polar and azimuthal angles. The initial disc normal points at the centre of the phantom. (c) At each of the 60 centre points, 17 adjoint detector discs with different orientations are defined.

This implies that in total 1020 beams around the head are modelled. These 1020 adjoint detector discs are also the virtual adjoint disc detectors in the APDT and the beam exits in the forward MC method. All calculations, for all 1020 beams, are performed for beam diameters of 5 cm, 10 cm and 15 cm. The source energy spectrum is taken from the BNCT treatment beam called HB11 as available in Petten. It consists of mainly 10 keV source neutrons and has a 2 degree divergence which can be regarded as mono-directional. The gamma source spectrum is taken uniform between the limits 0.01 MeV and 20.0 MeV.

In the next subsections the results will be discussed, starting with the calculation times of the forward MC and the two adjoint MC techniques. Thereafter, the results for this phantom head itself will be discussed by showing the optimum positions and orientations for the Petten neutron beam to irradiate from. The other feature coming out of the adjoint calculation, the optimum source neutron energies, is discussed last.

3.4.1 Calculation times of forward MC, APDT and LEXT

The calculation times of the forward MC, APDT and LEXT can be compared after setting the allowed relative error in the 20 ROI for the three methods to <5% (95% confidence interval). These relative errors are averaged values from the results of a certain number of beams. To save time, 255 out of the 1020 beams around the head are chosen and their relative errors in the tumours and OAR are averaged. Since the relative error of the results in Monte Carlo is 'scaled' with the square root of the number of tracked particles, it can be determined how many particles need to be run and consequently how much time it takes to get a certain relative error. All averaged relative errors are, before scaling, up to 15% in the 95% confidence interval. In case of the LEXT, the post-processing time is linear proportional with the MCNP time to obtain the PTRAC file. The resulting times for the three methods are summarized in Table 3.2. In the column containing the forward MC results, the absolute times are given in days. The calculation times of the adjoint techniques are normalised towards these forward MC times and written in bold face. It is clear from Table 3.2 that in the case of the head phantom example, the smallest beams (5 cm) are

calculated most quickly with forward MC for both neutrons and gammas. In the case of neutrons, the 10 cm and 15 cm beams are 6 and 20 times faster calculated with the LEXT respectively. The APDT lacks from the fact that the adjoint thermal neutrons scatter a lot due to the hydrogen in the tissues, for which each time, a contribution to the adjoint point detector is determined. In many cases the contribution cannot be made for the reason described at the end of section 3.3.1.

Table 3.2. The total calculation times for the three methods.

Diameter of adjoint detector/ beam exit [cm]	Time to calculate 1020 beams Normalised to forward		
	FORWARD	APDT	LEXT
NEUTRONS			
5	1.00 (=140 days*)	27.40	1.52
10	1.00 (=113 days*)	18.42	0.15
15	1.00 (=88 days*)	12.94	0.05
GAMMAS			
5	1.00 (=53 days*)	1.57	1.47
10	1.00 (=42 days*)	0.52	0.55
15	1.00 (=27days*)	0.33	0.30

*) Results gathered on a Pentium IV with a 3 GHz processor and 512 Mb of memory.

For gammas, for the 10 cm and 15 cm beam exits, the calculation times for the APDT improve because gammas interact far less with the head phantom materials. The calculation times for these large beam exits are similar to the LEXT in case of 20 ROI. One can imagine that when less ROI and/or less gamma beams are involved, less APDT calculations are needed and the APDT becomes preferable to the LEXT. An overview of when forward MC calculations are faster than the two presented adjoint MC techniques, as a function of the number of ROI against the number of beams, is given in Figures 3.5 and 3.6, for neutrons and gammas respectively. Every figure contains 3 lines belonging to each beam exit diameter. Above the line of a certain beam diameter, the calculations are faster using forward MC, below the line by adjoint MC. Figures 3.5 and 3.6 are based on scaling the calculation times of the forward MC, APDT and LEXT head phantom results according to:

$$\text{Forward MC} \propto \text{number of beams}$$

$$\text{APDT} \propto \text{number of beams and number of ROI}$$

$$\text{LEXT MCNP} \propto \text{number of ROI}$$

$$\text{LEXT Post Proc.} \propto \text{number of beams and number of ROI}$$

The increase of MCNP calculation time due to the increasing complexity of the geometry when more ROI are involved is not taken into account. Due to this, in reality, the LEXT results will be somewhat better than presented because of the post processing time which does not depend on the complexity of the geometry.

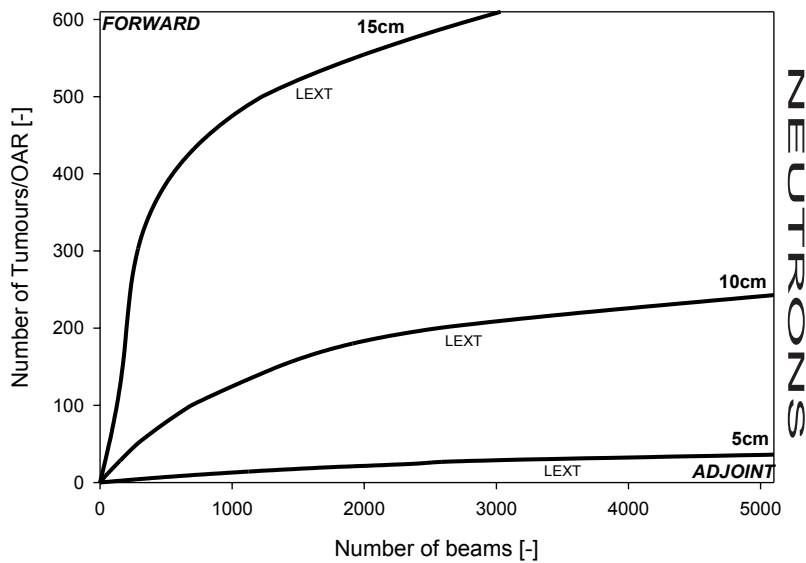


Figure 3.5. Number of neutron beams with different diameters vs. number of tumours/OAR for which adjoint or forward MC is preferable. For a given beam diameter, the region below the line is the area where adjoint MC is preferable.

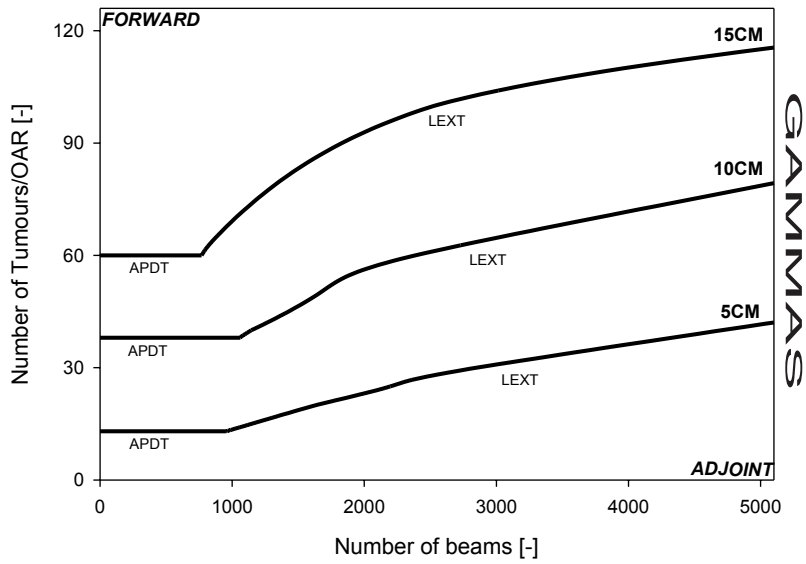


Figure 3.6. Like Figure 3.5 but for gamma beams with different diameters.

The exercise presented here can also be performed for a fixed beam diameter but as a function of ROI size/volume. The same kind of curves would be expected, as presented in Figures 3.5 and 3.6, although the largest beam diameters will represent the smallest ROI and vice versa.

3.4.2 Optimum irradiation locations and directions

The following results are obtained with the LEXT for the Petten neutron beam with a diameter of 15 cm. The differences between the LEXT outcomes and 255 controlling forward calculations are within the statistical uncertainties. From this point, the thermal neutron fluxes used are chosen to be the average fluxes over all tumours and the average over all OAR. Due to this averaging, the statistics improve and therefore an optimum treatment plan can be obtained more quickly. It is subject for further research to see if such an approach can hold in comparison with a treatment plan which is optimised taking into account every single tumour and OAR. Figure 3.7 shows the optimum orientation out of the 17 discrete orientations the Petten beam can have at each of the 60 positions around the phantom head as shown in Figure 3.4.

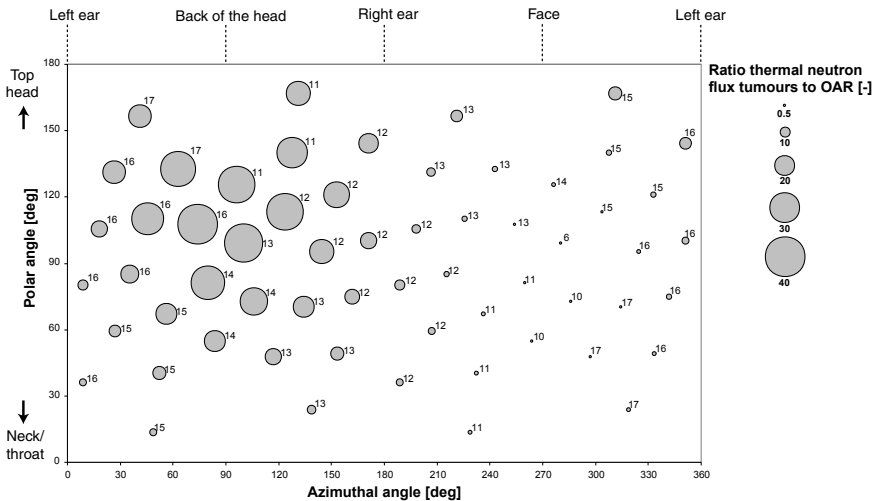


Figure 3.7. An example outcome for treatment planning with the 15 cm neutron beam in Petten: the maximum ratios of the thermal neutron fluxes in tumours to OAR at each of the 60 positions around the phantom head example.

This optimum is defined as to have the highest ratio of thermal neutron flux in the tumours to OAR. As a constraint, it is chosen that the thermal neutron flux in the tumours has to be $>75\%$ of the maximum attained thermal neutron flux in the tumours for that beam position. This constraint prevents the situation that the flux in the tumours is low but the flux in the OAR is close to zero which gives anyhow a high ratio. However, the time the patient needs to be irradiated becomes too long. The optimum ratios around the head are also given in the grey histogram in Figure 3.8; the 60 beam positions are ordered with the azimuthal angle. The polar angles

and orientation numbers information is omitted. For instance at beam position 13 in Figure 3.8, around 40 times more thermal neutrons are delivered in the tumours than in the OAR. It is clear that the best locations to irradiate the tumours are from the back of the head. Therefore, with the LEXT, 20 times faster than with normal forward MC, the whole head has been ‘scanned’ by 1020 beams and the treatment planner can obtain the best positions and orientations for irradiation. It is nearly impossible to have ‘missed’ a good beam configuration. This is therefore a good starting point to combine the best beams and optimise the treatment plan.

3.4.3 Optimum source neutron energy group

The optimum source particle energy can also be obtained with the adjoint technique. This is simply the source particle energy giving the highest contribution of interest in the tumour and the lowest in the OAR. In terms of adjoint MC, this means that only a few (or ideally none) adjoint source particles originating from the OAR will reach the adjoint detector. This results in a large accompanying relative error. Of course one has to be confident that enough histories have been run in order to assure that the result has converged. It is expected that obtaining acceptable relative errors within various bins at several adjoint detectors around the phantom when using an isotropic adjoint source, is a good indicator that the MC run has converged. This problem of having large errors in some ROI will not occur rapidly in the results with the Petten beam, as many energy groups are involved by which the statistical uncertainty decreases after integration. In the case of single source neutron energy groups, it is for now impossible to draw conclusions on the absolute ratio values of the thermal neutron flux in the tumours to OAR. It is expected that MCNP variance reduction techniques are needed to overcome this problem of the large relative errors in the OAR. This is subject for further investigations. Another approach would be the use of deterministic codes.

For our phantom head example, irradiated with a 15 cm diameter neutron beam, the maximum ratios of the thermal neutron flux in the tumours to OAR are displayed in Figure 3.9. The grey levels indicate the maximum ratios out of 17 orientations, for 17 energy groups as a function of the 60 positions around the head. For this purpose, the 172 energy groups are condensed to 17 groups (the first 12 groups and 16 times 10 groups) in order to improve the statistics and be more realistic regarding obtaining a certain energy group; it is impossible to obtain neutrons in a very narrow energy range apart from having them in a great number. In Figure 3.9, the accompanying optimum orientation is not indicated. The maximum ratios have to meet two additional constraints concerning the thermal neutron flux in the tumours: (1) It has to be $>75\%$ of the highest possible thermal neutron flux at that position for a certain orientation and energy group. (2) The relative error has to be $<5\%$ in the 95% confidence interval. When these constraints are not met the ratio is displayed as zero. Constraint 1, in particular, truncates the results in Figure 3.9 by which no results are obtained for the lowest and highest energy groups; the values are shown in white. The order of the 60 beam positions in Figure 3.9 is similar to Figure 3.8 and it can be seen that the beams irradiating the back of the head prefer lower source neutron energies. The white histogram in Figure 3.8 shows the ratios obtained similar to those discussed earlier for the Petten beam results, but for the optimum

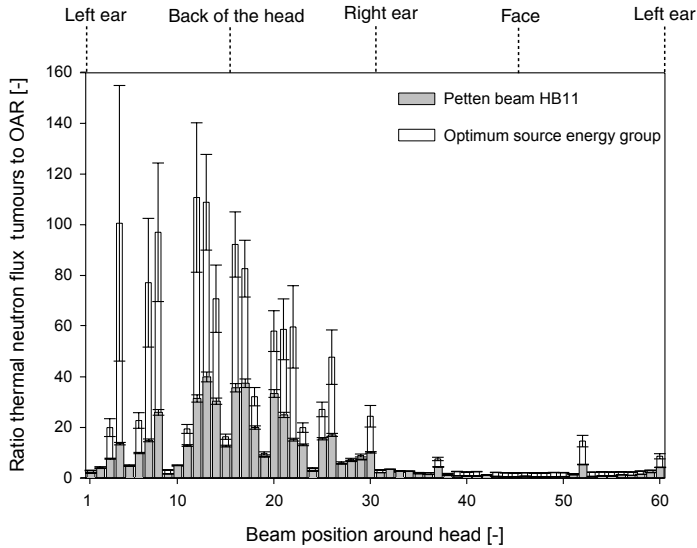


Figure 3.8. Maximum ratios thermal neutron flux in tumours to OAR of the Petten beam in 60 positions around the phantom head example.

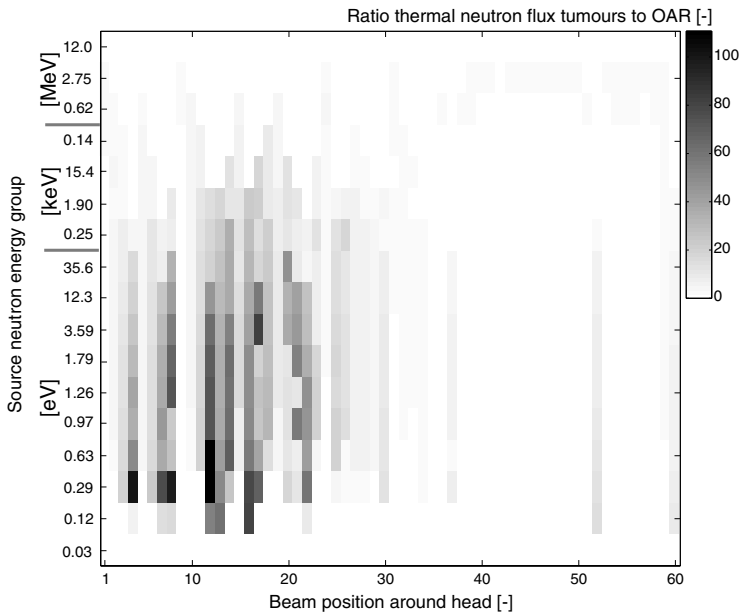


Figure 3.9. Maximum ratios of the thermal neutron flux in the tumours to OAR out of 17 orientations for 17 source neutron energy groups around the phantom head.

energy groups. Because of the high relative errors for the OAR, these ratio values are not trustworthy but nevertheless presented to indicate the kind of improvements that can be expected. In any case, less thermal neutrons in the OAR means that the tumours can be irradiated longer and more boron reactions can be realised.

3.5 Conclusions

Application of the adjoint MC for mono-directional neutron beams enables the optimum irradiation directions and positions for a BNCT treatment plan to be obtained more quickly. The next step would be investigating how to optimise the treatment plan by selecting the best beams out of all information provided by the adjoint. The adjoint also provides information on which source energies give high contributions to the tumours and small to the OAR. It needs investigating further how to deal with the accompanying large relative error in the OAR since this makes it difficult to judge the absolute improvements when using single energy groups. Nevertheless, the adjoint outcome suggests using low source neutron energies, in case of the head phantom example. This has to be further investigated with respect to the skin dose and the dose given to the deepest seated tumours.

Chapter 4

Thermal neutron field facility

4. Design of a homogeneous thermal neutron field facility for BNCT

The BNCT treatment of organs suffering from cancer which are irradiated extra-corporally becomes more and more interesting after the promising results obtained by researchers in Italy [88-90]. Furthermore, researchers in the field of drug development for BNCT desire a facility containing a homogeneous thermal neutron field for in-vitro studies. In this chapter, a measure for homogeneity is defined as the ratio of minimum thermal neutron flux to maximum thermal neutron flux in a volume. As explained in Chapter 1, the thermal neutron flux is a perfect indicator for the ^{10}B absorptions.

In section 4.1, the description of a facility especially designed for liver treatment by an epithermal neutron beam is given, while section 4.2 discusses the best design for a facility if a new neutron beam would be constructed.

4.1 Design of an irradiation facility for the extra-corporal treatment of liver cancer with an existing epithermal beam

In Pavia (Italy), two livers of patients suffering from haematogenous metastasis of colorectal cancer, were treated extra-corporally with BNCT. The first patient lived for almost 4 years (communication from A. Zonta, Pavia Italy) while the second patient died a month after the operation due to heart failure. The success of the first patient, which implies undeniable evidence that BNCT can be a promising treatment, encouraged us to investigate whether extra-corporal liver irradiations can be performed with the existing epithermal neutron beam at the High Flux Reactor in Petten (The Netherlands). The study has the aim to design a facility in which a homogeneous thermal neutron field can be obtained with epithermal source neutrons; the BNCT treatment beam in Petten itself cannot be tailored due to the ongoing clinical trials concerning BNCT of brain tumours {REF 5,6}. As the treatment will be extra-corporal, there is a limit which the patient may be anhepatic, which when corrected for the loss of transportation time, according to the liver surgeon, allows an irradiation time of at most 180 minutes. The study has the additional goal to obtain the same thermal neutron fluence of 4×10^{12} (+/- 20%) cm^{-2} as was applied in Pavia. Another requirement (according to the Pavia researchers) is that the liver should not exceed a total weighted dose (as defined in [4] of 15 Gy [89]. The weighting factors (explained in Chapter 1) for the different dose components are those as applied for BPA: $\text{RBE}_\text{B}=1.3$ or 3.8 (healthy or tumour tissue) ; $\text{RBE}_\text{p} = 3.2$; $\text{RBE}_\text{n}=3.2$; $\text{RBE}_\text{g}=1.0$. An important issue that should be investigated thoroughly after a facility has been built is the dose limit for healthy liver. In this chapter, the focus is mainly on obtaining the homogeneous thermal neutron field. This means finding the parameters with the greatest influence, obtaining their optimum values and describing the choice of the materials. More details about the project to treat extra-corporal livers in Petten are given in Paper III.

4.1.1 Design parameters and selected materials

The BNCT neutron beam at Petten has an epithermal neutron flux of $3.3 \times 10^8 \text{ cm}^{-2}\text{s}^{-1}$ with an average energy of 10 keV [29]. The skin, cranium and brain tissues are used to thermalise the neutrons by the elastic scattering properties of the prevailing hydrogen to $E < 0.5 \text{ eV}$. This thermalisation effect is indicated in Figure 4.1: The epithermal neutron flux decreases while the thermal neutron flux increases when the neutrons travel into a cube or sphere of H_2O which has similar properties to human tissue. The thermal neutron flux has a maximum at around 2.5 cm depth, the so-called thermal maximum. The thermal neutron flux in the sphere (with diameter of 25.0 cm) is higher than in the cube (sides of 20.0 cm) at deeper positions; the thermal flux is distributed over a larger area.

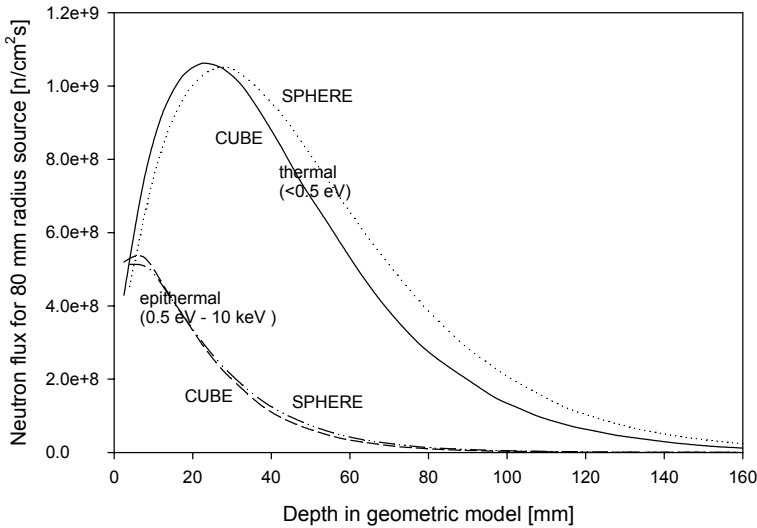


Figure 4.1. The epithermal and thermal neutron flux along the beam centre-line as a function of distance in a cube and sphere of H_2O .

The fixed parameters in the existing Petten set-up are all source related: Energy and spatially dependent source intensity and a maximum radius R_{src} of the irradiation beam of 8.0 cm. At the edges of the Petten beam, the neutron intensity drops rapidly. An average liver has a weight of around 1.7 kg [91] and would fit in an imaginary cube with sides of 12.0 cm. From Figure 4.1 it can be seen that the liver would need to be irradiated from more than one side in order to get a flat neutron fluence distribution.

By extrapolating the idea of irradiating a body from more than one side, the step to irradiate a rotating body which is rotational-symmetric seems straightforward. The simulation of the rotation is discussed in subsection 4.1.2. A spheroid shaped liver holder with a polar axis R_{pol} and an azimuthal axis R_{azi} is chosen, see Figure 4.2. The advantage of a spherical design is that the intensity fall off near the edges of the beam is compensated by the presence of less liver material to irradiate near the

bottom and top of the sphere. R_{pol} can be chosen to be the same as R_{src} . The R_{azi} should be chosen to be a compromise between large enough to create space for the liver and still provide enough thermal neutrons at the centre of the liver. In fact the thermal neutron profile, as shown in Figure 4.1, is distributed over a volume resembling a torus due to rotation of the spheroidal liver holder.

At the edges of the liver holder the tori-volumes are larger, which will decrease even more the already low thermal neutron flux density since this flux is ‘smeared out’ over this larger volume. This has to be compensated by surrounding the holder by neutron- moderating and reflecting materials in order to increase the number of thermal neutrons at the edges. In addition to selecting appropriate materials, the dimensions of the materials are also variable. Typical dimensions that can be varied in order to optimize are $q1, q2, q3, q4$ and $q5$ as indicated in Figure 4.2.

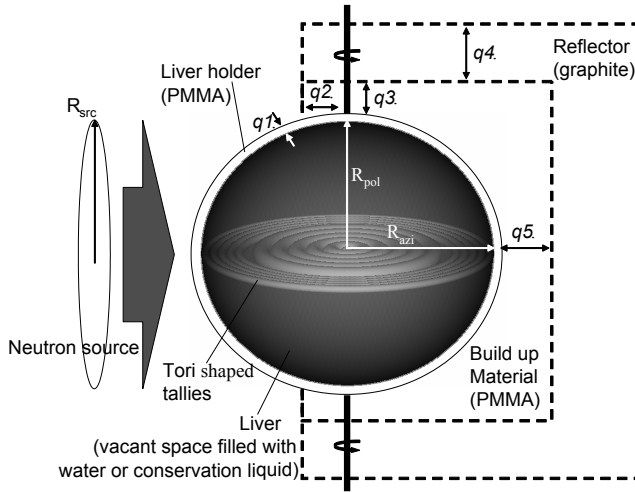


Figure 4.2. Schematic overview of the liver irradiation set-up with all the design parameters and some 3D drawn tori for tallying neutrons simulating rotation.

For moderation of the epithermal source neutrons, a scattering medium containing a lot of hydrogen should be selected. This requirement is met by the plastic polymethylmethacrylate (PMMA) which is solid and stiff. PMMA has a mass fraction for hydrogen which is around 20% less compared with liver tissue. This difference is reduced to 10% due to the higher density of the plastic. PMMA is non-toxic and transparent and therefore suitable for the liver holder. A disadvantage of hydrogen is the production due to neutron capture of 2.2 MeV gammas. For this reason the rotating liver holder is surrounded by sufficient PMMA to create the necessary thermal neutron build-up and supplemented by graphite for more scattering of the neutrons with less production of gammas. In Figure 4.2 these two materials are defined as build-up and reflector respectively. After selecting these materials, the Monte Carlo code MCNP [7] is used to simulate the neutrons and gammas through the geometry. By varying the parameters $q1$ to $q5$, one at a time

and observing the changes, the optimum set-up can be approximated. During this phase the thermal neutron flux is monitored at certain characteristic positions, i.e. at the centre, the thermal maximum, the equator, top and bottom, to obtain a homogeneous neutron flux density. At the same time, it is desired to have as low as possible gamma production. When these criteria are closely met, the thermal neutron flux is calculated everywhere in the liver by simply programming many tori evenly distributed inside the liver. After calculating the entire thermal neutron field inside the liver holder for several combinations of promising parameter settings, the most homogeneous result is chosen. In the calculations the liver tissue composition is taken from ICRU 46 [8]).

4.1.2 Simulating rotation with the Monte Carlo code

By programming tori, only one MCNP calculation is needed in which the beam irradiates the liver from one direction. MCNP adds all the track lengths of the neutrons or gammas inside the torus volume and gives, when dividing by the volume of the torus (V_{torus}), the neutron and/or gamma flux. From another point of view, the flux can be seen as a time-averaged flux inside the rotating liver. Mathematically, the above explanation of the calculation of a flux in a rotating torus is as follows: Imagine the torus to be fixed and that the beam is rotating around it with a revolution time T . This means that the angular flux $\phi(\vec{r}, \Omega, E, t)$, as defined in Bell and Glasstone [69] at \vec{r} within the torus becomes a function of time t . The angular flux is also depending on the direction Ω and energy E of the neutrons. Integrating over time T and dividing by T gives a time averaged angular flux, as shown between the brackets in equation (4.1). In fact:

$$\bar{\phi}_{V_{torus}}^{rev} = \frac{1}{V_{torus}} \int_{V_{torus}} dV \int_{\Omega} d\Omega \int_E dE \left\{ \frac{1}{T} \int_T dt \phi(\vec{r}, \Omega, E, t) \right\} = \bar{\phi}_{V_{torus}} \quad (4.1)$$

gives the total flux averaged over V_{torus} per revolution (*rev*). This is in fact what MCNP calculates with the so called F4 tally [92].

4.1.3 Results of the designed liver facility at the HFR Petten

Two liver irradiation facility designs are discussed which represent the two extremes: As large as possible irradiated volume with acceptable homogeneity and the smallest acceptable volume with a high homogeneity. The first design has a volume of 2.4 litres and is restricted by the homogeneity demand of $\pm 20\%$ in the thermal neutron fluence distribution. The second design has a volume of 1.6 litres and is restricted by the minimum volume of liver (together with the conservation liquid) that can be expected. After several MCNP calculations, the optimum parameter settings are obtained which are presented in Table 4.1.

Table 4.1. Optimal parameter settings for liver irradiation set-ups.

	R_{pol}	R_{azi}	$q1$	$q2$	$q3$	$q4$	$q5$
	[cm]						
1.6ℓ holder	8.0	7.0	1.0	3.5	3.5	15.0	1.0
2.4ℓ holder	8.0	8.5	0.5	3.0	3.5	15.0	1.0

Parameters $q1$, $q2$, $q3$ are of direct influence in the Petten set-up while $q4$ and $q5$ are of little importance; as long as the graphite thickness $q4 > 15.0$ cm. The graphite increases by up to 15% of the thermal neutron flux at the edge of the holder volume. It appeared that the build up PMMA around the holders almost doubles the number of thermal neutrons inside the holder. Figure 4.3 shows the cross sections of the thermal neutron flux distributions in the two liver holders and Table 4.2 contains an overview of the characteristic thermal neutron flux, the maximum weighted dose rates and the resulting irradiation times.

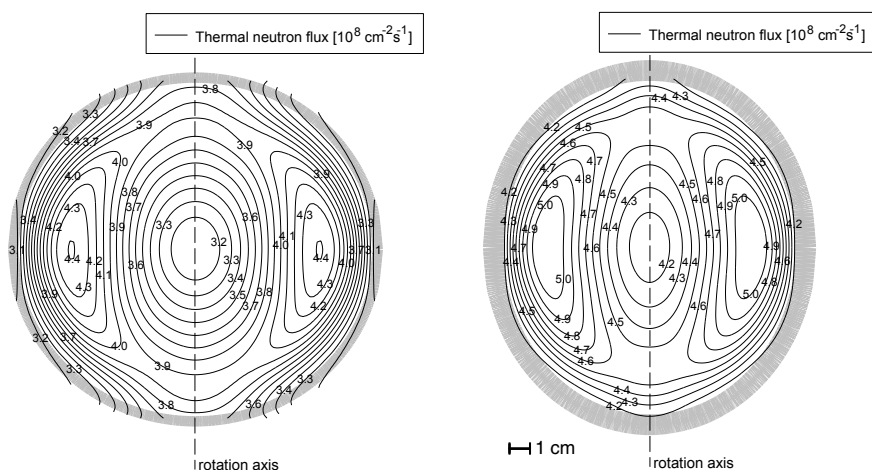


Figure 4.3. Left: The thermal neutron flux in the 2.4 litres liver holder. Right: same for 1.6 litres holder.

Table 4.2. Characteristic fluxes and weighted dose rates in both liver holders.

Description:	2.4ℓ holder	1.6ℓ holder
Average thermal neutron flux	$3.8 \times 10^8 \text{ cm}^{-2} \text{ s}^{-1}$ -20% minimum +17% maximum	$4.7 \times 10^8 \text{ cm}^{-2} \text{ s}^{-1}$ -12% minimum +9% maximum
Time to deliver $4 \times 10^{12} \text{ cm}^{-2}$	175 min	142 min
Maximum weighted dose rate (point) 8 ppm ^{10}B	5.8 Gy h^{-1}	6.5 Gy h^{-1}
Time to deliver 15 Gy maximum dose	155 min	138 min

It is due to the smaller R_{azi} in the 1.6 litres holder that a better homogeneity can be obtained. In both holders the minimum flux is at the edge and centre of the liver volume and the maximum is as to be expected at the position near to the thermal maximum (see Figure 4.3). The thermal maximum is still present and recognizable in both holders. However in the largest holder, the ratio of maximum over minimum within 8.5 cm is 1.5 instead of almost 4 as seen in Figure 4.1. The 2.4 litres holder is

sufficient to hold livers up to 2.1 kg, which do exist (private communication M. Malago and W. Sauerwein, University Hospital Essen, Germany).

In the 1.6 litres holder, the time to deliver the thermal neutron fluence and the time after which the tolerance dose is exceeded is roughly in agreement. For the largest holder, there seems to be no improvement in homogeneity over the Pavia thermal neutron flux distribution; it has to be recalled that the Petten beam is rather small for such a large organ. Although the required fluence of $4 \times 10^{12} \text{ cm}^{-2}$ can be given within 180 minutes, the maximum prescribed dose will be exceeded when applying this fluence. This is partly caused by the higher photon dose rate, compared with Pavia, due to the beam photons. Nevertheless, this result is promising enough to proceed first with dosimetry and after that animal studies.

4.2 Optimum neutron beam design and holders for extra-corporal BNCT irradiations

The facility described in section 4.1 for irradiating an extra-corporal liver with epithermal source neutrons, tailored specifically for the HFR in Petten, is designed around a given source description. The 'Forward SCX technique' (see Chapter 3) that gives the expected detector contribution of the source particles which is numerically the same as the result of the adjoint method, can be applied for the inverse exercise: To find a neutron source distribution and spectrum that provides a homogeneous thermal neutron field in a given volume.

Actually, the best shape of the holder, i.e. cuboid, cylindrical or spherical (see Figure 4.4) has a direct dependence on the design of a new optimum neutron beam. It is chosen to study these models with volumes of 2, 4 and 6 litres. Despite of the previous sections, in all models, it is chosen to surround the liver only by PMMA and omit the graphite in order to simplify the set-up at this stage. The holder thicknesses are 0.5 cm while a surrounding PMMA block for build up and scattering of neutrons, is $50 \times 50 \text{ cm}^2$ (width x height). In case of the cylinder and sphere, the block starts 2 cm before the rotation axis.

The new beam exit is chosen to be shaped according to the cross-sectional area of the model: this means a rectangular shape for the cuboid and cylinder and circular for the spherical holder. In the calculations, the dimensions of the beam exit (width and height or diameter) are chosen such that there is always sufficient overlap to each side of the cross-sectional area of the maximum investigated liver volume; $30 \times 40 \text{ cm}^2$ for the cuboid, $25 \times 39 \text{ cm}^2$ for the cylinder and a diameter of 32 cm for the sphere. In fact, these dimensions ensure that the beam area is two times the cross-sectional area of the largest holder (see dimensions of the 6 litres holders in Figure 4.4). The new beam will have a zero divergence and the desired neutron energy in the liver volume is $< 0.5 \text{ eV}$ and the liver tissue contains 15 ppm of ^{10}B homogeneously distributed in the liver.

4.2.1 Set-up of the holder models

In the simulation, every holder model contains smaller cells which are the MCNP detectors. In these cells, the expected detector contributions of the source neutrons are obtained. This is necessary to monitor the homogeneity in the entire model during optimisation as will be further explained in section 4.2.3. Due to symmetry

only a quarter of the cuboid model and half of the cylindrical and spherical models have to be filled by these cells. Figure 4.4 shows the holder models and the surrounding PMMA with on the left the defined neutron sources.

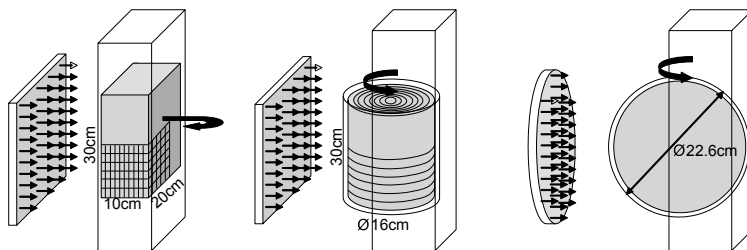


Figure 4.4. Cuboid shaped, cylindrical and spherical holder models (all 6 litres) in which the expected detector contributions are calculated together with the neutron beam exits.

The cell structure per model is organized in the following way:

* **Cuboid:** A quarter of the 6 litre cuboid model is filled with 300 rectangular parallelepiped shaped cells; width x height x depth=5 x 6 x 10 cells. The cuboid holder is irradiated from two sides (see arrow in Figure 4.4). In reality, the holder is turned half-way the irradiation time. For the 2 and 4 litre holders, the optimisation is performed over fewer cells; the outside cells are not taken into account whereby the thickness remains always 10 cells=10 cm. Separate MC calculations for these smaller volumes are not performed since the effect of the presence of 10% more hydrogen in liver tissue compared with PMMA is regarded to be insignificant compared with other influences such as the actual environment and beam characteristics.

* **Cylinder:** Half of the cylinder consists of 48 ring-shaped cells; diameter x height=8 x 6 rings. The cylindrical holder is rotating along a vertical axis. Similar to the cuboid model: the volume of the cylindrical holder is decreased by not taking into account the lowest 16 and 32 rings for the 4 and 2 litre holders, respectively, during the optimisation process.

* **Sphere:** The top half of the sphere is filled (not drawn) with 13 tori-shaped cells. The 4 ‘tori’ along the vertical rotation axis are actually spheres. In every volume, the tori fill the space evenly. The straight arrow, drawn in the spherical holder model, in Figure 4.4 indicates that the diameter of the holder can be decreased, whereby the tori will be redistributed.

4.2.2 Expected contributions of the source neutrons inside the models

The forward source is chosen to have two uniform spectra; of 33 and 43 energy groups between the limits 1×10^{-5} eV to 27.4 keV and 1×10^{-5} eV to 19.6 MeV, respectively. These values of the upper limits come from the XMAS energy structure. By investigating these two spectra, the optimum source spectrum is obtained with and without the influence of the damaging fast neutrons. The energy groups are condensed groups of the 172 energy groups library described in Chapter 3. Everywhere, the statistical uncertainties in all the calculations presented are <5%

(95% confidence interval). In order to keep the graphs surveyable, only 10 cells of the cuboid model and 8 rings of the cylinder are considered. The results for the 6 litre holder models are presented in the Figures 4.5 to 4.7.

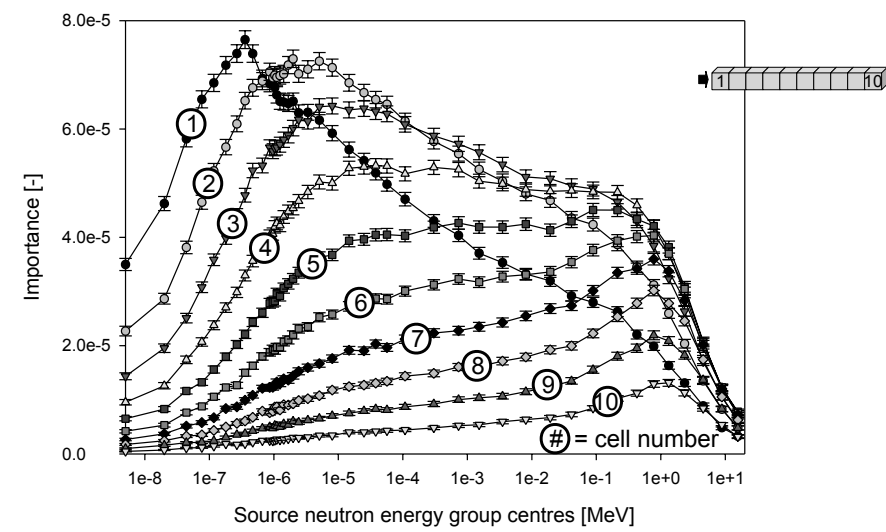


Figure 4.5. Expected detector contributions of the source neutrons of 10 cells along and nearest to the beam centreline inside the cuboid model when irradiated from one side.

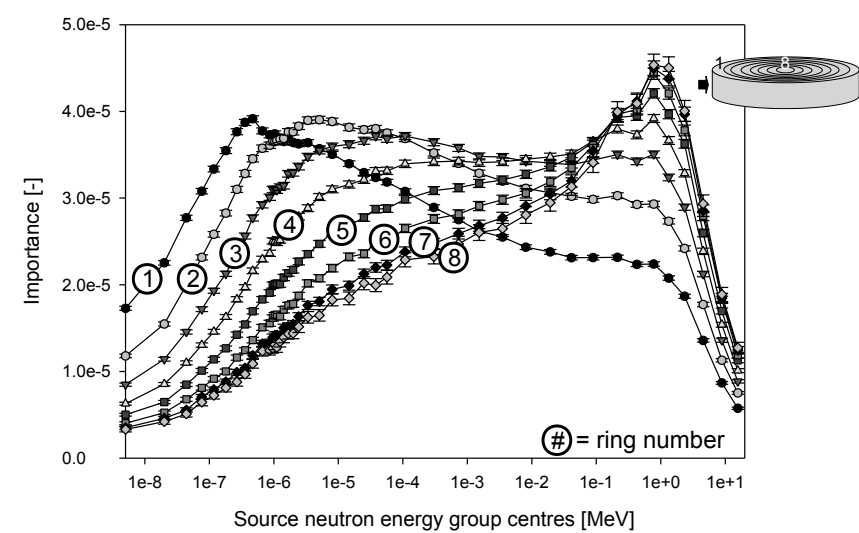


Figure 4.6. Expected detector contributions of the source neutrons of 8 rings nearest to the beam centreline inside the cylindrical model.

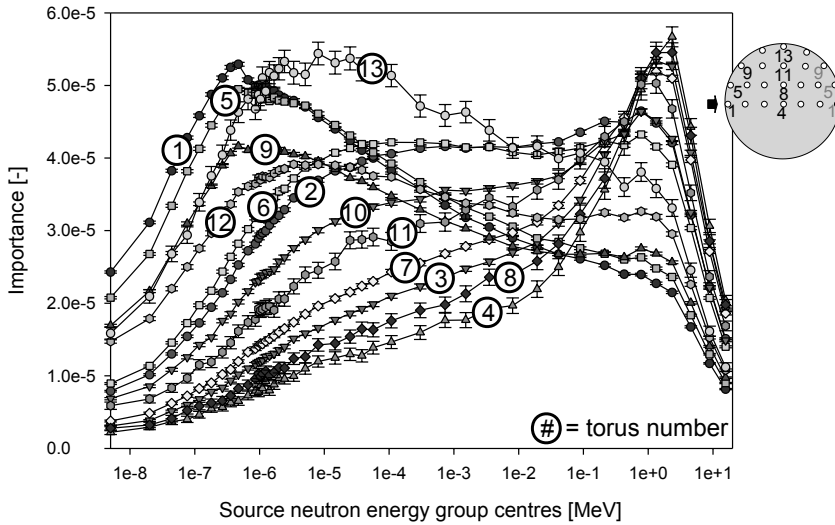


Figure 4.7. Expected detector contributions of the source neutrons of 9 tori and 4 spheres.

In Figure 4.5, 10 cells from the cuboid model, indicated at the upper right, are the nearest to the beam centre line and their expected detector contributions of the source neutrons are shown. Cell 1 is defined here as closest to the beam exit which explains the peaked preference at around 0.5 eV source neutrons. The accompanying importance value of 8.0×10^{-5} implies that for every 12,500 source neutrons of around 0.5 eV leaving the 1200 cm^2 source with 43 energy groups, only 1 neutron contributes to neutrons $< 0.5 \text{ eV}$ in this cell 1. Cell 10, farthest away from the beam exit, has a preference for 1 MeV source neutrons. In Figure 4.6, the expected detector contributions of the source neutrons of 8 coaxial rings nearest to the beam centre line are shown. The outer ring has a preference for thermal source neutrons while the thermal neutrons in the centre ring come mainly from fast source neutrons. The expected detector contributions of the source neutrons of the rings in-between are shaped according to a transition from thermal to fast with plateau-shapes for ring 3 and 4. All the expected detector contributions of the source neutrons of the 13 tori of the spherical model (diameter of 22.6 cm) are given in Figure 4.7. There is a great similarity with the expected detector contributions of the source neutrons obtained in the cylindrical model, e.g. the curves are sharply peaked at the fast source neutrons in the tori (actually spheres) at the centre of the models.

Since the cuboid holder will be irradiated from two sides, the curves shown in Figure 4.5 are added such that cell 1 and cell 10 are added, cell 2 and cell 9, etc. The result is presented in Figure 4.8 for cells 1 to 5. The other 5 cells are similar due to symmetry.

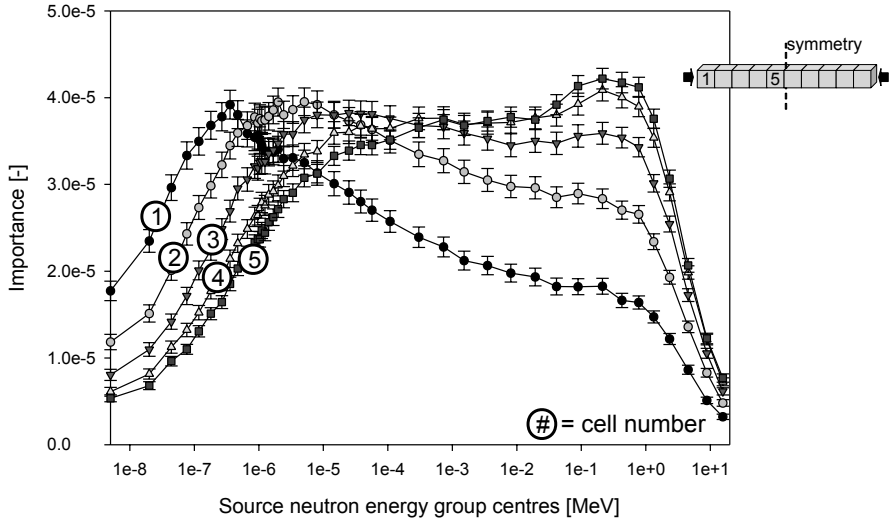


Figure 4.8. Expected detector contributions of the source neutrons when 10 cells are irradiated from two sides. Due to the symmetry only 5 cells are shown. The cells are along and nearest to the beam centreline inside the cuboid model.

4.2.3 Optimum source neutron energies

In order to realise homogeneity in the holder models, it is desirable to produce the same number of thermal neutrons ($E < 0.5$ eV) in every cell. It is not to be expected that a high homogeneity can be obtained by using a single source neutron energy group. Therefore, it is shown here that by combining the contributions of source neutrons of different energy groups k with weight a_k , a better homogeneity is attained. The contributions are labelled as the ‘importance’ (*imp*) and the sum of the weighed importances over all energy groups in every cell j is called WI_j . Due to the direct relation between the number of source neutrons and importance, homogeneity can be defined as:

$$Homogeneity = \frac{\min_{j=1,J}(WI_j)}{\max_{j=1,J}(WI_j)}, \quad \text{where } WI_j = \sum_{k=1}^G a_k \cdot imp(k,j)$$

The closer to unity the better is the homogeneity. The minimum and maximum are selected after summing the weighed importances up to G energy groups in every cell j (J cells in total); G is 33 or 43 energy groups. The weighs a_k of the source energy groups are determined by using a linear optimisation scheme. The so-called Simplex method (described in [93-95]) can maximise an objective function Z under the constraints provided, whenever there is a solution. The scheme to solve is:

Objective function:

$$Z = \max \left(\sum_{j=1}^J WI_j \right)$$

3 constraints:

$$WI_j < L$$

$$WI_j \geq Homogeneity \cdot L \text{ with } 0 < Homogeneity < 1$$

$$\sum_{k=1}^G a_k = 1$$

That is: the optimization process will provide the maximum number of thermal neutrons in the liver under the constraint that the ratio of the minimum and maximum WI_j , among all cells, is between the *Homogeneity* and unity. Similar to the a_k 's, L is a variable that will be solved during the optimisation. It is needed to prevent setting an absolute constraint which is already done with constraint 3; this keeps the total number of source neutrons constant. The system is solved each time with a given *Homogeneity* that increases in small steps from 0 towards 1. The maximum homogeneity is found for the last value of the *Homogeneity*, for which the Simplex method is able to provide a solution; if the *Homogeneity* increases further, the constraints cannot be satisfied.

In Figures 4.9 and 4.10, the Simplex solution vectors are shown containing the weights a_k of the energy groups, for the three holder models and three volumes. Figure 4.9 shows the result when source neutrons up to 19.6 MeV may be used while Figure 4.10 is limited up to 27.4 keV.

It is clear from both figures that the maximum homogeneity is reached when using the 'lowest' in combination with the 'highest' neutron energy groups, regardless of the holder model or volume; one exception is the 6 litre spherical holder when no fast neutrons may be used (see Figure 4.10).

For the results of all the "homogeneity vs. neutron source spectrum", the calculations are summarised in Table 4.3. The last two columns of Table 4.3 give the obtained homogeneities for the spectra shown in Figures 4.9 and 4.10.

Table 4.3. Obtained optimal homogeneities in the models for different neutron source spectra.

Model	Volume (litres)	Petten spectrum	Uniform source spectrum			Optimum source spectrum (Simplex)	
Energy range		0eV-19.6MeV	0eV-27.4keV	<1eV	>1keV<27.4keV	0eV-27.4keV	0eV-19.6MeV
CUBE	2	0.63	0.77	0.48	0.54	0.96	0.98
	4	0.63	0.77	0.48	0.54	0.95	0.97
	6	0.62	0.76	0.47	0.52	0.93	0.95
CYLINDER	2	0.67	0.46	0.26	0.73	0.82	0.99
	4	0.67	0.46	0.26	0.72	0.81	0.99
	6	0.67	0.46	0.26	0.65	0.78	0.88
SPHERE	2	0.62	0.45	0.31	0.60	0.72	0.87
	4	0.44	0.30	0.19	0.55	0.65	0.90
	6	0.36	0.23	0.12	0.44	0.52	0.91

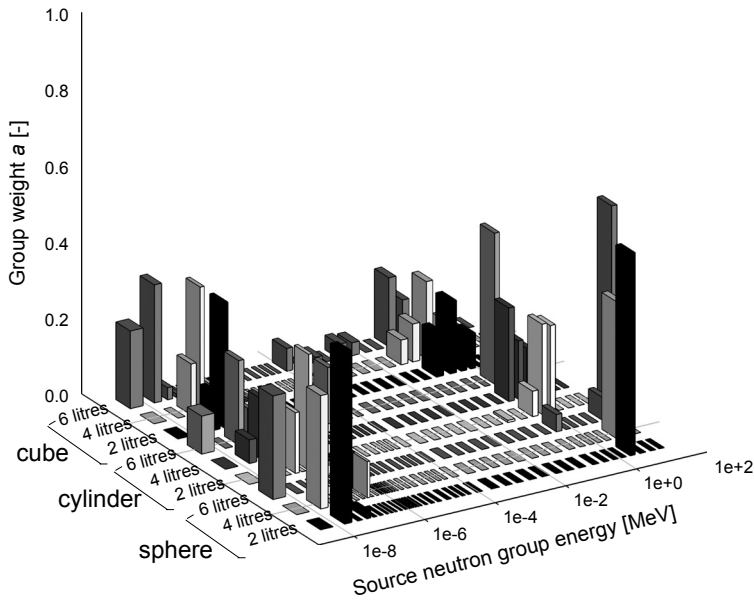


Figure 4.9. The optimum source neutron spectra with a 19.6 MeV upper limit for the 3 geometrical models (3 volumes) to obtain the maximum homogeneity.

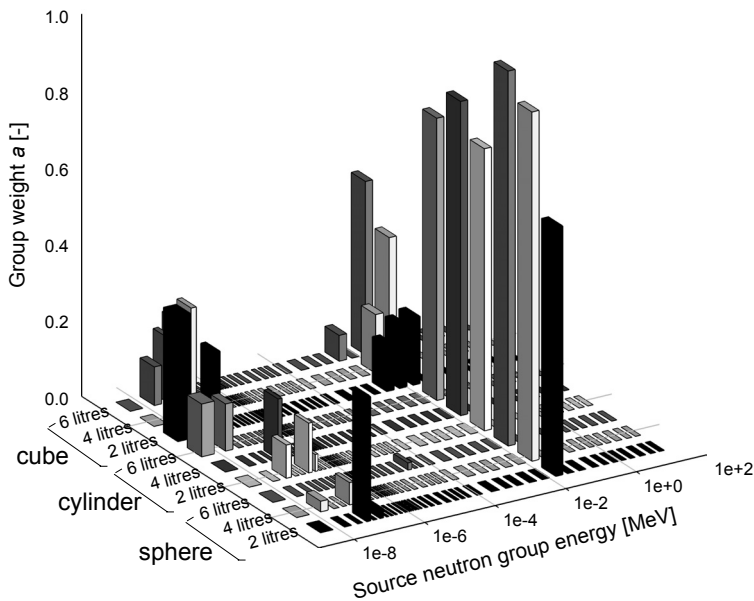


Figure 4.10. The optimum source neutron spectra with a 27.4 keV upper limit for the 3 geometrical models (3 volumes) to obtain the maximum homogeneity.

It can be seen that the cylindrical and spherical holders improve significantly whenever fast source neutrons are allowed. The cuboid liver holder provides the best homogeneous thermal neutron field. In studying all Simplex outcomes, it is concluded that the homogeneities will not change significantly compared to the optimum solution when another nearby energy group is selected or the weights are slightly changed. The numbers presented in the last two columns of Table 4.3 are the arithmetical optima. The table also shows the maximum homogeneities when using source neutrons with either a uniform spectrum up to 27.4 keV, or only thermal or only epithermal energy groups. For all spectra in Table 4.3, the fact that the homogeneity of the cuboid and cylindrical models does not vary greatly with decreasing volume suggests that the dimensions of the beam exit can be reduced. Furthermore, Table 4.3 shows that the Petten design presented in section 4.1, might have been improved by choosing a cylindrical liver holder instead of the spherical one. Unfortunately, this is not possible due to the rather small beam opening in Petten. The right choice for the spherical design in the Petten set-up is also conferred when taking into account the minimum summed weighed importance (WI_j) obtained in the holder model; this means a minimum number of delivered thermal neutrons. In Figure 4.11, this minimum WI_j is shown for every solution of the Simplex method (27.4 keV upper limit case) somewhere in the liver as a function of Homogeneity.

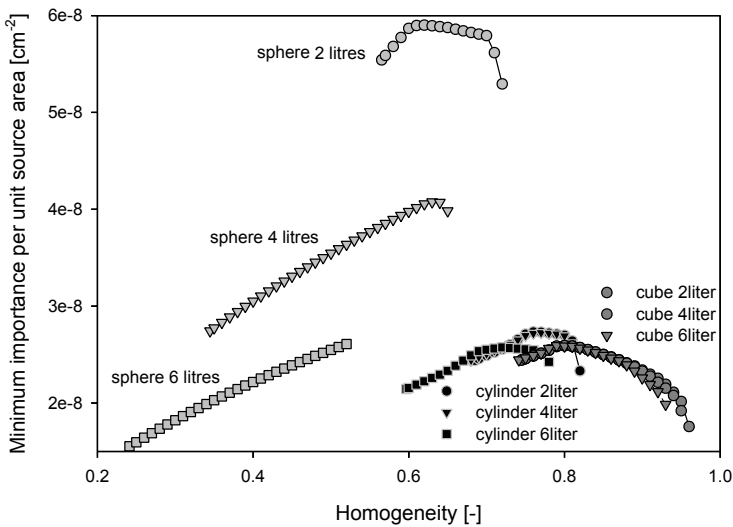


Figure 4.11. The minimum reached importance in a certain cell inside the 3 geometrical models, for 3 volumes each, as a function of the homogeneity.

Normalised to per source area, this minimum WI_j is highest in the 2 and 4 litre spherical holder models. In these models, the source neutrons can be said to be at their most effective. Therefore, given the small existing beam opening and intensity, as in Petten, the spherical holder seems from this graph to be the best choice. The curves in Figure 4.11 are based on the source areas as defined in section 4.2. In order to have the same ratio of beam area to cross-sectional area for all models with the

same volume, the curves for the spherical holders of 2 and 4 litres have to be multiplied with 0.67 and 0.84, respectively. It can be seen that even then, the contributions of the source neutrons in these spherical models are still higher.

Describing Figure 4.11 in terms of the Simplex method: For low values of the *Homogeneity* in the constraints, the objective function is maximised by having large WI_j 's in many cells at the cost of low WI_j 's in a small number of cells. For the 2 litres spherical and for all the cylindrical and cuboid shaped holders, it can be seen that the minimum WI_j somewhere in the holders, first increase then decrease towards the maximum homogeneities. This means that for the maximum homogeneities, the source neutrons are less effective and more source neutrons are needed to reach a certain effect. This does not mean immediately that it will take longer to irradiate since that depends on the available source neutron energy spectrum in combination with the source strength.

4.3 Conclusions

To conclude, it seems that the cuboid shaped model would be the best option when a new neutron beam is to be designed and constructed. The investigated thickness of 10 cm is sufficient for both livers and other similarly shaped volumes, such as for example the irradiation of cell cultures, for which also a homogenous thermal neutron field is required. The disadvantage, namely the rather large beam exit, can be circumvented by transporting the cuboid holder up and down (or left and right) through a smaller neutron beam with a high intensity. Furthermore, for neutron sources that may have relatively low strength, the 2 and 4 litre spherical holder models would be the preferred configuration which is practically the case with the present epithermal neutron beam in Petten. Note that the obtained homogeneity in the 2.4 litre spheroid liver holder (0.68) of section 4.1 is close to the optimum, as can be concluded from the spherical results in Table 4.2; the spheroid shape improves the result even further.

Chapter 5

Conclusions

The quest for the optimal source neutrons for BNCT was investigated from three viewpoints:

* In the first point of view, as there is no consensus among radiobiologists about the proper values of the parameters influencing the biologically weighted dose, e.g. RBE values and tolerance doses, almost all of these parameters were varied. For brain tumours located between 20 mm up to 80 mm from the skin it was found that for most parameter configurations, epithermal source neutrons, between 1 keV and 10 keV, are optimal. Only the parameters related to ^{10}B and fast neutrons result in diverging optimal source neutron energies. For example, low values for the ^{10}B concentrations and the accompanying CBE for the boron dose result often in lower than modal source neutron energies to be optimal. Smaller values for the RBE of the fast neutron dose enable higher source neutron energies to be optimal and thus more destructive in the tumour. These parameters are of influence in the tissue in which the tolerance dose is reached first. This is depending on the ratio of the tolerance dose set for skin to brain. It is likely that in the future, boron compounds will be available which give ^{10}B concentrations close to zero in skin and other healthy tissues. Furthermore, it is possible that in the future BNCT treatment modalities (e.g. extra-corporeal, at low temperatures) the recoil protons are found to be less damaging for the cells. Of course this needs to be investigated.

This parameter study shows that having three neutron beams, one nearly thermal (5 eV) and two epithermal (500 eV and 10 keV), assures an optimal treatment, no matter what the influencing biologically weighted dose parameter values may be.

* Two newly developed adjoint Monte Carlo (MC) techniques, the Legendre Expansion Technique (LEXT) and the Adjoint Point Detector Technique (APDT), enable the simulation of mono-directional gamma, as well as neutron, beams. When the beam diameters are larger than 5 cm, the results for 1020 beams are calculated 1.8 up to 20 times faster than when compared with results from forward MC. Overall, for small diameter neutron and gamma beams (around 5 cm), the adjoint MC techniques are preferred when thousands of different locations and orientations of a mono-directional beam need to be calculated and when there are no more than ten tumours and/or organs at risk (OAR). For larger beam diameters is adjoint MC preferable up to hundreds of regions of interest whenever even a 'few' hundred of mono-directional beams are investigated. Overall, in order to take advantage of the adjoint technique, the user has to be interested in beam positions at many locations around the irradiated patient or phantom. Apart from BNCT, the LEXT and APDT are of value in conventional radiotherapy since most of the treatment beams are mono-directional or have just a small divergence. Thereby, the conventional radiotherapy community would be interested to implement MC for dose

calculations, since the results are closer to the measurements than the results of other dose calculation techniques. For the LEXT, it is expected that other base functions than Legendre polynomials, will give improvements whenever they are more appropriate to describe the angular adjoint functions in a certain problem (e.g. particle type, geometry). At present, the divergence of a beam is easy to simulate with the APDT, just by changing the position of the adjoint point detector. However, a problem occurs when the optimal source neutron energy is investigated with adjoint MC because by definition the optimal source neutrons give a high contribution to the tumours and a low contribution to the OAR. As a consequence, the values of interest in the OAR have a large relative error, and no judgement can be given on the outcome. Nevertheless, preliminary results for a model with ten tumours in the brain showed that only thermal and low epithermal source neutrons can give significant improvements to the ratio of the thermal neutron flux in tumours to the thermal neutron flux in the OAR, when compared with the ratio resulting from the Petten BNCT beam. Further analysis in the field of treatment planning optimisation is obviously the next step.

* The last point in this thesis is the investigation to obtain the optimal source neutrons for future BNCT applications such as the extra-corporeal irradiation of organs (e.g. liver). The first part of this research shows that it is possible to irradiate a large liver, with a volume of 2.4 litres, at the current BNCT facility in Petten. This requires rotation of the liver in a spheroid holder in order to obtain thermal neutron fluence as homogeneous as possible with the rather small epithermal beam. The homogeneity is defined as the ratio of the minimum to the maximum thermal neutron flux in the liver holder. Simulation of the doses and fluxes in the rotating liver was performed with MCNP by programming torus shaped tallies in the liver and irradiating from one side. Averaging the flux and/or dose over the volume of the torus provides the answer as if the torus is rotating around the symmetry axis. The homogeneity in the designed and constructed 2.4 litre liver holder is 0.68. Since more researchers are interested in a volume with a homogenous thermal neutron field, e.g. for cell experiments, a systematic investigation was started in which also the neutron source could vary in shape and energy. In cubic volumes a homogeneity of around 0.95 can be realised when the source neutrons are mixed in a composition of around 30% thermal (around 0.1 eV) and 70% epithermal (around 10 keV). In spherical volumes the homogeneities cannot exceed 0.72, but these spherical shapes are preferred when high effectiveness per source neutron is required. This is necessary in case of a low source strength in combination with a limited irradiation time.

To conclude: in 1941, Zahl *et al.* {REF} proposed the use of epithermal instead of thermal source neutrons in BNCT. The outcome of the three parts of this thesis has shown that 3 neutron energy regimes should be prescribed. Besides the 10 keV epithermal source neutrons, low epithermal source neutrons of around 1 eV and thermal source neutrons with energies of 0.1 eV must also be used. With these source neutrons available, BNCT treatment planning can be optimised, whatever the biological factors may be, wherever the tumours are located, or wherever the patient

or the patient's organ is situated. This work shows that significant improvements in the delivery of a therapeutic radiation dose can be given if a new neutron filter is designed in order to provide a variable neutron spectrum as described above.

APPENDIX

Normalisation of adjoint MCNP results for mono-directional detector contributions

In Monte Carlo calculations, the probability that adjoint particles cross a certain detector with a certain angle is nearly zero. Knowing even that more of these particles are necessary to improve the statistics of the result indicates that it will be impossible to calculate such tasks with standard Monte Carlo. Therefore, a forward calculation concerning mono-directional source particles cannot be derived with the adjoint method by means of ‘basic’ MCNP. Figure A.1 shows schematically this forward set-up with a disc shaped source and spherical tumour as a detector. This figure and also the Figures A.2, A.3 and A.4 contain the parameter descriptions as used throughout this appendix and the characteristics as will be later used in Table A.1

In fact, a surface crossing estimator (EST_{sc}) should have been used for mono-directional adjoint particles. So the detector response function should be like

$$\frac{1}{A_{src}} \delta(\Omega + \Omega_{src}) \delta(y - y_{src}) \text{ with } (x, z) \text{ within the detector area.}$$

Although it can be performed with ‘basic’ MCNP, this is not a feasible estimator for a Monte Carlo calculation, as no particle (like the grey arrow in Figure A.2) will have exactly the direction $-\Omega_{src}$. Therefore, a next-event estimator would be required which calculates from a given collision site the probability of scattering $p(-\Omega_{src})$ in the right direction and the attenuation $e^{-\xi}$ to get to the source disc as illustrated in Figure A.3. ξ is the number of mean free paths from the collision point to the detector (in fact to the source plane). Hence, the required estimator should be

$$EST_{sc} = p(-\Omega_{src}) \frac{e^{-\xi}}{A_{src}} \quad (a.1)$$

As such an estimator is not present in MCNP, this estimator is replaced by the next-event point detector estimator of MCNP, as illustrated in Figure A.4. The point detector estimator (EST_{pd}) gives for a particle entering a collision

$$EST_{pd} = p(\Omega_{det}) \frac{e^{-\xi}}{s^2} \quad (a.2)$$

where $p(\Omega_{det})$ is the probability of scattering into the direction Ω_{det} towards the point detector and s is the distance between the collision site and the detector. This is provided with the F5 tally in MCNP [7]. If the position of the point detector is sufficiently far away, Ω_{det} will be sufficiently equal to the (opposite) source direction Ω_{src} . If the system dimensions are small compared to the

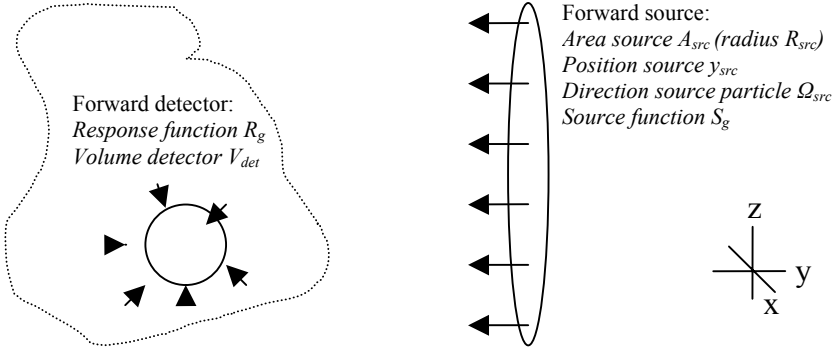


Figure A.1. Forward set-up.

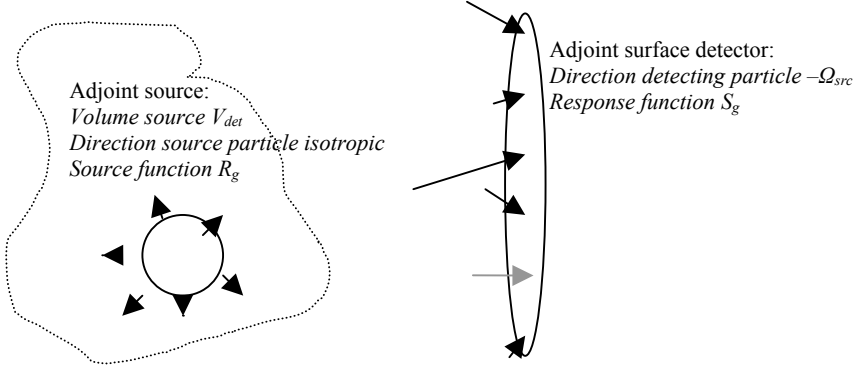


Figure A.2. Adjoint ‘basic’ set-up.

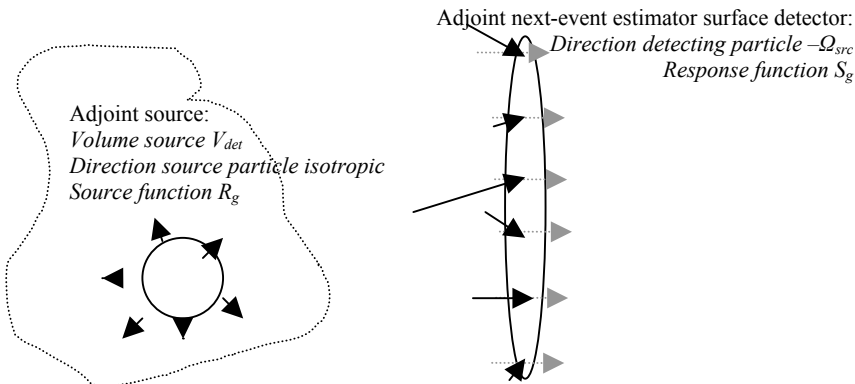


Figure A.3. Adjoint ‘required’ set-up.

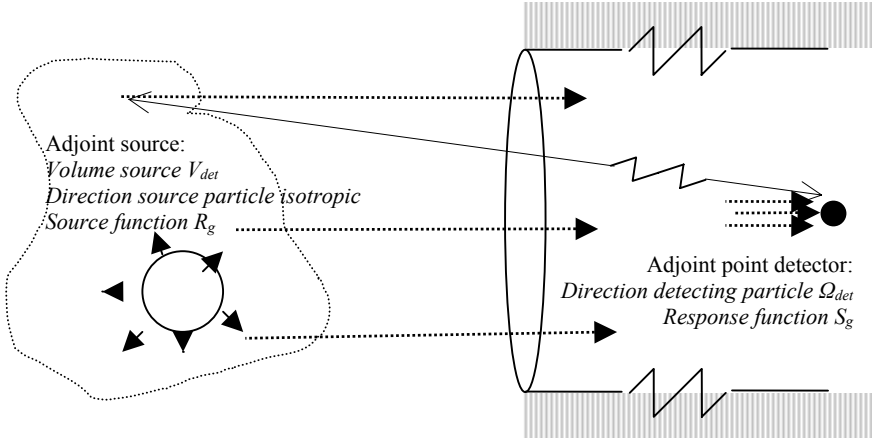


Figure A.4. Adjoint 'point detector' set-up.

distance to the detector, s can be considered constant and equal to the distance between the centre of the system and the point detector.

According to the methodology introduced by Wagner *et al* [70], Table A.1 can be composed for the geometry drawn in the Figures A.1 up to A.4 with the volume averaged flux in the tumour as the forward detector. Practically, after filling in the source and detector densities in Table A.1, the normalization factor is the product of the entries in the forward problem column divided by the product of the entries in the adjoint problem column.

The 3 columns for an adjoint calculation are (by approximation) equivalent with respect to the intention of the estimator. Comparing the results from the columns for the forward and the 'basic' adjoint equation (for a flat source spectrum and a flat detector energy response) a multiplicative normalization factor in the adjoint equation should be 4π . The estimator suggested for the adjoint 'required' calculation is equivalent to adjoint 'basic' and here also the normalization factor 4π results. By approximation this estimator is also equivalent to the adjoint point detector, but from comparison of the relevant columns, the factor s^2 must be compensated, as well as a factor A_{src} . Hence, for the actually calculated adjoint point detector the normalization factor F_{norm} , with which the result of the adjoint calculation must be multiplied becomes

$$F_{norm} = \frac{4\pi}{A_{src}} s^2 = \frac{4}{R_{src}^2} s^2 \quad (\text{a.3})$$

Note that here the situation is given for the total response over energy. If the response for one group is required, the adjoint source is limited to this group and the source density in energy is 1 instead of $1/G$ where G is the number of energy groups. This gives another factor $1/G$ in the normalization.

Table A.1. Normalisation form for the sample problem illustrated in the Figures A.1 up till A.4

dimension	forward	adjoint 'basic'	adjoint 'required'	adjoint 'point detector'
SOURCE				
space	$\frac{1}{A_{src}} \delta(y - y_{src})$	$\frac{1}{V_{det}} \quad r \in V_{det}$	$\frac{1}{V_{det}} \quad r \in V_{det}$	$\frac{1}{V_{det}} \quad r \in V_{det}$
direction	$\delta(\Omega - \Omega_{src})$	$\frac{1}{4\pi}$ (isotropic)	$\frac{1}{4\pi}$ (isotropic)	$\frac{1}{4\pi}$ (isotropic)
energy	$S_g / \sum_{g'} S_{g'}$ $= 1/G$ for flat source	$R_g / \sum_{g'} R_{g'}$ $= 1/G$ for flat response	$R_g / \sum_{g'} R_{g'}$ $= 1/G$ for flat response	$R_g / \sum_{g'} R_{g'}$ $= 1/G$ for flat response
DETECTOR				
space	$\frac{1}{V_{det}} \quad r \in V_{det}$	$\frac{1}{A_{src}} \delta(y - y_{src})$	$\frac{e^{-\xi}}{A_{src}}$	$\frac{e^{-\xi}}{s^2}$
direction	1	$\delta(\Omega + \Omega_{src})$	$p(-\Omega_{src})$	$p(\Omega_{det})$
energy	R_g $=1$ for flat response	S_g $=1$ for flat source	S_g $=1$ for flat source	S_g $=1$ for flat source

Acknowledgement

The exact derivation of the normalisation factors presented here is performed by J.E. Hoogenboom.

NOMENCLATURE

A	surface area	m^2
a	weigh of source energy group	-
C	concentration	ppm
CBE	compound related biological effectiveness factor	-
d	coefficient of orthonormal basis functions	-
D	physical dose	Gy
E	energy	eV
EST _{pd}	next-event point detector estimator	m^{-2}
EST _{sc}	surface crossing estimator	m^{-2}
f	arbitrary function	-
F _{norm}	normalization factor for adjoint results	-
G	number of energy groups	-
J	number of cells	-
L	variable	-
N	number of samples	-
p	direction probability function	-
Q	source function	$cm^{-3} s^{-1}$
q1:q5	dimensions (thickness, distance)	m
r	position	-
R	radius	m
RBE	relative biologically effectiveness factor	-
R _g	group wise response function	-
s	distance between collision site and detector	m
S _g	group wise source function	-
T	revolution time	s
t	time	s
V	volume	m^3
w	weight of Monte Carlo particle	-
WI	sum of weighed importances	-
x	spatial coordinate	m
y	spatial coordinate	m
Z	objective function	-
z	spatial coordinate	m

Greek symbols

ϕ^+	adjoint function	-
ϕ	forward flux	$cm^{-2} s^{-1}$
$\bar{\phi}_V$	volume averaged forward flux	$cm^{-2} s^{-1}$
α	arbitrary angle	rad
β	arbitrary angle	rad
δ	Dirac-function	-
λ	ratio source gammas to source neutrons	-

ξ	number of mean free paths to detector	-
Σ_d	detector response function	cm^{-1}
ψ	orthonormal basis functions	-
Ω	direction	ster

Subscripts

azi	azimuthal
B	boron-10
b γ	beam gamma related
det	detector
i	index for samples
j	index for cells
k	index for energy groups
l	index for coefficients
m	index for coefficients
n	fast neutron related
p	thermal neutron related
pol	polar
rev	revolution
src	source
w	biologically weighted
γ	induced gamma related

ABBREVIATIONS

APDT	Adjoint Point Detector Technique
BNCT	Boron Neutron Capture Therapy
BNL	Brookhaven National Laboratory
BPA	Borono-phenylalanine
BSH	Borocaptate Sodium
CBE	Compound related Biological Effectiveness
DNA	Deoxyribonucleic acid
EELS	Electron Energy Loss Spectroscopy
EORTC	European Organisation for Research and Treatment of Cancer
EST	Estimator
FET	Functional Expansion Technique
HFR	High Flux Reactor
IAEA	International Atomic Energy Agency
ICRU	International Commission on Radiation Units & measurements
JRC	Joint Research Centre
KERMA	Kinetic Energy Released per unit Mass
LET	Linear Energy Transfer
LEXT	Legendre EXpansion Technique
MC	Monte Carlo
MCNP	Monte Carlo N-Particle transport code
MIT	Massachusetts Institute of Technology
OAR	Organs At Risk
PMMA	Polymethyl Methacrylate)
PNR	Physics of Nuclear Reactors
RBE	Relative Biological Effectiveness
ROI	Regio Of Interest

REFERENCES

1. T. HARTMAN, J. CARLSSON, "Radiation dose heterogeneity in receptor and antigen mediated boron neutron capture therapy," *Radiother Oncol.* 31(1), 61-75 (1994).
2. J. A. CODERRE, J. C. TURCOTTE, K. J. RILEY, P. J. BINNS, O. K. HARLING, W. S. KIGER, III, "Boron Neutron Capture Therapy: Cellular Targeting of High Linear Energy Transfer Radiation," *Technology in Cancer Research & Treatment* Volume 2, Number 5, October (2003).
3. J.J. DUDERSTADT, L.J. HAMILTON, *Nuclear reactor analysis*, John Wiley & Sons Inc, New York (1976).
4. International Atomic Energy Agency IAEA: Current status of neutron capture therapy. IAEA-TECDOC-1223. Vienna (2001).
5. J.A. CODERRE, G.M. MORRIS, "The radiation biology of boron neutron capture therapy," *Rad. Res.*, 151, 1-18, (1999).
6. E.H. ELOWITZ, R.M. BERGLAND, J.A. CODERRE, D.D. JOEL, M. CHADHA, A.D. CHANANA, "Biodistribution of p-boronophenylalanine in patients with glioblastoma multiforme for use in boron neutron capture therapy," *Neurosurgery* 42(3), 463-8 (1998).
7. J.F. BRIESMEISTER, MCNP - A General Monte Carlo N-Particle Transport Code, Version 4C. LA-13709-M (2000).
8. ICRU 46. Photon, electron, proton and neutron interaction data for body tissues. International Commission on Radiation Units and Measurements. Bethesda. MD (1992).
9. G. M. MORRIS, J. A. CODERRE, J. W. HOPEWELL, P. L. MICCA, M. REZVANI, "Response of Rat Skin to Boron Neutron Capture Therapy with p-boronophenylalanine or Borocaptate Sodium," *Radiother. Oncol.* 32, 144-153 (1994).
10. A.H. SOLOWAY, H. HATANAKA, M.A. DAVIS, "Penetration of Brain and Brain Tumor. VII. Tumor-binding Sulfhydryl Boron Compounds," *J. Med. Chem.*, 10:714-717, (1967).
11. H. C. MILLER, N. E. MILLER, E. L. MUETTERTIES, "Synthesis of Polyhedral Boranes," *J. Am. Chem. Soc.* 85(23), 3885 – 3886 (1963).
12. H.R. SNYDER, A. H. REEDY, W. LENNARZ, "Synthesis of Aromatic Boronic Acids. Aldehyde Boronic Acids and a Boronic Acid Analog of Tyrosine," *J. Am. Chem. Soc.* 80, 835-838 (1958).
13. Y. MISHIMA, C. HONDA, M. ICHIHASHI, H. OBARA, J. HIRATSUKA, H. FUKUDA, H. KARASHIMA, T. KOBAYASHI, K. KANDA, K. YOSHINO, "Treatment of Malignant Melanoma by Single Thermal Neutron Capture Therapy with Melanoma-seeking 10B-compound," *Lancet* II, 388-389 (1989).
14. K.H.I. PHILIPP, Tolerance of normal brain tissue to Boron Neutron Capture Irradiation, PhD Thesis, Katholieke Universiteit Nijmegen (2004).
15. J. CHADWICK, "The Existence of a Neutron," *Proc. Roy. Soc., A*,

- 136, 692-708 (1932).
16. E. RUTHERFORD, "Nuclear Constitution of Atoms," *Proc. Roy. Soc. A* 97, 374-400 (1920).
 17. H.J. TAYLOR, M. GOLDBERGER, "Detection of nuclear disintegration in a photographic emulsion," *Nature (Lond.)* 135, 341-348 (1935).
 18. G.L. LOCHER, "Biological effects and therapeutic possibilities of neutrons," *Am. J. Roentgenol. Radium. Ther.* 36, 1-13 (1936).
 19. P. G. KRUGER, "Some Biological Effects of Nuclear Disintegration Products on Neoplastic Tissue," *Proc.Natl.Acad.Sci.* 26, 181-192 (1940).
 20. P.A. ZAHL, F.S. COOPER, "Physical and biological considerations in the use of slow neutrons for cancer therapy," *Radiology* 37, 673-682 (1940).
 21. P. A. ZAHL, F. S. COOPER, J. R. DUNNING, "Some in vivo Effects of Localized Nuclear Disintegration Products on a Transplantable Mouse Sarcoma," *Proc.Natl.Acad.Sci.* 26, 589-598 (1940).
 22. P. A. ZAHL, F. S. COOPER, "Localization of Lithium in Tumor Tissue as a Basis for Slow Neutron Therapy," *Science*, 64-65 (1941).
 23. L.E. FARR, W.H. SWEET, J.S. ROBERTSON, S.G. FOSTER, H.B. LOCKSLEY, D.L.SUTHERLAND, M.L. MENDELSON, E.E. STICKEY, "Neutron Capture Therapy with Boron in the Treatment of Glioblastoma Multiforme," *Am. J. Roentgenol.*, 71, 279-291 (1954).
 24. W. H. SWEET, "Medical aspects of boron slow-neutron capture therapy," In: *Workshop on Neutron Capture Therapy*, Report BNL-51994, eds. R.G. Fairchild, V.P. Bond (Brookhaven Natl. Lab., Upton, NY), 173-177 (1986).
 25. H. HATANAKA, Y. NAKAGAWA, "Clinical results of long-surviving Brain Tumor Patients who underwent boron neutron capture therapy," *Int. J. Radiat. Oncol. Biol. Phys.* 28, 1061-1066 (1994).
 26. H. HATANAKA, "Clinical results of boron neutron capture therapy," *Basic Life Sci.* 54, 15-21 (1990).
 27. R.L. MOSS, "Progress towards boron neutron capture therapy at the High Flux Reactor Petten," *Basic Life Sci.* 54, 169-83 (1990).
 28. G. DETLEF, R. MOSS, editors, *Boron neutron capture therapy: toward clinical trials of glioma treatment (HB)*, Plenum Press, New York (1992).
 29. R.L. MOSS, O. AIZAWA, D. BEYNON, R. BRUGGER, G. CONSTANTINE, O. HARLING, H.B. LIU, P. WATKINS, "The requirements and development of neutron beams for neutron capture therapy of brain cancer," *J. Neuro-Onc.* vol 33, 27-40 (1997).
 30. L. KANKAANRANTA, T. SEPPÄLÄ, M. KALLIO, J. KARILA, C. ASCHAN, T. SEREN, M. KORTESNIEMI, P. KOTILUOTO, E. JÄRVILUOMA, M. KULVIK, J. LAAKSO, A. BRANDER, J. JÄÄSKELÄINEN, J. VÄHÄTALO, I. AUTERINEN, S. SAVOLAINEN, M. FÄRKKILÄ, H. JOENSUU, "First clinical

- results on the Finnish study on BPA-mediated BNCT in glioblastoma,” - NCT Osaka 2000. 9th International Symposium on Neutron Capture Therapy for Cancer, Program & Abstracts. Osaka, JP, 2 - 6 Oct., 31-32 (2000).
31. J. CAPALA, B.H. STENSTAM, K. SKOLD, P.M. AF ROSENSCHOLD, V. GIUSTI, C. PERSSON, E. WALLIN, A. BRUN, L. FRANZEN, J. CARLSSON, L. SALFORD, C. CEBERG, B. PERSSON, L. PELLETTIERI, R. HENRIKSSON, “Boron neutron capture therapy for glioblastoma multiforme: clinical studies in Sweden,” *J.Neurooncol.* 62(1-2), 135-44 (2003).
 32. B.T.S. THIRUMAMAGAL, X.B. ZHAO, A.K. BANDYOPADHY, S. NARAYANASAMY, J. SAMUEL, R. TIWARI, D.W. GOLIGHTLY, V. PATEL, B.T. JEHNING, M.V. BACKER, R.F. BARTH, R.J. LEE, J.M. BACKER, W. TJARKS, “Receptor-Targeted Liposomal Delivery of Boron-Containing Cholesterol Mimics for Boron Neutron Capture Therapy (BNCT),” *Bioconjugate Chem.* 17 (5), 1141 -1150 (2006).
 33. J. CARLSSON, E.B. KULLBERG, J. CAPALA, S. SJÖBERG, K. EDWARDS, L. GEDDA, “Ligand Liposomes and Boron Neutron Capture Therapy,” *J.Neuro-Oncology* 62, Number 1, 47-59 (2003).
 34. G.C. KRIJGER, M.M. FRETZ, R. CARVALHO, O. STEINEBACH, W. JISKOOT, G. STORM, G.A. KONING, “Tumor targeted liposomes for neutron capture therapy,” *Radiochim.Acta* 93, 589-593 (2005).
 35. G.A. KONING, M.M. FRETZ, U. WORONIECKA, G. STORM, G.C. KRIJGER, “Targeting liposomes to tumor endothelial cells for neutron capture therapy,” *Appl. Radiat. Isot.* 61 (5), 963-967 (2004).
 36. R.A. WATSON-CLARK, M.L. BANQUERIGO, K. SHELLY, M.F. HAWTHORNE, E. BRAHN, “Model studies directed toward the application of boron neutron capture therapy to rheumatoid arthritis: Boron delivery by liposomes in rat collagen-induced arthritis,” *Proc.Natl.Acad.Sci.* 95, 2531–2534 (1998).
 37. J.C. YANCH, S. SHORTKROFF, R.E. SHEFER, S. JOHNSON, E. BINELLO, D. GIERGA, A.G. JONES, G. YOUNG, C. VIVIEROS, A. DAVISON, C. SLEDGE, “Boron Neutron Capture Synovectomy: Treatment of Rheumatoid Arthritis Based on the $^{10}\text{B}(\text{n},\alpha)^7\text{Li}$ Nuclear Reaction,” *Medical Physics* (26)3, 364-375 (1999).
 38. P. VAN LENT, “Selective Elimination of Synovial Macrophages by Boron Neutron Capture Therapy prevents onset of Murine Experimental Arthritis,” 12th International Congress on Neutron Capture Therapy, Proceedings of ICNCT-12 Takamatsu, JP, 9 – 13 Oct. (2006).
 39. Y. SAKURAI, K. ONO, S. MIYATAKE, A. MARUHASHI, “Improvement effect on the depth-dose distribution by CSF drainage and air infusion of a tumour-removed cavity in boron neutron capture therapy for malignant brain tumours,” *Phys. Med. Biol.* 51, 1173-

- 1183 (2006).
40. K. YOKOYAMA, S. MIYATAKE, Y. KAJIMOTO, S. KAWABATA, A. DOI, T. YOSHIDA, T. ASANO, M. KIRIHATA, K. ONO, T. KUROIWA, "Pharmacokinetic study of BSH and BPA in simultaneous use for BNCT," *J. Neuro-Oncology* 78 Number 3, 227-232 (2006).
 41. J. MICHEL, G. BALOSSIER, A. WITTIG, W. SAUERWEIN, K. ZIEROLD, "EELS spectrum-imaging for boron detection in biological cryofixed tissues," *Instr.sci.technol.* 33 no6, 631-644 (2005).
 42. K.J. RILEY, P.J. BINNS, D.D. GREENBERG, O.K. HARLING, "A Physical Dosimetry Intercomparison for BNCT," *Med.Phys.* 29 (5), May (2002).
 43. P.J. BINNS, K.J. RILEY, O.K. HARLING, W.S. KIGER 3RD, P.M. MUNCK AF ROSENSCHOLD, V. GIUSTI, J. CAPALA, K. SKOLD, I. AUTERINEN, T. SEREN, P. KOTILUOTO, J. UUSI-SIMOLA, M. MAREK, L. VIERERBL, F.SPURNY, "An international dosimetry exchange for boron neutron capture therapy. Part I: Absorbed dose measurements," *Med.Phys.* 32(12), 3729-36 (2005).
 44. J. BENCZIK, T. SEPPÄLÄ, M. SNELLMAN, H. JOENSUU, G. M. MORRIS, J. W. HOPEWELL, "Evaluation of the Relative Biological Effectiveness of a Clinical Epithermal Neutron Beam Using Dog Brain," *Radiat. Res.* 159, 199-209 (2003).
 45. J. GUEULETTE, P.J. BINNS, B.M. DE COSTER, X-Q. LU, S.A. ROBERTS, K.J. RILEY, "RBE of the MIT fission converter beam for crypt cell regeneration in mice," *Radiat. Res.* 164, 805-809 (2005).
 46. R.G. FAIRCHILD, "Development and Dosimetry of an Epithermal Neutron Beam for Possible Use in Neutron Capture Therapy, I. 'Epithermal' Neutron Beam Development," *Phys.Med.Biol.* 10 No. 4, 491-504 (1965).
 47. R.G. FAIRCHILD, "Development and Dosimetry of an Epithermal Neutron Beam for Possible Use in Neutron Capture Therapy, II. Absorbed Dose Measurements in a Phantom Man," *Phys.Med.Biol.* 11 No. 1, 15-30 (1966).
 48. O.AIZAWA, "Research on neutron beam design for BNCT at the Musashi Reactor," *Basic Life Sci.* 54, 109-24 (1990).
 49. G. TRACZ, L. DABKOWSKI, D. DWORAK, K. PYTEL, U. WOZNICKA, "The filter/moderator arrangement-optimisation for the boron-neutron capture therapy (BNCT)," *Radiat. prot. dosim.* 110 no1-4, 827-831 (2004).
 50. J.M. VERBEKE, A.S. CHEN, J.L. VUJIC, K.N. LEUNG, "Optimization of Beam-Shaping Assemblies for BNCS Using the High-Energy Neutron Sources D-D and D-T," *Rad.Biol.Med.* 134(3), 278-293 (2001).
 51. T. KOBAYASHI, Y. SAKURAI, K. KANDA, Y. FUJITA, K. ONO,

- "The Remodeling and Basic Characteristics of the Heavy Water Neutron Irradiation Facility of the Kyoto University Research Reactor, Mainly for Neutron Capture Therapy," *Rad.Biol.Med.* 131(3), 354-378 (2000).
52. T. MATSUMOTO, H.B.LIU, R.M.BRUGGER, "Design studies of an epithermal neutron beam for neutron capture therapy at the Musashi reactor," *J. Nucl. Sci. Technol.* 32 no2, 87-94 (1995).
53. H.B. LIU, R.M. BRUGGER, D.C. RORER, P.R. TICHLER, J.P. HU, "Design of a high-flux epithermal neutron beam using ²³⁵U fission plates at the Brookhaven Medical Research Reactor," *Med Phys.* 21(10), 1627-31 (1994).
54. J.C. YANCH, X.L. ZHOU, G.L.BROWNELL, "A Monte Carlo Investigation of the dosimetric properties of monoenergetic neutron beams for neutron capture therapy," *Radiat.Res.* 126, 1-20 (1991).
55. J.C. YANCH, O.K. HARLING, "Dosimetric Effects of Beam size and collimation of epithermal neutrons for Boron Neutron Capture Therapy," *Rad.Res.* 135, 131-145 (1993).
56. E. BISCEGLIE, P. COLANGELO, N. COLONNA, P. SANTORELLI, V. VARIALE, "On the optimal energy of epithermal neutron beams for BNCT," *Phys.Med.Biol.* 45, 49-58 (2000).
57. D.L. BLEUEL, R.J. DONAHUE, B.A. LUDEWIGT, J. VUJIC, "Development of a Neutron Energy-Biased In-Air Figure of Merit for Predicting In-Phantom BNCT Neutron Beam Characteristics," In: *Proceedings of the 8th International Symposium on Neutron Capture Therapy for Cancer*, La Jolla, CA, Sep. 13-18, (1999).
58. H.D. THAMES, J.H. HENDRY, *Fractionation in Radiotherapy*, Taylor & Francis Books Ltd., London (1987).
59. J.F. FOWLER, "Biological factors influencing optimum fractionation in radiation therapy," *Acta Oncologica* 40(6), 712-717 (2001).
60. D.T. GOODHEAD, J. THACKER, R. COX, "Effects of radiations of different qualities on cells: molecular mechanisms of damage and repair," *Int.J.Radiat.Biol.* 63, 543-556 (1993).
61. E.J. HALL, A. GIACCIA, *Radiobiology for the Radiologist*, Lippincott Williams and Wilkins, Philadelphia, San Francisco, Sixth Edition (2005).
62. A.L. BROOKS, G.J. NEWTON, L.J. SHYR, F.A. SEILER, B.R. SCOTT, "The combined effects of alpha-particles and X-rays on cell killing and micronuclei induction in lung epithelial cells," *Int.J.Radiat. Biol.* 58, 799-811 (1990).
63. Y. FURUSAWA, M. AOKI, M. DURANTE, "Simultaneous exposure of mammalian cells to heavy ions and X-rays, *Advances in Space Research*," 30, 877-884 (2002).
64. A. WITTIG ET AL., Early phase II study on BNCT in metastatic malignant melanoma using the boron carrier BPA, EORTC protocol 11011 (2003).
65. W. SAUERWEIN ET AL., Postoperative Treatment of glioblastoma

- with BNCT at the Petten Irradiation Facility, EORTC Protocol 11961 (1999).
66. K. HIDEGHETY, W. SAUERWEIN, A. WITTIG, C. GOTZ, P. PAQUIS, F. GROCHULLA, K. HASELSBERGER, J. WOLBERS, R. MOSS, R. HUIKAMP, H. FANKHAUSER, M. DE VRIES, D. GABEL, "Tissue uptake of BSH in patients with glioblastoma in the EORTC 11961 phase I BNCT trial," *J.Neurooncol.* 62(1-2), 145-56 (2003).
 67. D.W. NIGG, "Some recent trends and progress in the physics and biophysics of neutron capture therapy," *Progr. In Nuclear Energy* 35 No 1, 79-127 (1999).
 68. C. VROEGINDEWELJ, F. WHEELER, F. STECHER-RASMUSSEN, R. HUIKAMP, "Microdosimetry Model for Boron Neutron Capture Therapy. II. Theoretical Estimation of the Effectiveness Function and Surviving Fractions," *Rad. Res.* 155, 498-502 (2001).
 69. G. I. BELL, S. GLASSTONE, *Nuclear Reactor Theory*, Van Nostrand Reinhold Company, New York, NY (1970).
 70. J.C. WAGNER, E.L. REDMOND II, S.P. PALMTAG, J.S. HENDRICKS, "MCNP: Multigroup/Adjoint Capabilities," LA-12704, Los Alamos National Laboratory (1994).
 71. J.E. HOOGENBOOM, "Methodology of Continuous-Energy Adjoint Monte Carlo for Neutron, Photon, and Coupled Neutron-Photon Transport," *Nucl. Sci. Eng.* 143, 99-120 (2003).
 72. F.C. DIFILIPPO, "Forward and adjoint methods for radiotherapy planning," *Med. Phys.* 25(9), 1702-10 (1998).
 73. J.V. SIEBERS, M. LAUTERBACH, S. TONG, Q. WU, R. MOHAN, "Reducing dose calculation time for accurate iterative IMRT planning," *Med.Phys.* 29(2), 231-237 (2002).
 74. W. ULMER, J. PYYRY, W. KAISSEL, "A 3D photon superposition/convolution algorithm and its foundation on results of Monte Carlo calculations," *Phys.Med.Biol.* 50, 1767-1790 (2005).
 75. Q. WU, D. DJAJAPUTRA, M. LAUTERBACH, Y. WU, R. MOHAN, "A fast dose calculation method based on table lookup for IMRT optimization," *Phys.Med.Biol.* 48, N159-N166 (2003).
 76. C.M. MA, E. MOK, A. KAPUR, T. PAWLICKI, D. FINDLEY, S. BRAIN, K. FORSTER, A. L. BOYER, "Clinical implementation of a Monte Carlo treatment planning system," *Med.Phys.* 26(10), 2133-2143 (1999).
 77. J.J. DEMARCO, I.J. CHETTY, T.D. SOLBERG, "A Monte Carlo tutorial and the application for radiotherapy treatment planning," *Med.Dosim.* 27(1), 43-50 (2002).
 78. R. JERAJ AND P. KEALL, "Monte Carlo-based inverse treatment planning," *Phys. Med. Biol.* 44, 1885-96 (1999).
 79. M. GOLDSTEIN, "The adjoint Monte Carlo - a viable option for efficient radiotherapy treatment planning," *Proc. of the 19th Conf. of*

- the Israeli Nucl. Soc. 11-2 (1996).
80. S. YOO, M.E. KOWALOK, B.R. THOMADSEN, D.L. HENDERSON, "Treatment planning for prostate brachytherapy using region of interest adjoint functions and greedy heuristic," *Phys.Med.Biol.* 48, 4077-90 (2003).
 81. B. WANG, M. GOLDSTEIN, X.G. XU, N. SAHOO, "Adjoint Monte Carlo method for prostate external gamma beam treatment planning: an application to 3D patient anatomy," *Phys.Med.Biol.* 50, 923-935 (2005).
 82. R.A. LILLIE, "BNCT filter optimisation using two-and three-dimensional discrete ordinates," In: *Proceedings of the 3-D Deterministic Radiation Transport Computer Programs: Features, Applications and Perspectives*, vol. 1, Paris, France, 379 (1996).
 83. B.L. BEERS, V.W. PINE, "Functional Expansion Technique for Monte Carlo Electron Transport Calculations" *IEEE Trans. Nucl. Sci.* 23, No. 6 (1976).
 84. D.P. GRIESHEIMER, W.R. MARTIN, "Monte Carlo Based Angular Flux Distribution with Orthogonal Function Expansion," *Trans. Am. Nucl. Soc.* 89 (2003).
 85. J.P. BOYD, *Chebyshev and Fourier spectral method*, Dover Publications, New York (2000).
 86. J.T. WEST III, "SABRINA, an Interactive Three-Dimensional Geometry-Modeling Program for MCNP," Los Alamos National Laboratory Report LA10688M (1986).
 87. K.A. VAN RIPER, "A CT and MRI scan to MCNP input conversion program," *Rad.Prot.Dos.* 115 No. 1-4, 513-516 (2005).
 88. T. PINELLI, A. ZONTA, S. ALTIERI, S.BARNI, A. BRAGHIERI, P. PEDRONI, P. BRUSCHI, P. CHIARI, C. FERRARI, C. ZONTA, "TAOrMINA: From the first idea to the application to the human liver," In: W. Sauerwein, R. Moss, A. Wittig, eds *Research and Development Neutron Capture Therapy*. Bologna: Monduzzi Editore, 1065-72 (2002).
 89. T. PINELLI, S. ALTIERI, F. FOSSATI, A. ZONTA, C. FERRARI, U. PRATI, L. ROVEDA, S. NGNITEJEU TATA, S. BARNI, D.M. FERGUSON, "Operative modalities and effects of BNCT on liver metastases of colon adenocarcinoma," In: M.F. Hawthorne, K. Shelly, R.J. Wiersema, eds. *Frontiers in Neutron Capture Therapy*. New York: Kluwer Academic, Plenum Publishers, 1427-40 (2001).
 90. R. NANO, S. BARNI, P. CHIARI, T. PINELLI, F. FOSSATI, S. ALTIERI, C. ZONTA, U. PRATI, L. ROVEDA, A. ZONTA, "Efficacy of boron neutron capture therapy on liver metastases of colon adenocarcinoma: optical and ultrastructural study in the rat," *Oncol.Rep.* 11, 149-153 (2004).
 91. H. GRAY, *Anatomy of the Human Body*. Philadelphia: Lea & Febiger; 1918. Thoroughly revised and re-edited by WH. Lewis New York: Bartleby.com (2000).

92. J.A. FAVORITE, Memorandum: Proposed Changes to the Tallies Section of the MCNP4C Manual, Chapter 2, Secs. V.A-V.C, X-5:02-017(U), LA-UR-02-1892 (2002).
93. G.B. DANTZIG, Linear Programming and Extensions. Princeton, NJ Princeton University Press (1963).
94. Numerical Recipes in Fortran 77: The art of scientific computing. Copyright (C) 1986-1992 by Cambridge University Press.
95. T. COLEMAN, M. A. BRANCH, A. GRACE, Optimization Toolbox For Use with MATLAB, User's Guide Version 2, The MathWorks, Inc. (1999).

ACKNOWLEDGEMENT

I am willing to defend the proposition that says that without any of you mentioned in the acknowledgement, there would have been no thesis and list of propositions at all! One could argue that some people are not directly involved but I would reply that these people enjoy(ed) my life which is most important when trying to achieve something like a Ph.D. While writing this acknowledgement at the last moment (of course), I am afraid that I might forget to thank someone which would destroy my latest proposition immediately. Therefore, as a solution:

Many thanks to! How could I ever forget you? Sorry.

As you can imagine, it is impossible for me to start thanking all the persons in an order of 'importance'. There are the people who coached and helped me scientifically and there are the people who supported me privately in the dark moments I went through during this Ph.D. adventure. To be honest, I was at one moment close to giving up. I choose the 'proven' and therefore 'safe' order of thanking you which is roughly arranged from work-related friends to private friends to closest family.

In Delft, I want to thank the Professors Hugo van Dam and Tim van der Hagen for their trust, advice and support over the years. I learned a lot in the monthly meetings in which often one of you attacked my work while the other one protected me. Fortunately, Dr.ir. Jan Leen Kloosterman was always at my side in these meetings. However, outside the meetings Jan Leen pushed me hard to keep track of an imaginary schedule. Thank you for that, I know now that it is absolutely necessary. Always interested in my work was Dr.ir. Danny Lathouwers; the man with whom I baked bitterballen and vlammetjes during our duty in the IRI-bar (thank you Ruben for teaching us)! Let me continue with thanking Dr.ir. Eduard Hoogenboom, Ine, Riny, Piet, Camiel, Dick, August and Martin. Of course, we started more or less together, and finished it: Alexander, Marek and the Húngarian guy I forgot the name of (C15?). All students from PNR thank you for letting me feel welcome during my monthly returns to Delft.

In Petten, I want to thank our director Professor Kari Törrönen, Dr. Roberto May and Dr. Marc Becquet. Thank you Dr. Ray Moss. Of course, very important, Gerda, thank you for all your support. Mentioning Gerda, with tears in my eyes: where would I have been without TIM, TAS, Conge, WAB and Sysper2! Thank you all people of the JRC's administration and IT department for making impossible things possible. All my fellow colleagues and agents: Antoaneta, Jim, Arthur, Josselin, Lucien, Giuseppe, Günther, Andrzej, Yuan-DHL, Bart, Alain, Finn, Klaas, Anton and Francois. I really appreciate the friendliness and interest of all the people from NRG working around the reactor. Thanks und grüsse to the Essen crew in the persons of Professor Wolfgang Sauerwein, Dr. Andrea Wittig and Dr. Reinhard Hentschel. Thank you all BNCT colleagues and friends worldwide: Super Cecile, Silva, Andrea, Stead, Jingli, Stuart, Kent, Ray, Hiroaki, Saverio, Grazia, Simone, The Elisabetas, Jerome, Marjan, Gerard and Gerben. Thanks to Wilko and Corine for your Dutch BNCT support. Not to forget the people who encouraged me during my graduation work and motivated me to continue: Professor Rob Mudde, Dr. Hans

van Maanen and Jaap Beekman. Also related to this is Hanneke who encouraged me to go for it. Many thanks!

Okkebas, Het Eiland (Allan, Jan and Maikel) and Thijs G thanks for the great time. Please let me repeat it once again: no Cris and Haipo, no coffee, no thesis. Harold and Zoe thanks for also helping me with the linear programming. I will never forget the man who gave me a lot of support and who will make me feel very welcome in Hungary, whenever I go there: David!

Let me now thank my parents and family. Joop and Hedy, you are always there for me and this was once again proven as you helped us after the birth of Anna and Sofie. This was a very hectic period. Let me immediately add the name of Joke Wilkes. Many many thanks! Side support was given by Bert, Jorine, Eveline and Yvonne. I appreciated the support and understanding I received from my supervisors in Delft and Petten in this time.

My dear beloved Sabine, Anna and Sofie. I am very grateful to live my life with you every day. You gave me all the support possible to finish this thing. I am really looking forward to continue with you without having a thesis on my mind. This is for you!



Finally, I include here the first school-pictures of our daughters of whom we can be proud. With these pictures they have also something to look at in my thesis!

Petten, 10th of May 2007,
Sander

CURRICULUM VITAE

Victor Alexander Nievaart

Call name: Sander

Date of birth: June 19, 1973

Place of birth: Apeldoorn, The Netherlands

- 1985-1992: High school “Veluws College” in Apeldoorn; HAVO and VWO.
- 1992-2000: M.Sc. in applied physics at the Delft University of Technology, The Netherlands. Majored in the Transport Phenomena group on Laser Doppler Anemometry in multiphase flows.
- 2000-2004: Ph.D. student within a cooperation of the Section Physics of Nuclear Reactors of the Faculty of Applied Sciences of the Delft University of Technology and the Institute for Energy of the Joint Research Centre of the European Commission in Petten, The Netherlands. Ph.D. topic is ‘Spectral tailoring for Boron Neutron Capture Therapy’.
- 2004-2007: Continuing Ph.D. and involved in treatment planning in the BNCT clinical trials in Petten, investigating BNCT treatments of extra-corporeal livers and rheumatoid arthritis.

PART II

PAPERS I-III

